LOW-LYING EXCITED ENERGY STATES AND STRUCTURE OF DEFORMED NUCLEI

NOORA BINTI ROSLI

DISSERTATION SUBMITTED IN FULFILMENT OF THE REQUIREMENT FOR THE DEGREE OF MASTER OF SCIENCE

FACULTY OF SCIENCE
UNIVERSITY OF MALAYA
KUALA LUMPUR

2013

ABSTRACT

Low-lying excited states and structure of even-even, deformed, rare earth $^{152,154,156}Sm$ and $^{156,158,160,162,164,166}Dy$ nuclei are studied. A phenomenological model is used to understand the properties of deformed nuclei. The experimental data are analyzed by theoretical analysis within this model. Major steps in the derivation of cranking model are briefly presented. Harris parameterization for the energy and angular momentum are formulated and analyzed. The inertial parameters for the even-even deformed nuclei are defined using the Harris parameterization. The angular frequency of rotation is derived from the cubic equation of angular momentum. The values of angular frequency $\omega_{rot}(I)$ and rotational energy $E_{rot}(I)$ are calculated for the $^{152,154,156}Sm$ and $^{156,158,160,162,164,166}Dy$ nuclei at low spin $I \leq 10\hbar$. The energy spectra of positive-parity states which are in good agreement with the experimental data are presented. Few new states that are not available in the experimental data are predicted. At higher total angular momentum, deviation from the adiabatic theory is shown by the increment of energy difference between theoretical and experimental values. It is found that the non-adiabaticity of rotational energy bands occurred at high spin due to the Coriolis effect. The parameters fitted to the model are calculated. The complete low energy structures of $^{152,154,156}Sm$ and $^{156,158,160,162,164,166}Dy$ isotopes are calculated by taking into account the Coriolis mixing between states. The effect of $K^{\pi} = 1_{\nu}^{+}$ bands on low-lying $(K^{\pi} = 0_{1}^{+})$ ground states, $\beta_1 (K^{\pi} = 0_{2}^{+}) -$, β_2

$(K^{\pi}=0_3^{+})-$, and $\gamma\,(K^{\pi}=2^{+})-$ bands is studied. Larger values of Coriolis interaction matrix elements, $(j_x)_{K,K'}$ and the closeness between band head energies, ω_K induce strong states mixing.

ABSTRAK

Keadaan teruja paras rendah dan struktur bahagian nukleus tercangga genap-genap nadir bumi $^{152,154,156}Sm$ dan $^{156,158,160,162,164,166}Dy$ dikaji. Model fenomenologi digunakan untuk memahami sifat nukleus tercangga. Data eksperimen dianalisis secara teori dalam model ini. Langkah-langkah utama dalam penerbitan model "cranking" dibentangkan secara ringkas. Parameterisasi Harris untuk tenaga dan momentum sudut dirumuskan dan dianalisis. Parameter inersia untuk nukleus tercangga genap-genap ditakrifkan dengan menggunakan parameterisasi Harris. Frekuensi sudut putaran diterbitkan daripada persamaan kuasa tiga momentum sudut. Nilai-nilai frekuensi sudut $\omega_{rot}(I)$ dan tenaga putaran $E_{rot}(I)$ dikira untuk nukleus $^{152,154,156}Sm$ dan $^{156,158,160,162,164,166}Dy$ pada spin rendah $I \leq 10\hbar$. Spektrum tenaga keadaan berpariti positif yang bersetuju dengan baik dengan data eksperimen dibentangkan. Beberapa keadaan baru yang tidak terdapat di dalam data eksperimen diramalkan. Pada jumlah momentum sudut yang lebih tinggi, sisihan daripada teori adiabatik ditunjukkan oleh peningkatan beza tenaga antara nilai teori dan eksperimen. Ketidak-adiabatikan jalur tenaga putaran di dapati berlaku pada spin tinggi kerana kesan Coriolis. Parameter yang disesuaikan dalam model tersebut dikira. Struktur tenaga rendah isotop $^{152,154,156}Sm$ dan $^{156,158,160,162,164,166}Dy$ yang lengkap dikira dengan mengambil kira campuran Coriolis antara keadaan-keadaan. Kesan jalur $K^{\pi} = 1_{\nu}^{+}$ ke atas jalur-jalur keadaan dasar $(K^{\pi} = 0_1^{+})$, dan $\beta_1 (K^{\pi} = 0_2^{+})$, $\beta_2 (K^{\pi} = 0_3^{+})$, $\gamma (K^{\pi} = 2^{+})$

dikaji. Nilai elemen matriks saling tindakan Coriolis $(j_x)_{K,K'}$ yang besar dan kedekatan di antara tenaga kepala jalur ω_K mengaruhkan campuran keadaan yang kuat.

ACKNOWLEDGEMENTS

I praise and thank God for His grace in giving me strength to complete this project. And for the successful completion of my Master of Science project, I would like to express my sincere appreciations to many people for the motivation and support I have received.

In the first place, I would like to address my acknowledgements to my first supervisor, Assoc. Prof. Dr. Hasan Abu Kassim for his various suggestions and criticism throughout all stages of the research project. I am deeply thankful to my co-supervisor Dr. Abdurahim A. Okhunov for his valuable advice and guidance throughout the research project. He was never reluctant to assist despite his workload.

I am much indebted to Azni Abdul Aziz, Nor Sofiah Ahmad and the Theoretical Physics Research Group who have contributed, maybe unintentionally, to technically help and continuously guide in each step of my project. I would like to express my sincere gratitude to all my friends, who prevented frustration from creeping in.

To my grandparents, my father, my mother, my family and my dearest, this achievement is my gift to you. It was great to know that you have been around when I needed you. You have believed in me and have given me a grasp of my

own self-worth. My love to all of you that keeps me going. It derives my strength and inspiration. I love you all!

Last but not least, I would also like to thank University of Malaya for providing scholarship throughout my MSc. research project.

TABLE OF CONTENTS

LIST OF FIGURES

LIST OF TABLES

CHAPTER 1

INTRODUCTION

1.1 Rare-Earth Elements: *Samarium and Dysprosium*

Separated from the main body of the periodic table, one can see two rows of elements below the main body chart. These elements which include the lanthanides and actinides are called rare earth elements in the mass region of $150 < A < 190$. There are few opinions of the “rare” term. Some sources state that these elements are rare due to their scarcity [1-2]. The rare earth elements are typically dispersed and very difficult to find in concentrated form. The rarest rare earth metals are more abundant than gold, silver and lead. It took long and tedious processes to purify the metals from their oxides. But, the ion-exchange and solvent extraction processes used today which are low in cost can produce purer metals in short time [3-4].

There are common properties that can be applied on all of the rare earth elements. They appear as silvery-white or gray metals that have high luster. In air, these elements are very easy to oxide. The metals are very good electric conductors and have magnetic properties due to magnetic moment. Because of these common properties, it is very difficult to distinguish these elements from one another. Furthermore, they occur together in minerals naturally, e.g. in monazite sand. The elements themselves are not radioactive, but they are found in ore containing thorium and uranium.

Rare earth metals are vital to high-tech manufacturing. These metals are used in most electronic devices. Powerfulness and efficiency plus less in weight and

ability to pack energy in smaller space are the reasons why most electronic devices become smaller [2, 5].

Samarium and Dysprosium are categorized as lanthanides. They are quite well studied experimentally and theoretically [6-32]. Samarium is a fairly hard, pale silvery white metal as shown in Figure 1.1. Samarium has 30 known isotopes and the stable isotopes include ^{144}Sm, ^{150}Sm, ^{152}Sm and ^{154}Sm. The element ^{152}Sm is the most abundant isotope with 26.75% natural abundance. The element ^{148}Sm is extremely long-lived radioisotopes with half-life of 7×10^{15} yr. The naturally occurring element ^{146}Sm is also fairly long-lived radioisotopes with half-life of 1.03×10^{8} yr. The long lived isotopes, ^{146}Sm and ^{148}Sm are primarily decayed by alpha decay to isotopes of neodymium.

Figure 1.1 Samarium [33].

Samarium can ignite in dry air if heated above 150°C and form oxide coating if not stored in inert gas. Main application of the samarium is in samarium-

cobalt alloy magnets in electronic devices due to its high resistance to demagnetization and its ability to operate at high temperature up to $700^{\circ}C$. The long-lived radioisotopes of samarium are used in samarium-neodymium dating for determining the age relationships of rocks and meteorites [34-35].

Figure 1.2 Dysprosium [33].

Dysprosium is a soft and silvery-white rare earth metal as pictured in Figure 1.2. The stable isotopes of Dysprosium elements include ^{156}Dy, ^{158}Dy, ^{160}Dy, ^{162}Dy and ^{164}Dy. The most abundant isotope is ^{164}Dy at 28.18%. This metal reacts with cold water and dissolves in both dilute and concentrated acids. Dysprosium is an excellent neutron absorber that it is used in dysprosium-oxide-nickel cement in control rods in nuclear reactors. In addition, Dysprosium is used in data storage applications such as compact discs and hard discs [36].

1.2 Even- even Nuclei

Even-even nuclei have even number of protons and even number of neutrons, for example ^{154}Sm has 62 protons and 90 neutrons. According to the nuclear shell model, the ground state of even-even nuclei has zero angular momentum, $K^{\pi} = 0^{+}$ due to interaction of nucleons with equal magnitude and opposite direction of spins to form pairs. General property of even-even nuclei is, with the exception of the magic number nuclei, they have the lowest 2^{+} state energy. Figure 1.3 shows the energies of lowest 2^{+} states of even-even nuclei.

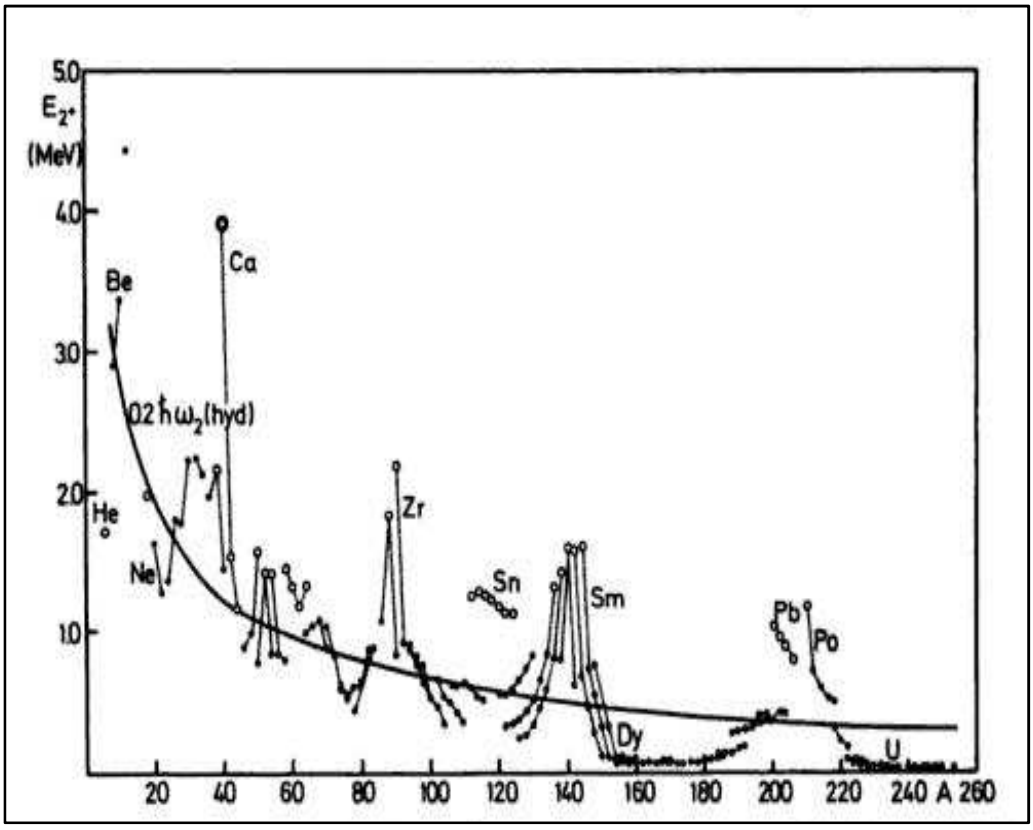

Figure 1.3 Energies of lowest 2^{+} states in even-even nuclei. The lines connect sequences of isotopes. The nuclei with closed neutron or proton shells are marked by open circles [37].

1.3 Collective Characteristic of Deformed nuclei

The isotopes $^{152,154,156}Sm$ and $^{156,158,160,162,164,166}Dy$ are classified as deformed nuclei. The valence nucleons of these deformed nuclei achieve low energy state for stability. Rotational and vibrational energy levels exist in these nuclei as they have nonspherically symmetric potential that is sensitive to collective motions. The collective characteristic of even-even deformed nuclei can be indicated by larger value of reduced transition probabilities, $B(E2;0^+ \rightarrow 2^+)$ and constant value of energy ratio for the excitation of lowest 4^+ and 2^+ states, $E_{4^+} / E_{2^+} = 3.33$. Rotation of a deformed charged object will emit electric quadrupole $E2$ radiation. The value $E_{4^+} / E_{2^+} = 3.33$ is equal to that of the pure rigid rotator value. Figures 1.4 and 1.5 show the remarkable

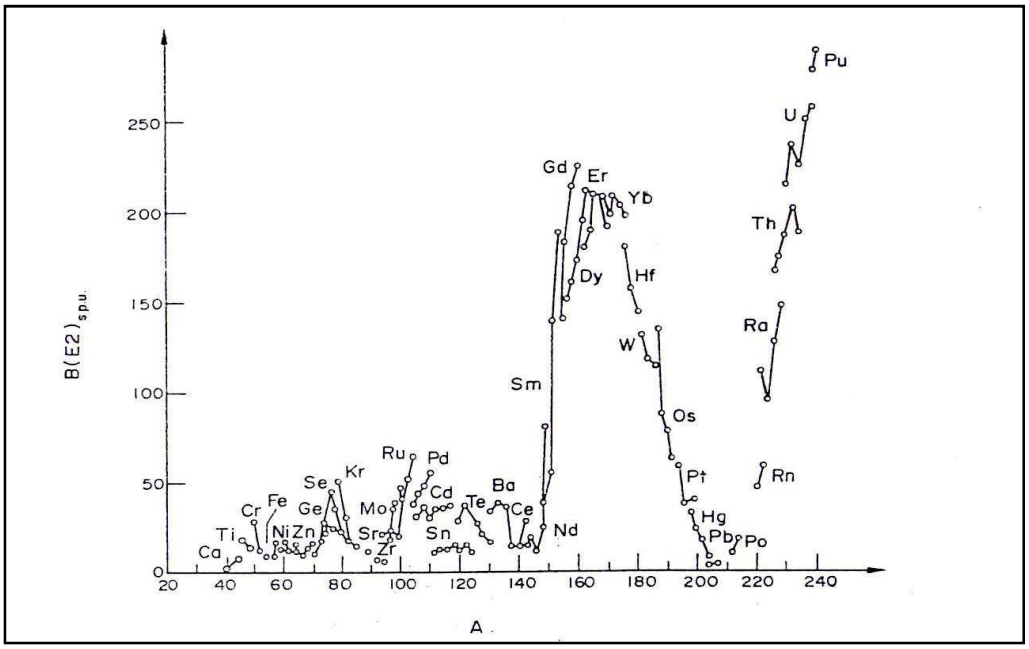

Figure 1.4 Reduced Transition Probabilities B(E2) for lowest 2^+ states of even-even nuclei [38].

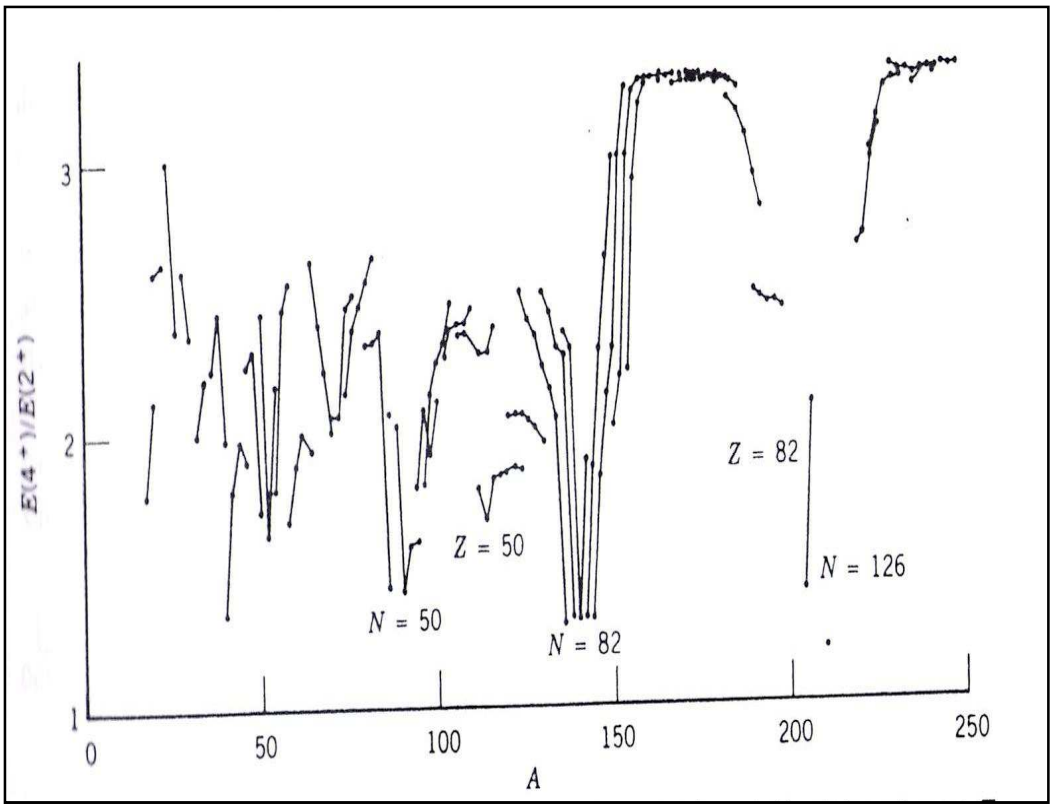

Figure 1.5 Energy ratio E_{4^+} / E_{2^+} for excitation of lowest 2^+ and 4^+ states in even-even nuclei. The lines connect sequences of isotopes [39].

behavior of nuclei in the rare earth mass regions which is consistent with the behavior of nuclei possessing large deformations.

Bohr and Mottelson suggested a theoretical direction to describe the deformed nuclei [40-41]. Nuclear behavior is predicted by angular frequency, moment of inertia and angular momentum induced by rotation.

For small values of angular momentum I, the rotational energy is expanded as a function of $I(I+1)$:

$$E_{rot}\left(I(I+1)\right) = AI(I+1) + BI^2(I+1)^2 + CI^3(I+1)^3 + \ldots$$

But, this law of $E_{rot} \sim I(I+1)$ is invalidate at high values of I. Prior to this weakness, more advance knowledge is explored to improve the understanding and explanation of nuclear behavior.

Nuclei as we know, made up of two different types of nucleons, i.e. protons and neutrons. These nucleons, as described by two-rotor model have dipole vibrational modes in which they oscillate around common axis in opposite phases. The oscillations generate isovector magnetic dipole resonance. The low-lying, collectively magnetic dipole excitations in deformed nuclei were discovered in the last decade [42]. Since then, interest to study the properties of the deformed nuclei has increased especially in the last few years [43-50]. It is evidently to state that the low-lying 1^+ states spread around the excitation energy of 3 MeV in energy spectrum [51].

Taking into account the Coriolis mixing of the isovector collective M1 states with low-lying states will lead for the non-adiabaticity of electromagnetic properties to occur [52-54].

1.4 Objectives

This study has two objectives:

1. To predict the energy spectra and study the low-lying excited energy states of $^{152,154,156}Sm$ and $^{156,158,160,162,164,166}Dy$ isotopes.
2. To analyze the wave function structure of nuclear band states of $^{152,154,156}Sm$ and $^{156,158,160,162,164,166}Dy$ isotopes.

The basic states of the Hamiltonian include $\left(K^{\pi}=0_{1}^{+}\right)$ ground state band, $\beta_{1}\left(K^{\pi}=0_{2}^{+}\right)-$, $\beta_{2}\left(K^{\pi}=0_{3}^{+}\right)-$, $\gamma\left(K^{\pi}=2^{+}\right)-$ vibrational bands and $K^{\pi}=1_{\nu}^{+}$ collective states (ν is the number of 1^{+} collective states).

1.5 Organization of Thesis

This thesis contains five chapters. The following chapter presents the overall theoretical and literature review done throughout the research. The description of nuclear models, the concepts of deformed nuclei, and the derivation of Harris parameterization from the cranking model are covered in Chapter 2.

The calculation and methodology of this study are demonstrated in Chapter 3. The structural work involving the analytical part is outlined with a flowchart presented in Figure 1.6.

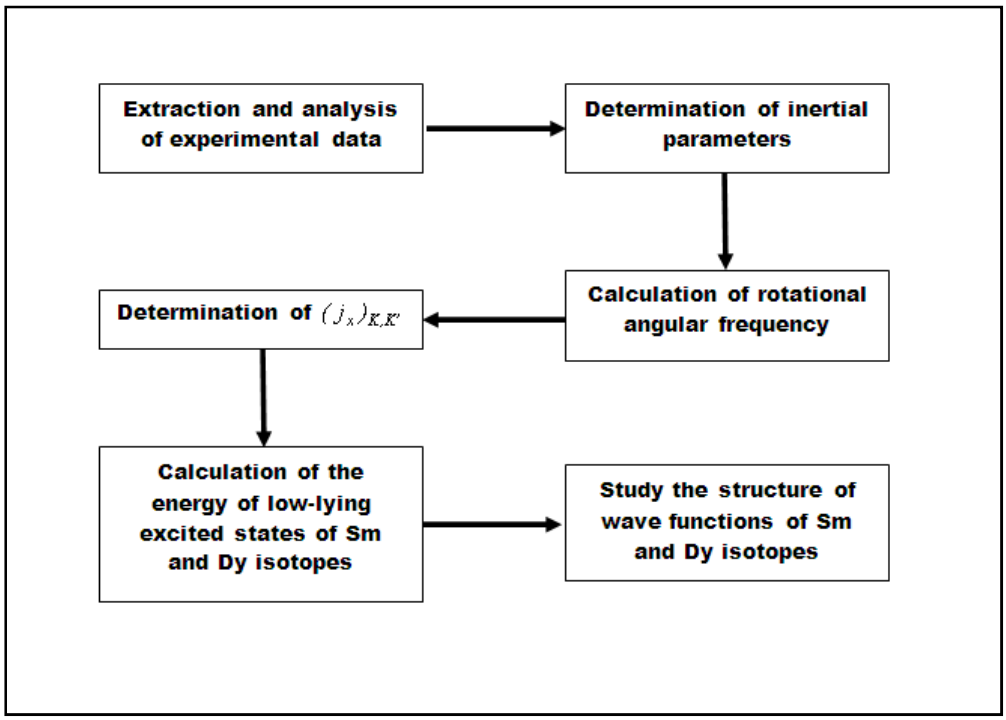

Figure 1.6 Work structure in the research.

Chapter 4 presents the results of the research. The results obtained for the determinations of inertial parameters, headband energies and the matrix elements of Coriolis mixing for $^{152,154,156}Sm$ and $^{156,158,160,162,164,166}Dy$ nuclei are presented in this chapter. The calculated values of the energy of low-lying excited states and the wave function structures of the nuclei are also included in this chapter. The explanations regarding the results obtained are discussed.

The final chapter summarizes the overall work done and concludes the study of low-energy structure in $^{152,154,156}Sm$ and $^{156,158,160,162,164,166}Dy$ nuclei. On-going and future works that may be explored are also included at the end of this chapter.

CHAPTER 2

NUCLEAR MODELS

The main problem of nuclear physics is to understand and explain the complex interaction in a nucleus. By 1934, scientists had found that the nucleus consists of protons and neutrons, but they did not have so much idea what is the general shape of nucleus and how these particles arrange themselves.

The nucleons inside an atomic nucleus are categorized as many-particle system that held by their mutual interaction via electromagnetic and strong forces. We are dealing with many-body problem of great complexity. Nuclear model is a simple way to look into a nucleus to give a wide range of its properties possible. A model is successful if it has the ability to predict measured nuclear properties that can be verified experimentally in the laboratory. The results predicted by the model must also be in good agreement with previous results. This chapter presents the chronology of nuclear model development relevant to this research.

2.1 The Liquid Drop Model: Semi-Empirical Mass Formula

A nucleus is not a simple collection of nucleons. In a reaction between A and b, there is an intermediate step C that delays the emission of particles X and y.

$$A + b \rightarrow C^{*} \rightarrow X + y$$

A Danish physicist, Niels Bohr proposed in the intermediate step, the energy is distributed among all nucleons and ends up on the emitted particles [55]. In

this model, the nucleons interacting via internal strong forces with their nearest neighbors in short range and results in the constantly oscillating and changing shape of the nucleus. In this respect, the nucleus is incompressible and not rigid as water droplet. As a consequence, the liquid drop model was suggested as early collective model in which the individual quantum properties of nucleons are completely ignored.

If two neighboring nucleons interact with each other, the total mass of the system is less than the sum of all the mass of individual nucleons. The mass defect is the difference in mass of the nucleus and its constituent nucleons; Z protons and N neutrons. The mass defect is defined by:

$$\Delta = \left(ZM_p + NM_n\right) - M\left(Z,N\right) \tag{2.1}$$

where M_p and M_n are the mass of the proton and neutron respectively. The stronger the interaction, the more the mass decreases.

To see how strong the nucleons are bound together, the mass defect is converted to the mass-energy equivalence which is the nuclear binding energy. The nuclear binding energy is given by:

$$B\left(Z,N\right) = \left[\left(ZM_P + NM_N\right) - M\left(Z,N\right)\right]c^2 . \tag{2.2}$$

The experimental nuclear binding energies of a wide range of nuclides are plotted in Figure 2.1. Binding energies per nucleon increase sharply as A reaches the peak of ~ 8 MeV/nucleon at iron (Fe) and then decreasing slowly

for the more massive nuclei. Above this value, the average binding energy per nucleon, B/A is relatively constant indicating that the nuclear density is almost constant and the nuclear force exhibits saturation properties.

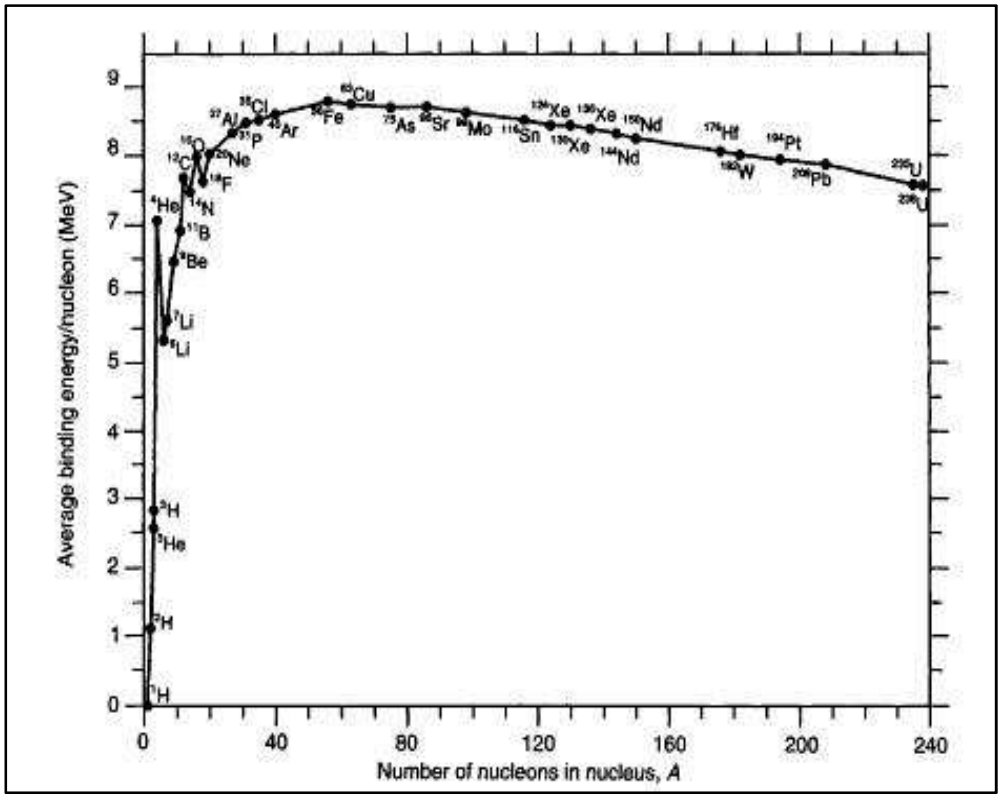

Figure 2.1 Binding energy per nucleon along the stability line [56].

On the basis of the liquid drop model, a systematic study leads to the completion of nuclear binding energy formula with few terms that shows the collective and the individual nucleons features of nuclei. Figure 2.2 shows the contribution of the correction terms in the semi-empirical formula:

$$B(Z,A) = a_v A - a_s A^{\frac{2}{3}} - a_c Z(Z-1)A^{-\frac{1}{3}} - a_{sym}\frac{(A-2Z)^2}{A} + \delta\,. \qquad (2.3)$$

The $a_v A$ term is proportional to the nuclear volume and represents the volume energy for the case of constant saturated binding energy per nucleon at 8 MeV. The $a_s A^{\frac{2}{3}}$ term corrects the binding energy formula due to the surface

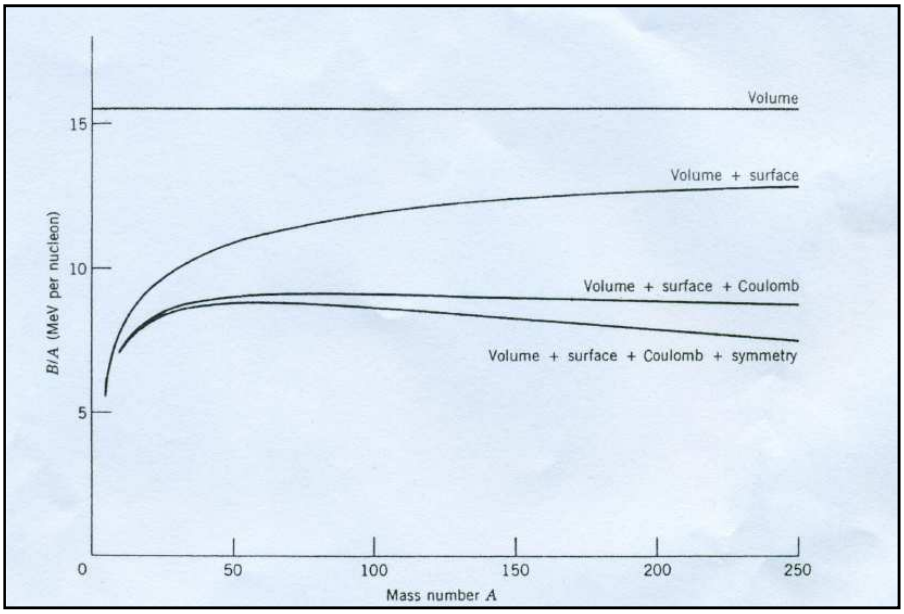

Figure 2.2 The contributions of various terms in the semiempirical mass formula to the binding energy per nucleon [57].

effect. The nucleons at the surface layer do not contribute to the binding energy as much as those in the central region. As in the raindrop, the force in the central core is saturated but drops to zero at the surface [58]. For lighter nuclei, the binding energy per nucleon is smaller because of larger surface-to-volume ratio.

The $a_c Z(Z-1)A^{-\frac{1}{3}}$ term is due to Coulomb repulsion between the Z protons in the nucleus. This Coulomb energy has destabilizing effect that reduces the binding strength. This term is very important for heavy nuclei because

additional neutrons are required for nuclear stability. The $a_{sym}\frac{(A-2Z)^2}{A}$ term is called symmetry energy. Unlike the Coulomb energy term, this term is important for light nuclei, for which $Z = N = A/2$ is strictly observed as presented in Figure 2.3.

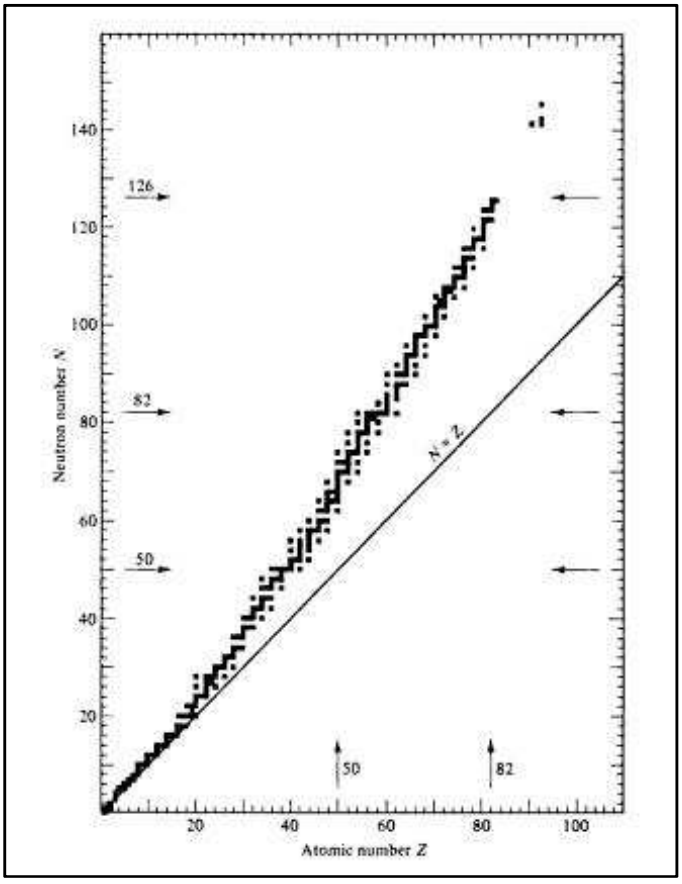

Figure 2.3 The plot of N versus Z for all stable nuclei [59].

The last term is called the pairing energy. This is due to nucleons tendency to form pairs with zero spin. When the value of both numbers of neutron and proton are odd, the odd proton is converted into a neutron (or vice versa), so that it gains binding energy to form a pair with its formerly odd partner. The pairing energy term of odd number of neutron and proton is subtracted from

the binding energy formula as opposed to that of the nuclei with even number of neutron and proton, which have greater stability. For nuclei with odd nucleon number, this term is taken as zero because such nuclei can be described without the last term.

The parameters a_v, a_s, a_c and a_{sym} are adjusted to give the best agreement with the experimental curve. By using this expression for B, the semi-empirical mass formula is formulated which is regarded as a first attempt to apply nuclear models. Since nucleons are bound, the binding energy must be subtracted from the total mass:

$$. M(Z,A) = ZM_P + NM_N - B(Z,N)/c^2 \quad . \tag{2.4}$$

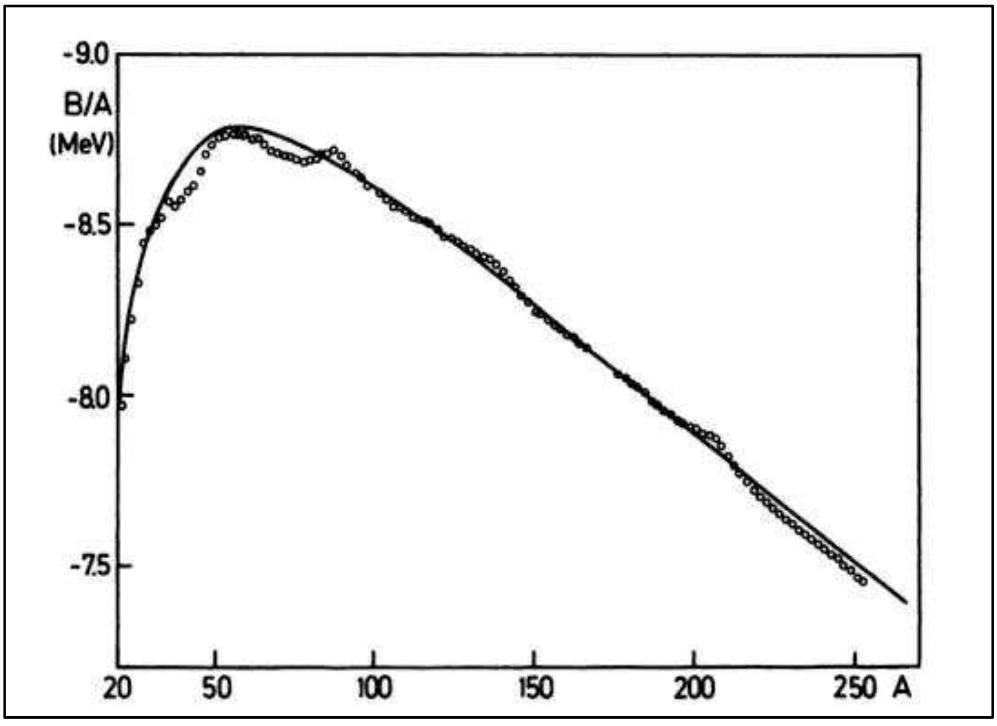

Figure 2.4 Deviation of the experimental values of the binding energy per nucleon from the semi-empirical values. The solid curve represents the semi-empirical binding energy formula, Equation (2.3) and the open circles are the experimental data [37].

However, it is proven in Figure 2.4 that the experimental values deviate from that of semi-empirical formula with large nuclear binding energy at certain number of neutrons and protons. These numbers are called the magic numbers of nuclei.

2.2 Spherical Shell Model

Nuclear shell model is obtained by analogous comparison with atomic shell model. The shell model accounts for many features of energy levels. In the atomic shell model, the shells are filled with electrons in increasing order of energy. Finally, the inert core of filled shells and valence electrons are obtained. The atomic properties are then determined by the valence electrons. This concept is applied on the nucleons in the nucleus. Some measured nuclear properties are remarkably in agreement with the prediction of the model.

The motion of each nucleon is governed by the average attractive force of all other nucleons. The resulting orbits of moving nucleons form shells. By Pauli Exclusion Principle, each nucleon is assigned a unique set of quantum numbers to describe its motion. The nucleons fill the lowest-energy shells as permitted by this principle. If the shells are fully filled, a nucleus would show unusual stability. Magic number represents shell closure occurs at proton and neutron numbers of 2, 8, 20, 28, 50, 82 and 126. These filled shells have total angular momentum $J^{\pi} = 0^{+}$. The next added nucleon, the valence nucleon determines the J^{π} of the new ground state. Thus, the shell model describes the energy required to excite nucleons and how the quantum numbers change.

However, there are some differences between the atom and nucleus. The well-known properties of atoms are the electrons move independently in an average atomic potential. Unlike the electrons, nucleons move in an average potential generated by other nucleons. Regarding large diameter of the nucleons relative to the nucleus itself, how can the nucleons move in well defined orbits without any collisions? The mean free path of a nucleon is very short compared to the length of its orbit. This objection can be encountered by the explanation of the Pauli Exclusion Principle and how the shells are filled. The collisions involve the energy transfer of nucleons to one another. Nucleon that gains energy must excite to the nearby levels but the filled shells cannot accept additional nucleons. To move up to the valence band, more energy is required than the transferred energy during collisions. Therefore, the collisions cannot occur, and the nucleons orbit as if they were transparent to one another.

In developing the shell model, the ordering and energy of the nuclear states can be calculated by solving the three-dimensional Schrodinger equation:

$$\left[-\frac{\hbar^2}{2m}\Delta + V(r)\right]\psi(\vec{r}) = E\psi(\vec{r}). \tag{2.5}$$

Assuming a nucleon moves in a spherical potential with spherical coordinates (r, θ, φ) using the relations

$$\Delta = \frac{\partial^2}{\partial r^2} + \frac{2}{r}\frac{\partial}{\partial r} - \frac{\vec{l}^{\,2}}{r^2}\frac{1}{\hbar^2} \tag{2.6}$$

and $\vec{l}\,(\theta, \varphi)$ is the angular momentum operator such that

$$\vec{l}^{\,2} = -\left[\frac{1}{\sin\theta}\frac{\partial}{\partial\theta}\left(\sin\theta\frac{\partial}{\partial\theta}\right) + \frac{1}{\sin^2\theta}\frac{\partial^2}{\partial\varphi^2}\right]\hbar^2. \tag{2.7}$$

By applying variables separation method, a wave function having radial and angular parts is obtained. The number of radial nodes *n* is the principle

quantum number. The angular part is spherical harmonic $Y_l^m(\theta,\varphi)$ with quantum numbers *l* and *m* corresponding to the angular momentum of the state and the projection of the angular momentum onto an axis. Solutions obtained are similar to the 3-dimensional harmonic oscillator.

Another more realistic potential to describe the forces applied on each nucleon is Wood-Saxon potential:

$$V(r) = -\frac{V_0}{1+exp[(r-R)/a]} \tag{2.8}$$

where potential well depth, $V_0 \approx 50\,\text{MeV}$, nuclear radius, $R = 1.2\,A^{-1/3}\,\text{fm}$, and a representing the surface thickness of the nucleus, $a = 0.5\,\text{fm}$.

The Wood-Saxon potential illustrated in Figure 2.5 is based on the assumption that each nucleon moves in an average interaction with all other nucleons. The force is attractive at increasing distance. When $r \approx R$ within a, the force towards the center is large. If $r - R >> a$, which means $r \to \infty$, the force rapidly approaching zero indicating the nature of short-distance of strong force.

However, if all the nucleons filled the particular states according to Pauli Exclusion Principle, the counted nucleons only agreed for the first three magic numbers. The prediction fails to fit the experimental observation. In 1949, Mayer and Jensen pointed out independently that the average potential felt by individual nucleons must include the spin-orbit term, $\vec{l} \bullet \vec{s}$ [60].

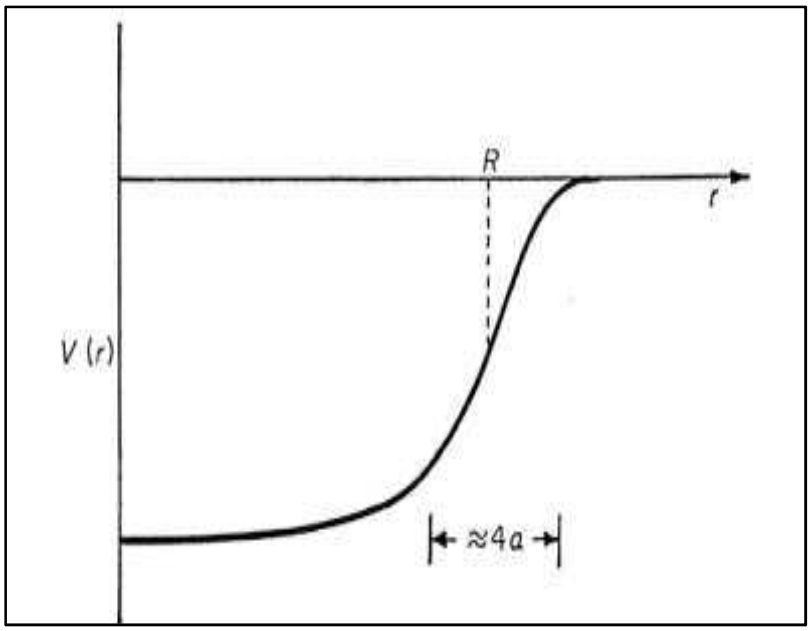

Figure 2.5 The Wood-Saxon potential [61].

The applicable potential is:

$$U(r) = -\frac{1}{2}m(\omega r)^2 + \beta l^2 + a\vec{l} \bullet \vec{s} \ . \tag{2.9}$$

The first term is the harmonic oscillator potential. The correct sequence of "magic numbers" is not reproduced by this potential. Only the first three magic number, 2, 8, and 20 emerging from this scheme. The individual nucleon not only interacts with all other nucleons, but also with itself. A nucleon is orbiting and also rotating. In Figure 2.6, we see that the spin angular momentum parallel to the orbital angular momentum is favored. Each nucleon orbit is split into two components, labeled by the total spin $\vec{j} = \vec{l} + \vec{s}$. All $\vec{j}$ for all nucleons will give the resultant angular momentum ($j - j$ coupling). However, this nuclear spin-orbit coupling is different from the one exists in atoms where total orbital angular momentum of all electrons, $\vec{L}$, combine with total of all spins $\vec{S}$ to form $\vec{J}$.

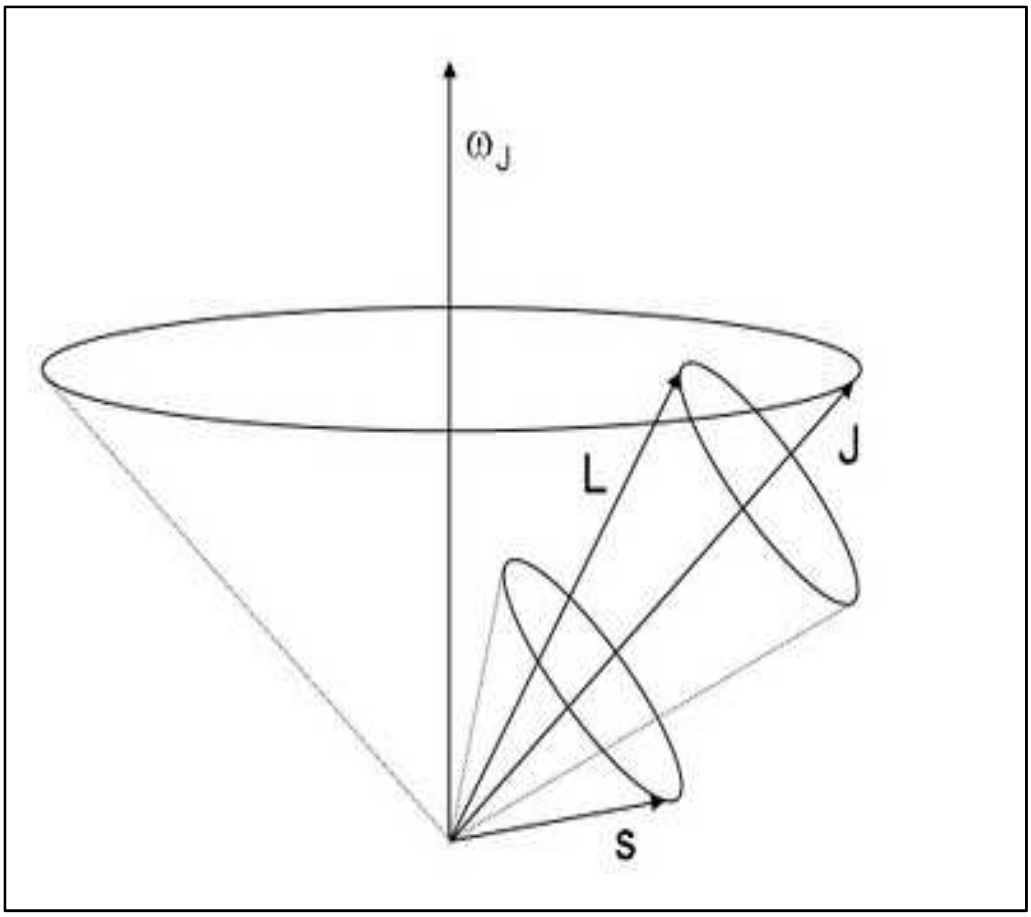

Figure 2.6 The coupling between the spin angular momentum and orbital angular momentum [62].

The introduction of the spin-orbit interaction is able to explain the experimental shell closure at 2, 8, 28, 50, 82, and 126 as pictured in Figure 2.7.

2.3 Nuclear Collective Model

For closed-shells configuration, the nucleus tends to be spherical. The addition of one or more nucleons produces small deformation. The nuclear shell model can explain this situation successfully. However, for the nuclei in the region

(rare-earths and actinides), the departing from the spherical shape cannot be ignored.

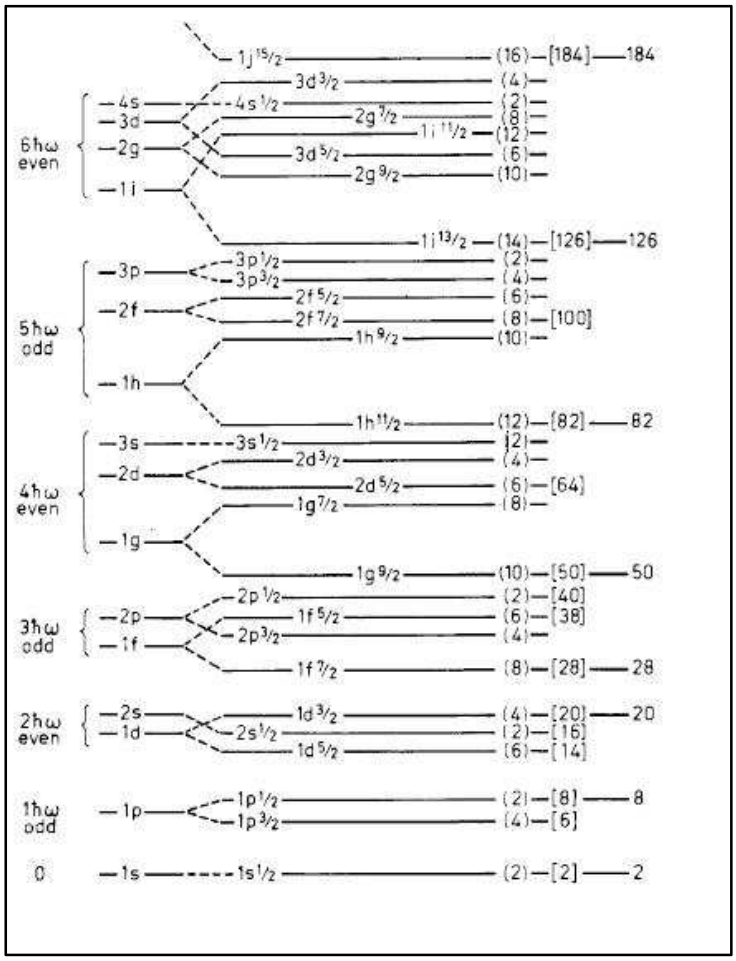

Figure 2.7 The magic number configuration reproduced by spin-orbit interaction [60].

The collective model proposed by Bohr and Mottelson [40], is inspired by the liquid drop model and the Rainwater proposal [63] about the intrinsically deformation of most nuclei away from closed shells with prolate quadrupole shape. The whole nucleus is deformed by single-particle motions and the observed electric quadrupole moment, Q is because of collective orbital distortions.

Analogous to liquid-drop idea, a nucleus consists of filled-shells as inner core and the outer valence nucleons as the surface of the liquid drop. In addition to the motion of individual nucleons, all the nucleons in the nucleus move coherently contributing to the collective excitation modes of the nucleus. A nucleus gains angular momentum either collectively by rotations and vibrations of the nuclear matter or by nucleons excitations. Practically, most nuclear states carrying large angular momentum are a mixture of these two modes.

2.3.1 Vibration

"Phonons" of multipolarity λ is the vibrational quanta that carry energy. The multipolarity λ is used to characterize the multipolarity of the nuclear surface. One can imagine the nuclear vibration as a liquid drop vibrating at high frequency. The nuclear average shape is spherical but the instantaneous shape is not spherical as illustrated in Figure 2.8. The nucleus is assumed to perform harmonic vibrations about the spherical shape [64].

The instantaneous coordinate $R(t)$ of a point on the nuclear surface at (θ, φ) is

$$R(t) = R_{av} + \sum_{\lambda \geq 1} \sum_{\mu=-\lambda}^{\lambda} \alpha_{\lambda\mu}(t) Y_{\lambda\mu}(\theta, \varphi). \tag{2.10}$$

Each spherical harmonic, $Y_{\lambda\mu}(\theta,\varphi)$ will have amplitude $\alpha_{\lambda\mu}(t)$. Due to reflection symmetry,

$$\alpha_{\lambda\mu} = \alpha_{\lambda-\mu}.$$

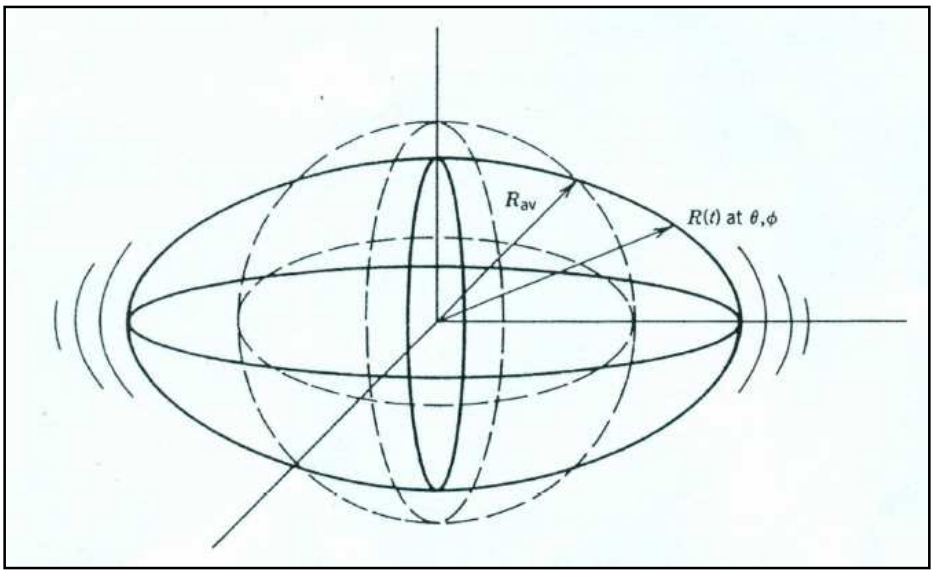

Figure 2.8 A vibrating nucleus with spherical equilibrium shape [57].

The $\lambda = 0$ (monopole) term corresponds to breathing mode of a compressible fluid. The nuclear shape is spherical with average radius $R_{av} = R_0 A^{-1/3}$. The typical dipole $(\lambda = 1)$ mode corresponds to overall translation of center of mass of the fluid. It occurs when the proton and neutron oscillate out of phase against each other. This is a collective isovector $(I = 1)$ mode. It has quantum number $K^{\pi} = 1^{-}$ (the parity of a phonon, π is given by $(-1)^{\lambda}$ in even-even nuclei and occurs at high energy. Low-energy quadrupole $(\lambda = 2)$ vibrations are dominant mode. This mode can have two forms in axially symmetric deformed nucleus. Variation of nuclear modes of vibration is shown in Figure 2.9.

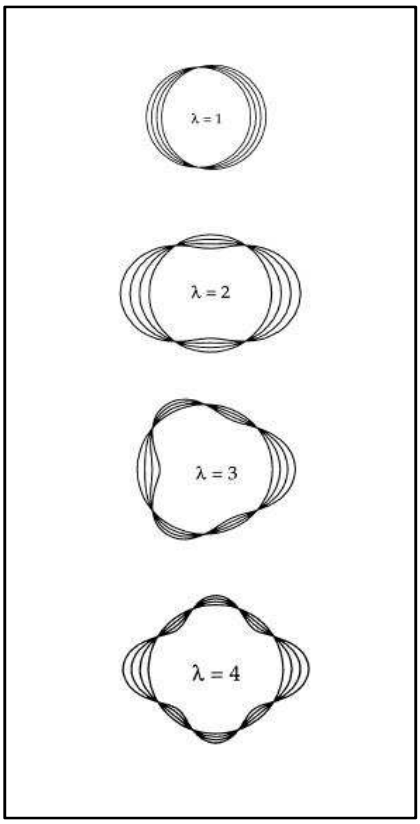

Figure 2.9 Modes of nuclear vibration [65].

The first, $\beta-$vibrations are the elongations along the symmetry axis. The angular momentum vector of such shape oscillations is perpendicular to the symmetry axis. Therefore, such bands are of $K^{\pi}=0^{+}$ states. The second type of vibration is $\gamma-$vibration which is the travelling wave with angular momentum vector points along the symmetry axis. This gives rise to $K^{\pi}=2^{+}$ bands.

2.3.2 Deformation

Assume an incompressible deformed nucleus with constant volume, the nuclear radius can be defined as the distance from the center of the nucleus to the surface at angle (θ,φ) and written as

$$R(\theta,\varphi) = R_{av}\left[1+\sum_{\lambda=2}^{\infty}\sum_{\mu=-\lambda}^{\lambda}\alpha_{\lambda\mu}Y_{\lambda\mu}(\theta,\varphi)\right] \tag{2.11}$$

where $\alpha_{\lambda\mu}$ are the coefficients of the spherical harmonics $Y_{\lambda\mu}(\theta,\varphi)$, the average radius $R_{av} = R_0 A^{-1/3}$ and R_0 is the radius of spherical nucleus having the same volume with the deformed nucleus. The value of λ determines the type of multipole deformations and μ is the projection of λ on the symmetry axis. The $\lambda = 2$ terms represent the quadrupole deformations.

For pure quadrupole deformation,

$$R(\theta,\varphi) = R_{av}\left[1+\alpha_{20}Y_{20}(\theta,\varphi)+\alpha_{22}Y_{22}(\theta,\varphi)+\alpha_{22}Y_{2-2}(\theta,\varphi)\right]. \tag{2.12}$$

Lund convention expressed the coefficients as:

$$\alpha_{20} = \beta_2 \cos\gamma$$

$$\alpha_{22} = \alpha_{2-2} = \beta_2 \sin\gamma$$

with β_2 is the eccentricity and γ is the non-axiality or degree of axiality. Figure 2.10 summarizes the nuclear shapes variation in the (β,γ) plane and how they repeat every $\gamma = 60^\circ$. The plane is divided into six parts by symmetries. In the 3-axis, the nucleus is in the prolate shape with one axis is long, and the other two axes equal, i.e. conventionally $x = y$.

For spheroidal nuclei, the nuclear radius is

$$R(\theta,\varphi) = R_{av}\left[1+\beta_2 Y_{20}(\theta,\varphi)\right]. \tag{2.13}$$

The spheroidal nucleus has axial symmetry, either oblate (two equal semi-major axes) $\gamma = 60^\circ$ or prolate (two equal semi-minor axes) $\gamma = 0^\circ$. This

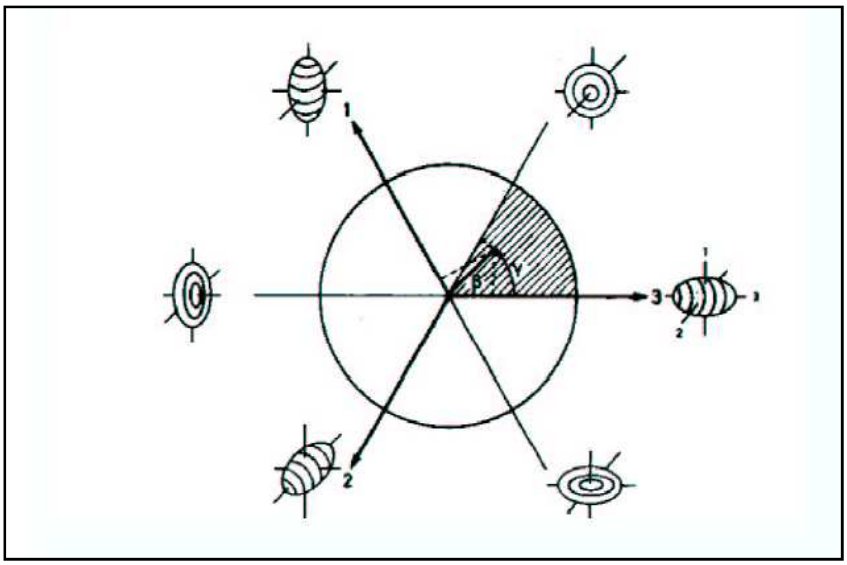

Figure 2.10 Nuclear shapes in the principal axes system as a function of γ for fixed β [37].

nucleus is in ellipsoidal shape that is its cross section is ellipse. One symmetry axis also is retained in this deformation. β_2 is derived using the Lund's definition:

$$\beta_2 = \frac{4}{3}\sqrt{\frac{\pi}{5}}\frac{\Delta R}{R_{av}}. \tag{2.14}$$

ΔR is the difference between the semi-major and semi-minor axes of the ellipsoid. Nuclear shapes variation in relation with eccentricity, β_2 is illustrated in Figure 2.11.

Nuclear charge distribution can be described by the effective shape of the nucleus through a parameter called nuclear electric quadrupole moment, Q .

The value of electric quadrupole moment is related to its deformations by the relation:

$$Q = \frac{4}{5}ZR_0^2\beta_2\left(1+\frac{1}{2}\beta_2+...\right). \tag{2.15}$$

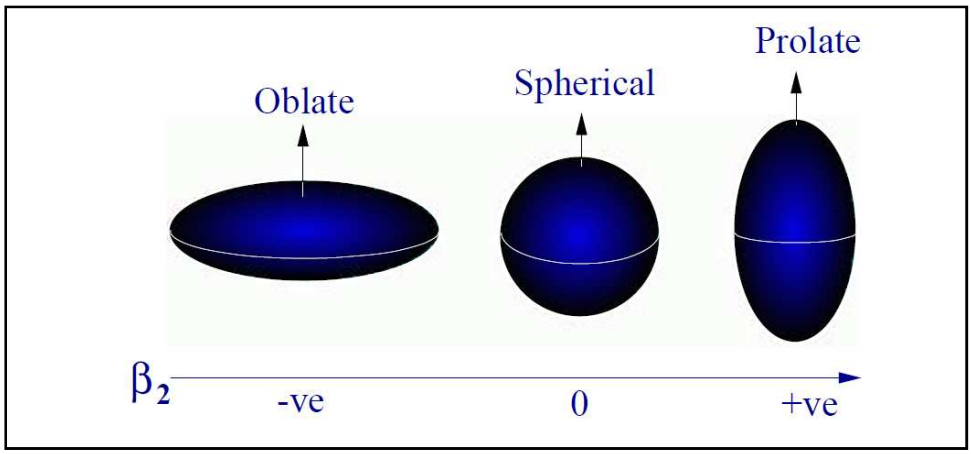

Figure 2.11 Nuclear shapes in relation with eccentricity, β_2 [66].

Nuclear shapes variation in relation with electric quadrupole moment, Q is illustrated in Figure 2.12. The non-zero value of electric quadrupole moment indicates that the charge distribution is not spherically symmetric. The positive value of Q represents the prolate shape of ellipsoid and negative value represents the oblate shape

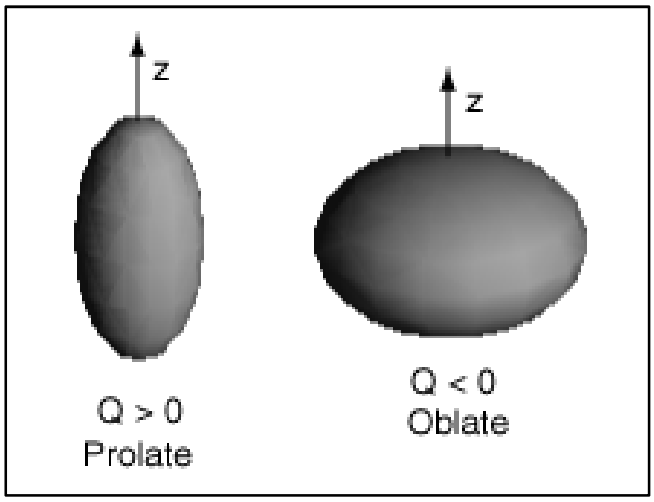

Figure 2.12 Nuclear shapes in relation with electric quadrupole moment, Q [67].

2.3.3 Axially Symmetric Ellipsoid Shape

Rotational motion can only be detected if the nucleus is in nonspherical shape. The rotational of spherical nucleus is always on symmetry axis and the orientation of the axes is indistinguishable quantum mechanically [68]. No collective rotations occur about the symmetry axes. In axial-symmetric deformed nucleus, the rotational symmetry is broken.

Imagine a deformed nucleus in a 3-dimensional (x, y, z) coordinate space with its center of mass is at $(0, 0, 0)$ coordinate. (x, y) plane is the rotational plane of the nucleus which perpendicular to z symmetry axis. By three infinitesimal rotations, the (x, y) plane is transformed into (x', y') plane.

No rotation will be observed if the rotational axes are parallel to z axis. The axially symmetric shape nuclei can only rotate along axes which are perpendicular to symmetry axis. As no rotation about z axis, moment of inertia about the other x' and y' axes are equal i.e. $\Im_{x'} = \Im_{y'} = \Im$ [69]. Only one value of $\Im$ is assigned for the rotational energy spectrum.

From Figure 2.13, the total angular momentum, $\vec{I}$ can be expressed as:

$$\vec{I} = \vec{R} + \vec{J}$$

where $\vec{R}$ is the vector of rotational angular momentum, and $\vec{J}$ is the angular momentum vector of intrinsic motion, and has its component on z axis, K.

Quantum numbers are constants of motion. Angular momentum of intrinsic motion j is not constant along with the rotation, so j cannot be considered as good quantum number for deformed nuclei. For simplicity, the angular

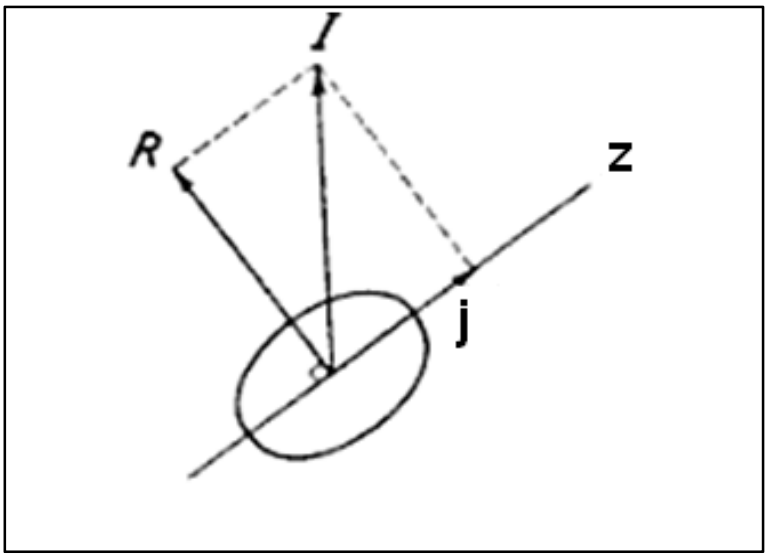

Figure 2.13 Coupling scheme for particle in slowly rotating spheroidal nucleus in 2-D coordinate system [70].

momentum of intrinsic motion is taken to be zero so that $\vec{R}$ is the total angular momentum:

$$\vec{I} = \vec{R}\,.$$

The angular momentum of rotation $\vec{R}$ is a constant of motion and is perpendicular to the symmetry axis z for an axially symmetric nucleus (See Figure 2.14). But, the quantum number K, the component of angular momentum summation of individual valence nucleons, $\Omega = \sum j$ about the symmetry axis has a fixed value for the rotational band [68].

If $\hat{R}_z$ is the operator for the angular momentum along the symmetry axis, then

$$\hat{R}_z \Psi = -i\hbar\left(\frac{\partial \Psi}{\partial \theta}\right) = 0\,. \qquad (2.16)$$

The axial-symmetric shape requires the Hamiltonian must be invariant with

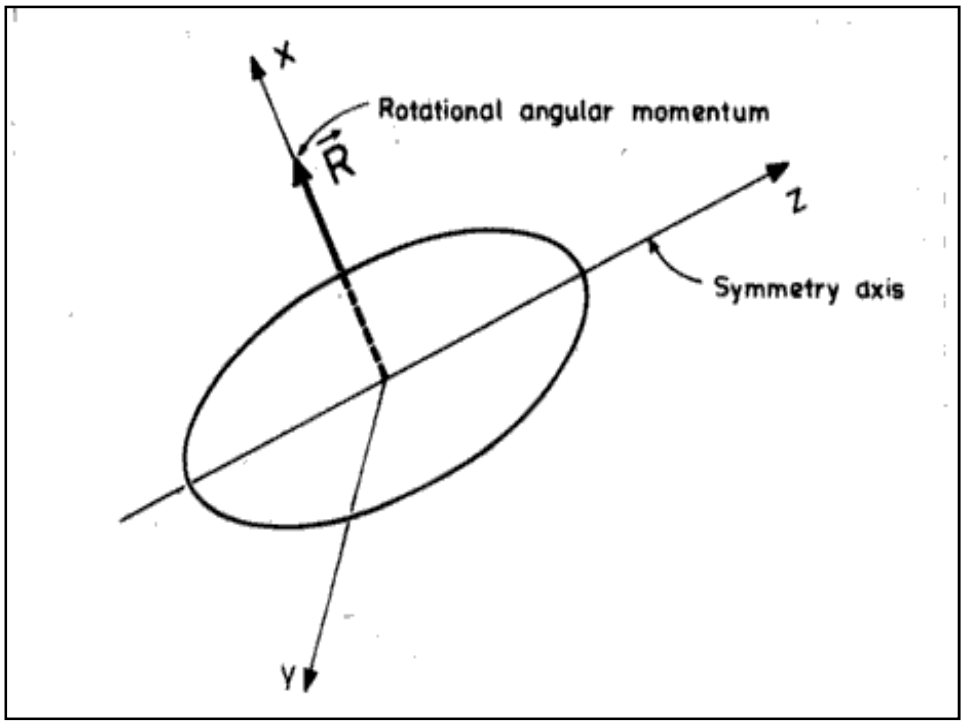

Figure 2.14 The rotational angular momentum R is not along the symmetry axis and the intrinsic angular momentum j is assumed to be zero, for simplicity.

respect to rotations about the symmetry axis, so there is no associated rotational energy about the symmetry axis. Only the phase is changing as the consequence of the rotation about the symmetry axis.

The even parity wave function that fulfill the symmetry relation is nonvanishing if

$$(-1)^I = 1.$$

Therefore the values for angular momentum are $I = 0, 2, 4, 6, \ldots$ or even parity wave function. The linear superposition of the wave will cancel out for odd I [60].

The degree of axial symmetry is zero with prolate shape.

2.3.4 Rotation Matrices

It is appropriate to introduce intrinsic (body-fixed) frame with (x', y', z') coordinates and laboratory (space-fixed) frame with (x, y, z) coordinates. Arbitrary rotation from (x, y, z) coordinates to (x', y', z') coordinates is described by the familiar Euler angle, $\theta = (\theta_1, \theta_2, \theta_3)$.

The following steps are done counterclockwise to arrive at the frame (x', y', z') from the original frame (x, y, z) [65, 71]:

a) The system is rotated through an angle θ_1 $(0 \le \theta_1 \le 2\pi)$ about z axis, thereby changing the position of x and y axes. This yields (x_1, y_1, z).

b) The second rotation is through θ_2 $(0 \le \theta_2 \le 2\pi)$ about the new position of y axis. This yields (x_2, y_1, z_2).

c) Finally, once again, rotation is done through θ_3 $(0 \le \theta_3 \le 2\pi)$ about the newest position of z axis. This yields (x', y', z') where $z' = z_2$.

These three infinitesimal rotations through Euler angles $\theta = (\theta_1, \theta_2, \theta_3) = (\alpha, \beta, \gamma)$ are defined in Figure 2.15.

If we specify the relationship between the representations of state vector, the rotated vector in the frame (x', y', z') is

$$|IK\rangle' = \Re |IK\rangle \tag{2.17}$$

where the rotation operator, $\Re = \exp(-\frac{i}{\hbar}\theta\hat{n} \bullet \vec{I})$. We have to define respective angular momentum operator for every infinitesimal rotation. Separating the

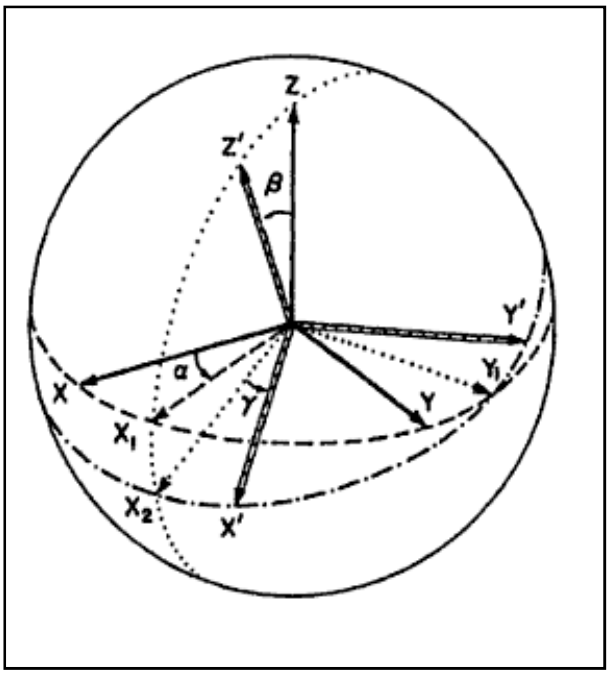

Figure 2.15 Rotation of the coordinate axes from (x, y, z) to (x', y', z') by Euler angles (α, β, γ) in three steps [41].

rotation operator to specify the ordered rotations through Euler angles,

$$\Re = \Re(\theta_3)\Re(\theta_2)\Re(\theta_1) = \exp(-\frac{i}{\hbar}\theta_3 \vec{I}_{z_2}) \exp(-\frac{i}{\hbar}\theta_2 \vec{I}_{y_1}) \exp(-\frac{i}{\hbar}\theta_1 \vec{I}_z) . \tag{2.18}$$

Fortunately,

$$\exp(-\frac{i}{\hbar}\theta_2 \vec{I}_{y_1}) = \exp(-\frac{i}{\hbar}\theta_1 \vec{I}_z) \exp(-\frac{i}{\hbar}\theta_2 \vec{I}_y) \exp(\frac{i}{\hbar}\theta_1 \vec{I}_z) \tag{2.19}$$

and

$$\exp(-\frac{i}{\hbar}\theta_3 \vec{I}_{z_2}) = \exp(-\frac{i}{\hbar}\theta_2 \vec{I}_{y_1}) \exp(-\frac{i}{\hbar}\theta_1 \vec{I}_z)$$

$$\times \exp(-\frac{i}{\hbar}\theta_3 \vec{I}_z) \exp(\frac{i}{\hbar}\theta_1 \vec{I}_z) \exp(\frac{i}{\hbar}\theta_2 \vec{I}_{y_1}) . \tag{2.20}$$

Finally, the full rotation in terms of angular momentum operator

$$\Re(\theta) = \exp(-\frac{i}{\hbar}\theta_1 \vec{I}_z) \exp(-\frac{i}{\hbar}\theta_2 \vec{I}_y) \exp(-\frac{i}{\hbar}\theta_3 \vec{I}_z) . \tag{2.21}$$

Using closure of the set $|IM\rangle$, we have the transformation of $|IK\rangle$ into

$$|IK\rangle' = \Re|IK\rangle = \sum_M |IM\rangle\langle IM|\Re|IK\rangle . \tag{2.22}$$

Figure 2.16 defines the relationship between the quantum numbers M and K .

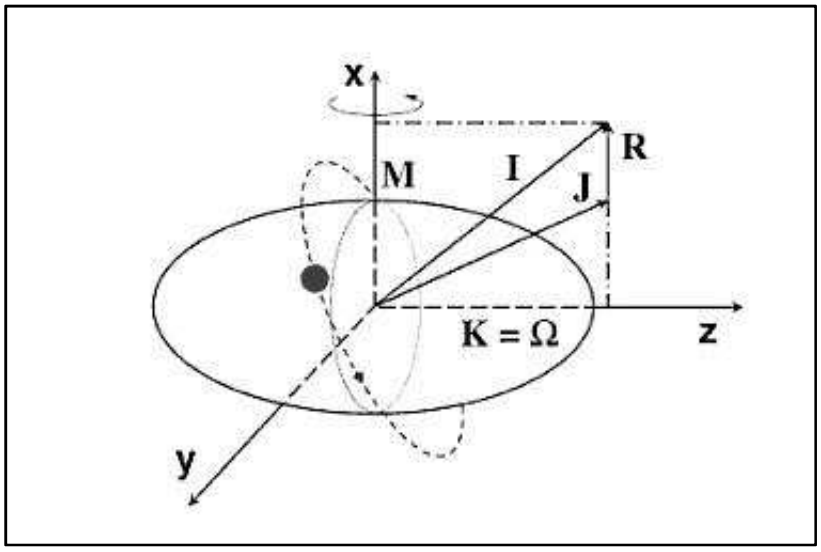

Figure 2.16 Relationship between the total angular momentum, $\vec{I}$, the intrinsic angular momentum, $\vec{J}$, the rotational angular momentum, $\vec{R}$ and the component of $\vec{I}$ along the rotational x axis, M and the symmetry axis in the body-fixed frame, K [72].

Defining the rotation matrices, or the $D-$functions for short as the coefficient of the relation

$$|IK\rangle' = \sum_M |IM\rangle D^I_{MK}(\theta) . \tag{2.23}$$

$$D^I_{MK}(\theta) = \langle IM\ |\Re(\theta)|IK\rangle . \tag{2.24}$$

$$D^I_{MK}(\theta) = \langle IM\,|\exp(-\frac{i}{\hbar}\theta_1\vec{I}_z)\exp(-\frac{i}{\hbar}\theta_2\vec{I}_y)\exp(-\frac{i}{\hbar}\theta_3\vec{I}_z)|IK\rangle . \tag{2.25}$$

Note that in Equation (2.21), the first and last operator is diagonal in the $|IK\rangle$, and $|IM\rangle$ is an eigenfunction of $\vec{I}_z$. The matrix is simplified to

$$D^I_{MK}(\theta) = \exp\left[-\frac{i}{\hbar}(\theta_1 M + \theta_3 K)\right]\langle IM|\exp(-\frac{i}{\hbar}\theta_2 \vec{I}_y)|IK\rangle. \tag{2.26}$$

$$D^I_{MK}(\theta) = \exp\left[-\frac{i}{\hbar}(\theta_1 M + \theta_3 K)\right] d^I_{MK}(\theta_2). \tag{2.27}$$

$d^I_{MK}(\theta_2)$ is the real function of reduced rotation matrix:

$$d^I_{MK}(\theta_2) = \langle IM|\exp(-\frac{i}{\hbar}\theta_2 \vec{I}_y)|IK\rangle. \tag{2.28}$$

$$d^I_{MK}(\theta_2) = \sum_s \frac{(-1)^s[(I+M)!(I-M)!(I+K)!(I-K)!]^{\frac{1}{2}}}{(I-M-s)!(I+K-s)!s!(M-K+s)!}$$

$$\times\left(\cos\frac{\theta_2}{2}\right)^{2I+K-M-2s}\left(-\sin\frac{\theta_2}{2}\right)^{2s+M-K}. \tag{2.29}$$

The summation is over all possible integer value of s for which the factorial arguments are zero or greater.

The conjugate of $D^I_{MK}(\theta)$:

$$|IK\rangle' = \sum_M D^{I*}_{MK}(\theta)|IM\rangle. \tag{2.30}$$

$$D^{I*}_{MK}(\theta) = \exp\left[\frac{i}{\hbar}(\theta_1 M + \theta_3 K)\right] d^I_{MK}(\theta_2). \tag{2.31}$$

The D^I_{MK} matrices are unitary,

$$\sum_M \left(D^I_{MK'}\right)^* D^I_{MK} = \delta_{KK'} \quad \text{and} \quad \sum_K \left(D^I_{M'K}\right)^* D^I_{MK} = \delta_{MM'}.$$

It follows that

$$|IM\rangle = \sum_K D^I_{MK}(\theta)|IK\rangle' \tag{2.32}$$

with the orthogonality relation between the $D-$functions,

$$\sum_{M'}\left(D^{I}_{M'K}\right)^{*} D^{I}_{M'M} = \sum_{M'} D^{I}_{MM'}\left(D^{I}_{KM'}\right)^{*} = \delta_{MK}$$

and

$$\int_0^{2\pi}\int_0^{2\pi}\int_0^{\pi} \sin\theta_2 \, d\theta_2 \, d\theta_1 \, d\theta_3 \left(D^{I}_{MK}\right)^{*} D^{I'}_{M'K'} = \frac{8\pi^2}{2I+1}\delta_{MM'}\delta_{KK'}\delta_{JJ'}.$$

where the δ_{ab} is the Kronecker delta with value unity if $a = b$ and zero otherwise.

2.3.5 Rotational Excitations

If nucleus is deformed, the core and valence nucleons will rotate collectively. The nonspherically symmetric potential is responsive to rotation because the different orientation is distinguishable. The wave functions of the nucleons that move collectively vary slowly with increasing angular momentum. For collective rotation of even-even nuclei, in the symmetric case, only one moment of inertia is defined leading to

$$H_{rot} = \frac{\vec{R}^2}{2\Im} \ . \tag{2.33}$$

Quantum mechanically, $\vec{R} = \sqrt{I(I+1)}\hbar$ for pure collective rotation [57, 68, 73, 74] that the total angular momentum, $\vec{R} = \vec{I}$. Then the spectrum will take a term that is consistent with the energy of rotational state. The rotational excitation band is similar to

$$T_{symmtop} = \frac{\hbar^2}{2\Im} I(I+1) \, . \tag{2.34}$$

In order of increasing excitation, the ground state band consists of

$$E_I = \frac{\hbar^2}{2\Im} I(I+1) \qquad \text{with} \qquad I = 0,\ 2,\ 4,... \tag{2.35}$$

as graphically shown in Figure 2.17. Only even sequence of I is allowed which gives the values:

$$E_{2^+} = 6\vartheta$$

$$E_{4^+} = 20\vartheta$$

$$E_{6^+} = 42\vartheta$$

where $\vartheta = \frac{\hbar^2}{2\Im}$.

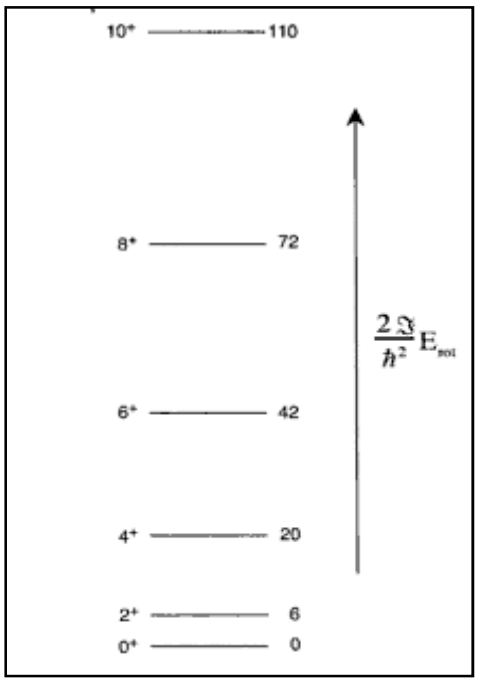

Figure 2.17 Rotational band built upon the ground state of a deformed, even-even nucleus in the rigid rotor approximation.

Thus, as shown in Figure 1.5, for an ideal rotating even-even nucleus in the ground band state, the energy ratio between the excitations of lowest 2^+ and 4^+ states are almost constant at 3.33 such that:

$$E_{4^+} / E_{2^+} = 3.33$$

directly indicates that the ideal rotating even-even nucleus is highly deformed and located at the $150 < A < 190$ and $A < 220$ mass region [39, 75]. This constant ratio is for extreme rigid rotator. It can be used as rigidity indicator of a nucleus. If a nucleus is subjected to centrifugal stretching, this ratio value will take a smaller value.

The ground states of the even-even nuclei have $K^{\pi} = 0^{+}$. The rotational energy law is only valid for small value of I. The deviation from $I(I+1)$ rule is increasing with the increment of spin I. Figure 2.18 shows the abrupt deviation of the $I(I+1)$ rule as the spin I increases where the dotted straight line is the predictions done by A. Bohr [76].

By analyzing Figure 1.3, the region of highly deformed, axially symmetric rotational nuclei and the spherical vibrational nuclei can be specified. The departure from the $I(I+1)$ rule of certain nuclei indicates the transitional regions between the highly deformed, axially symmetric rotational nuclei and the spherical vibrational nuclei that are found slightly outside the region of $150 < A < 190$ and $A < 220$. The value $E_{2^+} = 120\,\text{keV}$ is closer to those of axially symmetric rotators. On the other hand, the value the first 2^+ of level of ^{150}Sm is closer to those of single phonon vibrational energies of spherical nuclei [71].

For a given A, increasing deformation affecting on the moment of inertia by increasing it and lowering the excitation energy. This leads to smaller energy spacing. Nucleus with larger A has the larger value of moment of inertia [75] and smaller values of rotational energy. This is simply related to the

$$\Im = A^{\frac{5}{3}}. \tag{2.36}$$

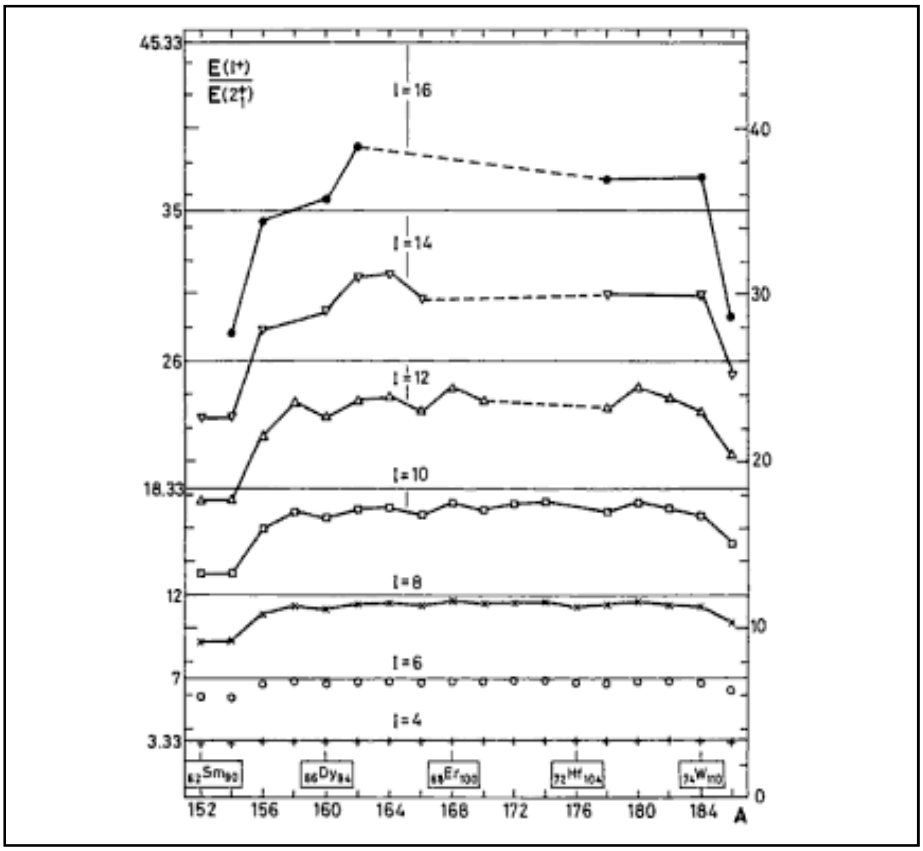

Figure 2.18 Energy ratio in the ground band state in the even-even nuclei in the 152 < A< 186. Data were taken from (Firestone et al. 1996) [76].

2.4 Nuclear Adiabatic Model (Unified Nuclear Model)

Nuclear adiabatic model is formulated by Bohr and Mottelson [41]. The model is formulated as an attempt to unify the concepts of collective model and shell model in the study of rotation-vibration interaction. The model states that the lowest excited state of axially symmetric ellipsoid even-even nuclei is related to rotational states with even angular momentum as a whole. The unified model also states that the strong coupling of nucleonic motions to the rotor and follow the rotational axis motion adiabatically.

The usual condition of adiabaticity is expressed as:

$$\omega_{rot} << \omega_{vib} << \omega_{\text{int}} \tag{2.37}$$

where ω_{rot} is the rotational angular frequency, ω_{vib} the vibrational angular frequency, and ω_{int} the intrinsic angular frequency. This condition implies the separation of rotational motions from the vibrations and single-particle excitations. These three motions are treated independently.

The adiabatic approximation is valid if the rotational motion is sufficiently slow without perturbing the nucleonic motion. Hence, the individual nucleon can continuously readjust its wave function without changing states and obliged to follow the deformations. The nucleus will change its shape in smooth manner without sudden change on the intrinsic motion. Large number of nucleons participates in the deformation [77].

In the unified nuclear model, the nuclear motion is expressed as three independent modes; the intrinsic motion, vibrational motion, and the rotation of the nucleus itself. Consequently, the Hamiltonian can be expressed as:

$$H = H_{int} + H_{rot} + H_{vib} \tag{2.38}$$

where H_{int} is the Hamiltonian for the intrinsic motion, H_{rot} the Hamiltonian for the rotational motion, and H_{vib} the vibrational Hamiltonian. For rigid rotation, the rotational Hamiltonian is

$$H_{rot} = \frac{1}{2\Im}\left(R_{x'}^2 + R_{y'}^2\right) + \frac{1}{2\Im_{z'}} R_{z'}^2 \tag{2.39}$$

where $R_{x'}$, $R_{y'}$ and $R_{z'}$ are the rotational angular momenta corresponding to x', y' and z'axes. Due to axial symmetry, $R_{z'} = 0$ and moment of inertia about the other x' and y' axes are equal i.e. $\Im_{x'} = \Im_{y'} = \Im$.

Using the equality from Figure 2.13:

$$\vec{R} = \vec{I} - \vec{J}$$

where $\vec{R}$ is the rotational angular momentum operator, decomposed into $\vec{I}$, the total angular momentum operator which rotates the whole system and acts only on the rotational wave function, and $\vec{J}$ is the angular momentum operator acting on intrinsic motion.

Now, the total Hamiltonian obtained is

$$H = H_{\text{int}} + T_{rot} + H_{cor} + H_{vib} \tag{2.40}$$

with

$$T_{rot} = \frac{I(I+1)}{2\Im} \tag{2.41}$$

and

$$H_{cor} = -\frac{1}{2\Im}(I_+ J_- + I_- J_+)\,. \tag{2.42}$$

H_{cor} is referred to as the Coriolis coupling which is the coupling of intrinsic and rotational motions. Coriolis interaction alters the projection of angular momentum on the symmetry axis, admixing different values of K. K is only a good quantum number when the potential is axially symmetry. $I_{\pm}$ acts on total angular momentum I, while $J_{\pm}$ acts on intrinsic angular momentum j. $I_+ J_-$ decreases K and $I_- J_+$ increases K. The nucleus is considered a good rotational nucleus when the Coriolis effect is relatively small with small reciprocal of moment of inertia $\frac{1}{2\Im}$, low angular momentum j, and low spin I [78]. This term is neglected by the adiabatic approximation. But at high spin

I , a small axial asymmetry is produced and the adiabatic theory is deviated [75].

2.4.1 Coriolis effect: Two states mixing

Mixing of two states is worth discussing in studying the effect of certain types of mixing on transition rate. The concept of two-state mixing is used in regards to its triviality and simple semi quantitative calculations without losing the sight of the basic physics.

Consider two perturbed states ψ_1 and ψ_2 with approximately same energy, spin and parity that can be written as combinations of pure wave functions

$$\psi_1 = \alpha\phi_1 - \beta\phi_2$$

$$\psi_2 = \beta\phi_1 + \alpha\phi_2$$

α and β are the normalization coefficients that represent the major and minor components of the wave functions such that, $\alpha > \beta$ and $\alpha^2 + \beta^2 = 1$. The two levels repel each other by difference of ε (See Figure 2.19) and change the moment of inertia.

Given the value of the perturbed (experimental) energies, $E^1_{\exp}$ and $E^2_{\exp}$, it is possible to calculate the interaction matrix element $\omega_{rot} j_x$ from the pure energies E^1_{theor} and E^2_{theor} , such that

$$\begin{pmatrix} E^1_{theor} & \omega_{rot} j_x \\ \omega_{rot} j_x & E^2_{theor} \end{pmatrix} \begin{pmatrix} \phi_1 \\ \phi_2 \end{pmatrix} = E^{1,2}_{\exp} \begin{pmatrix} \phi_1 \\ \phi_2 \end{pmatrix}. \qquad (2.43)$$

In general, the mixing depends both on the spacing of the initial unperturbed energies between two states ΔE_{theor} and on the strength of the matrix element

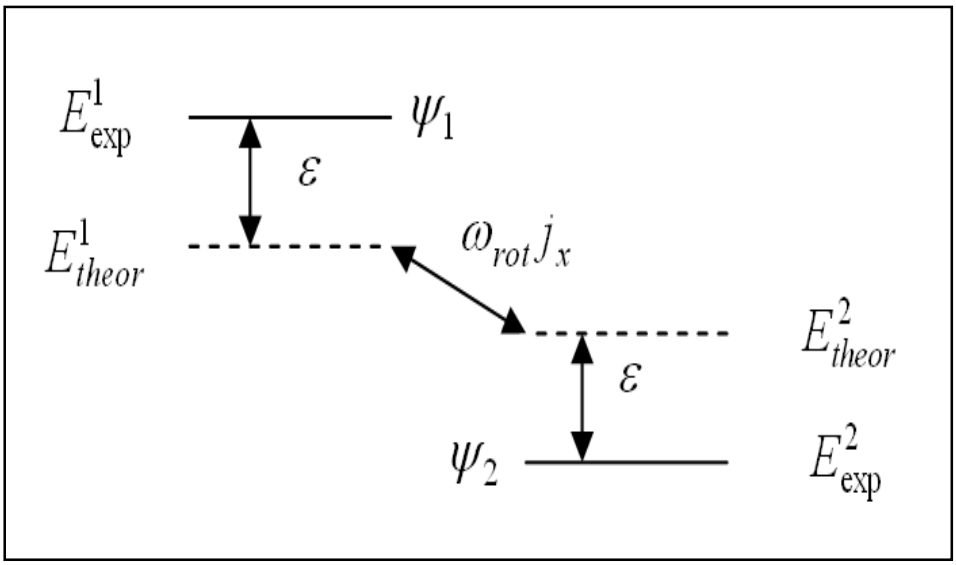

Figure 2.19 Two-level mixing.

j_x [54, 75]. There are two limiting cases to be considered i.e. infinitely strong and relatively weak mixing.

1. Suppose two initial states are degenerate. ($\Delta E_{theor} = 0$). The result is that, for any isolated two-state system, the final separation can never be closer than twice the mixing matrix element.

   But, suppose two levels mix. They can never cross but repel and can never be closer than twice the mixing matrix element after mixing. This behavior acts as an indication of strong mixing.

2. The weak mixing limit corresponds to the large separation of the initial unperturbed energies between two states relative to the mixing matrix element ($\Delta E_{theor} / j_x >> 1$).

The two-state mixing situation can be extended to define the description of two different bands K_1 and K_2 mixing which is more complicated. The band mixing can explain the back bending phenomenon [79].

2.5 Cranking Model

Rotational and vibrational motions are treated macroscopically in collective model. Based on deformation symmetry and adiabaticity, the Coriolis coupling does not appear explicitly, but manifests itself in low angular momentum dependence [41]. In order to determine the collective variables and parameters, microscopic modeling of both collective and single-particle excitations is needed. To bring these two excitations to unity, cranking model is added to deformed shell model. The effect of Coriolis coupling on the Hamiltonian will be taken into account by adding the cranking term to the quasiparticle energies. It is more practical to work in the intrinsic (body-fixed) system than in the laboratory (space-fixed) system. Cranking model is suitable to use as it can be extended to very high-spin states.

Cranking model as proposed by Inglis [80-81] is in semi classical context. The nuclear excited states are characterized by the classical quantity which is the angular momentum rather than the angular frequency. This model assumes that independent nucleons in the ground state of a nucleus move within deformed self-consistent many-particles potential react on external rotational force applied onto them [69]. In short, moment of inertia is derived by rotating the intrinsic wave. Further evaluation of the function can yield the energy increment [74].

The coordinate system which is rigidly fixed to that potential rotates with constant angular frequency ω. The angular frequency ω is conceived to be smaller compared to that of the collective motion. Due to adiabaticity, the intrinsic energies are larger than the rotational energies [73].

Considering a deformed potential well, U that is single-particle, self-consistent, and fixed shape rotating about an axis in space [74, 82]. With respect to rotational axis, spherical coordinate is introduced. At time $t=0$,

$$U(\vec{r};t)=U(r,\theta,\varphi-\omega t;0). \tag{2.44}$$

Nucleus is a dynamic system which depends on deformation variables and time derivative. If the deformed potential well U depends on φ , U is time dependence which means axial asymmetry is produced about rotational axis. As we consider axially-symmetric deformed nuclei in this research, the time dependence of the potential U will be eliminated later.

In laboratory system, we introduce time-dependent Hamiltonian H and a state function ψ describing the motion that satisfies the Schrodinger equation:

$$H\psi=\left(\frac{i\partial}{\partial}\right)\psi \ . \tag{2.45}$$

The nucleus is assumed to rotate slowly about the x axis. This rotational x axis is considerable to be perpendicular to the symmetry axis.

As mentioned before, the time dependence of the deformed potential U needs to be eliminated to maintain axially symmetric condition. To eliminate the time dependence, we can define unitary transformation, $U=exp(-iJ_x\omega t)$ such that

$$\psi=U(t)\varphi \tag{2.46}$$

where φ is the wave function in the latter system.

A transformation around rotational axis with angle, $\varphi=\omega t$ is induced.

Replacing (2.46) into (2.45) yields:

$$H\left(U(t)\varphi\right) = i\partial\left(U(t)\varphi\right)/\partial t$$

$$= i\varphi\frac{\partial\left(U(t)\varphi\right)}{\partial t} + U(t)\frac{\partial\varphi}{\partial t} \tag{2.47}$$

which rearranging the equation leads to:

$$U^{-1}\left\{HU\varphi - i\varphi\frac{\partial U}{\partial t}\right\} = \frac{i\partial\varphi}{\partial t}\ . \tag{2.48}$$

Equation (2.48) may be rewritten as:

$$\tilde{H}\varphi = i\partial\varphi/\partial t \tag{2.49}$$

where $\tilde{H}$ is given by:

$$\tilde{H} = U^{-1}\left\{HU - i\frac{\partial U}{\partial t}\right\}. \tag{2.50}$$

Note that we define unitary transformation for simplicity,

$$U = exp\left(-iJ_x\omega t\right) \tag{2.51}$$

and we can write $\tilde{H}$ as follows:

$$\tilde{H} = exp\left(-iJ_x\omega t\right)\{H\ exp\left(-iJ_x\omega t\right) - i[exp\left(-iJ_x\omega t\right)][-iJ_x\omega t]\}$$

$$= H_0 - \omega J_X\ . \tag{2.52}$$

The so-called general many-body Hamiltonian of the cranking model consists of two parts; the stationary state of the static Hamiltonian in the nuclear system and the cranking term.

The cranking term is treated as perturbation if ω is small enough. If the condition is fulfilled, the calculation of the quantity of the energy and function can be done by means of perturbation theory. We can write:

$$\tilde{H}\varphi = \tilde{E}\varphi \tag{2.53}$$

and the relation between the energy eigenvalues for the two systems with the Coriolis interaction $\vec{\omega}\bullet\vec{J}_X$ is:

$$E = \langle \psi \mid H \mid \psi \rangle \tag{2.54}$$

$$= \tilde{E} + \omega \langle \varphi \mid J_x \mid \varphi \rangle .$$

Inglis [72-73] developed the cranking formula for the moment of inertia:

$$\Im_{inglis} = 2\sum_{ik} \frac{|< i \mid J_x \mid k >|^2}{\varepsilon_i - \varepsilon_k} \tag{2.55}$$

where i and k are single particle bases and J_x is the rotational angular momentum operator. Figure 2.20 shows the plotted moment of inertia in rare earth nuclei.

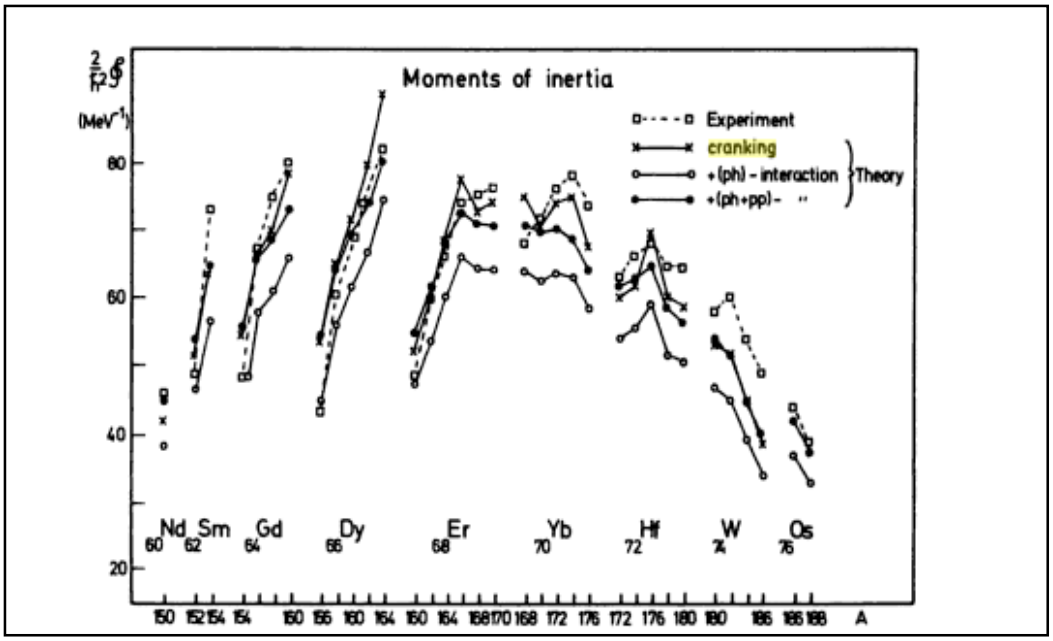

Figure 2.20 Moments of inertia in rare earth nuclei [37].

2.6 Harris Parameterization

From the previous section, Inglis cranking formula [80-81] for the moment of inertia is stated. But the cranking formula is the usual cranking model results from the use of second-order perturbation theory. Harris parameterization [82]

included terms up to fourth order in $H' = -\omega J_X$ by making use of fourth-order perturbation theory:

$$\tilde{\tilde{E}} = E_0 + \sum_m \frac{<0|H'|m><m|H'|0>}{E_0 - E_m}$$

$$+ \sum_{mnp} \frac{<0|H'|m><m|H'|n><n|H'|p><p|H'|0>}{(E_0 - E_m)(E_0 - E_n)(E_0 - E_p)} \qquad (2.56)$$

$$- \sum_{mn} |\frac{<0|H'|n>|^2 <0|H'|m>}{(E_0 - E_n)^2 (E_0 - E_m)^2}|^2 .$$

Here, φ must be calculated to third-order perturbation theory for proper normalization since terms up to fourth order is included in H':

$$\langle \varphi | H' | \varphi \rangle = -2 \sum_m \frac{<0|H'|m><m|H'|0>}{E_0 - E_m}$$

$$- 4 \sum_{mnp} \frac{<0|H'|m><m|H'|n><n|H'|p><p|H'|0>}{(E_0 - E_m)(E_0 - E_n)(E_0 - E_p)} \qquad (2.57)$$

$$+ 4 \sum_{mn} \frac{|<0|H'|n>|^2 <0|H'|m>|^2}{(E_0 - E_n)^2 (E_0 - E_m)^2} .$$

From (2.54), we obtain

$$E = E_0 - \omega^2 \sum_m \frac{<0|J_x|m><m|J_x|0>}{E_0 - E_m}$$

$$- 3\omega^4 \sum_{mnp} \frac{<0|J_x|m><m|J_x|n><n|J_x|p><p|J_x|0>}{(E_0 - E_m)(E_0 - E_n)(E_0 - E_p)} \qquad (2.58)$$

$$+3\omega^4\sum_{mn}\frac{|<0|J_x|n>|^2|<0|J_x|m>|^2}{(E_0-E_n)^2(E_0-E_m)^2}.$$

Basically, the rotational energy is related to rotational frequency ω and all terms containing the rotational frequency cannot be neglected. Expressed in terms of rotational frequency, the expression of the energy of the laboratory system is written in the form

$$E = E_0 + \frac{1}{2}\Im(\omega)\omega^2. \tag{2.59}$$

We finally obtain the moment of inertia dependence on the angular frequency expression:

$$\Im(\omega) = \Im_0 + 3C\omega^2 \tag{2.60}$$

where

$$\Im_0 = 2\sum_m \frac{|<m|J_x|0>|^2}{E_m - E_0} \tag{2.61}$$

which is the expression that completely very similar to the usual cranking formula obtained from the use of second-order perturbation treatment, and

$$C = 2\sum_{mnp}\frac{<0|J_x|m><m|J_x|n><n|J_x|p><p|J_x|0>}{(E_0-E_m)(E_0-E_n)(E_0-E_p)}$$

$$-\Im_0\sum_m\frac{|<0|J_x|m>|^2}{(E_m-E_0)^2}. \tag{2.62}$$

The expectation value for the angular momentum of the intrinsic state φ is

$$\langle\varphi|J_x|\varphi\rangle = \omega\left(\Im_0 + 2C\omega^2\right). \tag{2.63}$$

Since higher-order perturbation theories are used, the rapid convergence of the large correction terms in the perturbation series is often doubted. Self-consistency approach is used to overcome the doubt.

From (2.59), we write the energy in the form

$$E = E_0 + \frac{1}{2}\omega^2 \sum_{p=0}^{\infty} a_p \omega^{2p} \tag{2.64}$$

and from (2.63), the angular momentum is of the form as follows:

$$\langle \varphi \mid J_x \mid \varphi \rangle = \omega \sum_{p=0}^{\infty} b_p \omega^{2p} \,. \tag{2.65}$$

From (2.54),

$$E = \tilde{E} + \omega^2 \sum_{p=0}^{\infty} b_p \omega^{2p} \,. \tag{2.66}$$

Due to classical mechanics correlation,

$$\frac{\partial}{\partial \omega_{rot}} (E(\omega_{rot}) - \omega_{rot} \tilde{I}) = 0$$

where $\tilde{I} = \sqrt{I(I+1)}$.

Expression (2.66) is differentiated to give

$$\frac{\partial E}{\partial \omega} = \frac{\partial \tilde{E}}{\partial \omega} + \sum_p b_p (2p+2) \omega^{2p+1} \,. \tag{2.67}$$

For a stationary solution of

$$\tilde{H}(\omega)\varphi(\omega) = \tilde{E}(\omega)\varphi(\omega)$$

applying a theorem due to Feynmann, one has

$$\frac{\partial \tilde{E}}{\partial \omega} = < \varphi \mid \frac{\partial \tilde{H}}{\partial \omega} \mid \varphi > .$$

In this case,

$$\frac{\partial \tilde{E}}{\partial \omega} = - < \varphi \mid J_x \mid \varphi >$$

$$= -\omega \sum_{p=0}^{\infty} b_p \omega^{2p} \tag{2.68}$$

Combining (2.67) and (2.68), we obtain

$$\frac{\partial E}{\partial \omega} = \sum_p b_p (2p+1) \omega^{2p+1} \ . \tag{2.69}$$

From (2.59), we get

$$\frac{\partial E}{\partial \omega} = \frac{1}{2} \sum_p a_p (2p+2) \omega^{2p+1} . \tag{2.70}$$

By direct comparison, (2.69) and (2.70) are valid if $a_p(p+1) = b_p(2p+1)$ is obeyed for all p . If we write

$$E = E_0 + \frac{1}{2} \omega^2 \left(\Im_0 + 3C\omega^2 + 5D\omega^4 + 7F\omega^6 + \ldots \right) \tag{2.71}$$

and

$$\langle \varphi | J_x | \varphi \rangle = \omega \left(\Im_0 + 2C\omega^2 + 3D\omega^4 + 4F\omega^6 + \ldots \right), \tag{2.72}$$

self-consistency is achieved.

If $D = F = 0$, both equations agree with previous results. In, conclusion, the rotational energy and angular momentum of deformed nuclei are

$$E_{rot} = \frac{1}{2} \omega^2 \left(\Im_0 + 3C\omega^2 + 5D\omega^4 + 7F\omega^6 + \ldots \right) \tag{2.71'}$$

and

$$\sqrt{I(I+1)} = \omega \left(\Im_0 + 2C\omega^2 + 3D\omega^4 + 4F\omega^6 + \ldots \right). \tag{2.72'}$$

CHAPTER 3

THE MODEL

Interesting properties of $^{152,154,156}Sm$ and $^{156,158,160,162,164,166}Dy$ isotopes as deformed nuclei can be studied by applying the phenomenological model [52-53]. The basic states to be considered in this model include the $(K^{\pi}=0_1^+)$ ground state band, $\beta_1(K^{\pi}=0_2^+)-$, $\beta_2(K^{\pi}=0_3^+)-$, $\gamma(K^{\pi}=2^+)-$ vibrational bands and $K^{\pi}=1_{\nu}^+$ collective states (ν is the number of 1^+ collective states).

In order to explain the Coriolis mixing effect on the basis states of a nucleus within the phenomenological model, we shall start the formulation of the model with a stable deformed nucleus with a set of intrinsic axes connected to the rotation of laboratory axes by Euler angles, θ. We begin by introducing the nuclear Hamiltonian containing rotational part $H_{rot}\left(I^2\right)$ and the Coriolis interaction dependence part:

$$H = H_{rot}\left(I^2\right) + H^{\sigma}_{K,K}(I)\ . \tag{3.1}$$

The Coriolis interaction dependence part of the Hamiltonian is

$$H^{\sigma}_{K,K'}(I) = -\omega_K \delta_{K,K'} - \omega_{rot}(I)(j_x)_{K,K'}\chi(I,K)\delta_{K,K'\pm 1}\ . \tag{3.2}$$

In Equation (3.2), $(j_x)_{K,K'}$ is the matrix element describing the Coriolis coupling of rotational bands, $\omega_{rot}(I)$ is the angular frequency of core rotation, yielded from

$$\omega_{rot}(I) = \frac{dE_{rot}(I)}{dI} \tag{3.3}$$

(note that, for convenience, we have removed the factor $\hbar$ from each angular momentum operator throughout this thesis.), and ω_K is the band head energy of respective the K^π bands which is the lowest energy level and

$$\chi(I,0)=1,\ \chi(I,1)=\left[1-\frac{2}{I(I+1)}\right]^{\frac{1}{2}}. \tag{3.4}$$

The Kronecker delta , $\delta_{K,K'}=1$ if $K=K'$ or $\delta_{K,K'}=0$ if otherwise.

It is well established that a nucleus contains strongly interacting Fermi particles that obey the Pauli Exclusion Principle. Fermions must have anti-symmetric wave functions under the interchange of particles. The wave function of the nuclear Hamiltonian

$$\phi^I_{MK}=\sum_{K'}\psi^I_{KK'}\left|IMK\right\rangle$$

$$=\sqrt{\frac{2I+1}{16\pi^2}}\left\{\sqrt{2}\psi^I_{gr,K}D^I_{M,0}+\sum_{K'}\frac{\psi^I_{K',K}}{\sqrt{1+\delta_{K',0}}}\left[D^I_{M,K'}(\theta)b^+_{K'}+(-1)^{I+K}D^I_{M,-K}(\theta)b^+_{-K'}\right]\right\}\left|0\right\rangle$$

. (3.5)

$\psi^I_{K',K}$ are the amplitudes of basis states mixing from the $(4+\nu)$ bands includes the $(K^\pi=0^+_1)$ ground state band, and the single-phonon $b^+_{\lambda=2,K}\left|0\right\rangle=b^+_K\left|0\right\rangle$ with $\beta_1\,(K^\pi=0^+_2)-$, $\beta_2\,(K^\pi=0^+_3)-$, $\gamma\,(K^\pi=2^+)-$ vibrational bands and $K^\pi=1^+_\nu$ collective states (ν is the number of 1^+ collective states). The $1+\delta_{K',0}$ factor in the second term takes into account the difference in the normalization between $K^\pi=0^+_2$, 0^+_3 and $K^\pi=2^+$ bands.

By solving the Schrödinger equation

$$H^\sigma_{K,q}\psi^I_{K',q}=\varepsilon^\sigma_q\psi^I_{K,q} \tag{3.6}$$

one obtains wave function and energy of states with positive parity.

The total energy of states is taken to be

$$E_q^{\sigma}(I) = E_{rot}(I) + \varepsilon_q^{\sigma}(I) \ . \tag{3.7}$$

There are different methods available to determine the energy of rotational core $E_{rot}(I)$. Harris parameterization of the angular momentum and energy [82] is chosen to determine the energy of rotational core $E_{rot}(I)$:

$$E_{rot}(I) = \frac{1}{2}\Im_0\omega_{rot}^2(I) + \frac{3}{4}\Im_1\omega_{rot}^4(I) \tag{3.8}$$

$$\sqrt{I(I+1)} = \Im_0\omega_{rot}(I) + \Im_1\omega_{rot}^3(I) \tag{3.9}$$

where $\Im_0$ and $\Im_1$ are the adjustable inertial parameters of rotational core. A method of defining the even-even deformed nuclei inertial parameters using the experimental data up to $I \le 8\hbar$ for ground band is suggested in [83].

By solving the cubic equation, we obtain the rotational frequency of the core $\omega_{rot}(I)$. The resulting real root is as follows:

$$\omega_{rot}(I) = \left\{\frac{\tilde{I}}{2\Im_1} + \left(\left(\frac{\tilde{I}}{2\Im_1}\right)^2 + \left(\frac{\Im_0}{3\Im_1}\right)^3\right)^{\frac{1}{2}}\right\}^{\frac{1}{3}} + \left\{\frac{\tilde{I}}{2\Im_1} - \left(\left(\frac{\tilde{I}}{2\Im_1}\right)^2 + \left(\frac{\Im_0}{3\Im_1}\right)^3\right)^{\frac{1}{2}}\right\}^{\frac{1}{3}} \tag{3.10}$$

where $\tilde{I} = \sqrt{I(I+1)}$. Equation (3.10) gives value of $\omega_{rot}(I)$ at the given spin *I*.

3.1 Determination of $\omega_{rot}(I)$

In the cranking model, $\omega_{rot}(I)$ is the rotational angular frequency which is determined by imposing that the $J_x = \tilde{I} = \sqrt{I(I+1)}$

The inter-dependency of I and ω_{rot}^2 is introduced by Harris [82]:

$$E_{rot}(I) = \frac{1}{2}\Im_0\omega_{rot}^2(I) + \frac{3}{4}\Im_1\omega_{rot}^4(I) \tag{3.11}$$

$$\sqrt{I(I+1)} = \Im_0\omega_{rot}(I) + \Im_1\omega_{rot}^3(I). \tag{3.12}$$

Rearranging the expression:

$$\Im_0\omega_{rot}(I) + \Im_1\omega_{rot}^3(I) = \tilde{I}$$

$$\Im_0\omega_{rot}(I) + \Im_1\omega_{rot}^3(I) - \tilde{I} = 0$$

$$\omega_{rot}^3(I) + \frac{\Im_0}{\Im_1}\omega_{rot}(I) - \frac{\tilde{I}}{\Im_1} = 0.$$

By supposing $\Im_0/\Im_1 = q$, $-\tilde{I}/\Im_1 = r$ and setting $\omega_{rot}(I) = \omega$ to construct a simple new cubic equation which is

$$\omega^3 + q\omega + r = 0. \tag{3.13}$$

It is appropriate to replace $\omega = \nu + z$ into the simple cubic equation which gives

$$\nu^3 + 3\nu^2 z + 3\nu z^2 + z^3 + q\nu + qz + r = 0. \tag{3.14}$$

It is clear that Equation (3.14) is separable into two parts which if added together will equal to zero.

$$3\nu^2 z + 3\nu z^2 + q\nu + qz = 0 \tag{3.14a}$$

and

$$\nu^3 + z^3 + r = 0. \tag{3.14b}$$

By factorization of (3.14a),

$$(3\nu z + q)(\nu + z) = 0.$$

We note that either $3\nu z + q$ or $\nu + z$ might equal to zero. But obviously we can say that $\nu + z \neq 0$ because $\omega = \nu + z$ cannot be zero.

Here, we have two coupled equations: (3.14b) and

$$3v\,z + q = 0. \tag{3.13c}$$

Then, we have from (3.14c)

$$v\,z = -\frac{q}{3}$$

and later becomes

$$v^3 z^3 = -q^3/27. \tag{3.15}$$

Straightforwardly, we find from (3.14b)

$$v^3 + z^3 = -r. \tag{3.16}$$

The use of sum and product rules is a very convenient way to reduce the cubic equations to much simpler form of quadratic equation:

$$x^2 - \left(v^3 + z^3\right)x + v^3 z^3 = 0 \tag{3.17}$$

$$x^2 - \left(-r\right)x + \left(-q^3/27\right) = 0 \tag{3.17a}$$

such that $x = v^3$ or $x = z^3$.

From the general solution of quadratic equation, the solutions are

$$x = \frac{-r \pm \sqrt{r^2 - \left(4q^3/27\right)}}{2}$$

$$x = -r/2 \pm \sqrt{\left(\frac{1}{2}r\right)^2 + \left(\frac{1}{3}q\right)^3} \tag{3.18}$$

$$v = \left\{-\frac{r}{2} + \left(\left(\frac{1}{2}r\right)^2 + \left(\frac{1}{3}q\right)^3\right)^{\frac{1}{2}}\right\}^{\frac{1}{3}} \tag{3.19}$$

$$z=\left\{-\frac{r}{2}-\left(\left(\frac{1}{2}r\right)^{2}+\left(\frac{1}{3}q\right)^{3}\right)^{\frac{1}{2}}\right\}^{\frac{1}{3}} \tag{3.20}$$

Recall that $\omega=\nu+z$ and $\omega=\omega_{rot}(I)$ which yield

$$\omega_{rot}(I)=\left\{-\frac{r}{2}+\left(\left(\frac{1}{2}r\right)^{2}+\left(\frac{1}{3}q^{3}\right)^{\frac{1}{2}}\right)\right\}^{\frac{1}{3}}+\left\{-\frac{r}{2}-\left(\left(\frac{1}{2}r\right)^{2}+\left(\frac{1}{3}q^{3}\right)^{\frac{1}{2}}\right)\right\}^{\frac{1}{3}}. \tag{3.21}$$

Finally, we replace $q=\Im_0/\Im_1$, $r=-\tilde{I}/\Im_1$ in above expression, the rotational frequency of the core $\omega_{rot}(I)$ is now given by

$$\omega_{rot}(I)=\left\{\frac{\tilde{I}}{2\Im_1}+\left(\left(\frac{\tilde{I}}{2\Im_1}\right)^{2}+\left(\frac{\Im_0}{3\Im_1}\right)^{3}\right)^{\frac{1}{2}}\right\}^{\frac{1}{3}}+\left\{\frac{\tilde{I}}{2\Im_1}-\left(\left(\frac{\tilde{I}}{2\Im_1}\right)^{2}+\left(\frac{\Im_0}{3\Im_1}\right)^{3}\right)^{\frac{1}{2}}\right\}^{\frac{1}{3}}. \tag{3.22}$$

3.2 Determination of $\Im_0$ and $\Im_1$

The ground states of the even-even nuclei have $K^{\pi}=0^{+}$. The necessary condition for the rotational energy law to be valid is small value of I. The deviation from $I(I+1)$ rule is increasing with the increment of spin I.

Rotational angular frequency for the nucleus is:

$$\omega_{eff}(I)=\frac{E^{exp}(I+1)-E^{exp}(I-1)}{2} \tag{3.23}$$

where $E^{\exp}(I)$ is the energy from experiment [6-15].

Effective moment of inertia $\Im_{eff}(I)$ is written in terms of nuclear rotational angular frequency $\omega_{eff}(I)$:

$$\Im_{eff}(I) = \frac{\sqrt{I(I+1)}}{\omega_{eff}(I)} \ . \tag{3.24}$$

Evaluating the above expression, one obtains the effective moment of inertia for states $\Im_{eff}(I)$.

If we plot $\Im_{eff}(I)$ as a function of $\omega_{eff}^2(I)$ at low spin $I \leq 8\hbar$, the relation is verified to be mainly linear. This relation of the parameters is rephrased by using Harris two-parameter formula:

$$\Im_{eff}(I) = \Im_0 + \Im_1 \omega_{eff}^2(I). \tag{3.25}$$

Equation (3.25) defines the inertia parameters $\Im_0$ and $\Im_1$ for the effective moment of inertia $\Im_{eff}(I)$ when $I \leq 8\hbar$. The effective moment of inertia depends on the degree of rotation. The least square method is used in the equation to determine the numerical values of the parameters $\Im_0$ and $\Im_1$.

The inertial parameters, $\Im_0$ and $\Im_1$ have their interesting physical meanings. The parameter $\Im_0$ is the moment of inertia of the ground states band and the parameter $\Im_1$ represents the rigidity of the nucleus that leads to the centrifugal stretching effect [83-84].

3.3 Determination of $(j_x)_{K,K'}$

The lowest energies for ground-state and $\beta_n -$ bands were taken from experimental energies, since they are not affected by the Coriolis forces at spin $I = 0$:

$$\omega_{gr} = E_{gr}^{\exp t}(0) \text{ and } \omega_{\beta_n} = E_{\beta_n}^{\exp t}(0).$$

The band head energies for the collective 1^+ states in $^{152,154,156}Sm$ and $^{156,158,164,166}Dy$ nuclei are assumed to be $\omega_1 = 3\,\text{MeV}$ because the $K^\pi = 1^+$ bands have not been observed experimentally for these nuclei respectively [53]. Coriolis rotational states mixing matrix elements $(j_x)_{K,K'}$ and $\gamma-$ band head energies ω_γ are determined by using the least square fitting method of the diagonalize matrix

$$\begin{pmatrix} \omega_K - \varepsilon & \omega_{rot} j_x \\ \omega_{rot} j_x & \omega_{1^+} - \varepsilon \end{pmatrix} \begin{pmatrix} \phi_1 \\ \phi_2 \end{pmatrix} = \omega_K \begin{pmatrix} \phi_1 \\ \phi_2 \end{pmatrix}.$$

Currently, the experimental energy spectrum for the $0^+_{\beta_2}$ band in the ^{156}Sm and ^{166}Dy nuclei are not available. No calculations are done for this band in respective nuclei.

CHAPTER 4

RESULTS AND DISCUSSIONS

The values of the inertial parameters, $\Im_0$ and $\Im_1$ are obtained from Equation (3.25). $\Im_{eff}(I)$ is plotted as a function of $\omega_{eff}^2(I)$ at low spin, $I \leq 8\hbar$. The linear dependency of effective moment of inertia $\Im_{eff}(I)$ on the square of angular frequency $\omega_{eff}^2(I)$ is invalidating at higher spin. Figures 4.1-4.3 illustrate the linear dependency of $\Im_{eff}(I)$ on $\omega_{eff}^2(I)$ at low spin, $I \leq 8\hbar$ for isotopes $^{152,154,156}Sm$. Figures 4.7-4.12 show the same behavior of the relation for isotopes $^{156,158,160,162,164,166}Dy$. By using Equations (3.23) – (3.25) and utilizing least square method, $\Im_0$ and $\Im_1$ are deduced from the fitted straight lines. The values of the inertial parameters, $\Im_0$ and $\Im_1$ obtained are tabulated in Table 4.1 for isotopes $^{152,154,156}Sm$ and Table 4.6 for isotopes $^{156,158,160,162,164,166}Dy$.

From Tables 4.1 and 4.6, within same number of protons, for constant total angular momentum i.e. for ground band state, the moment of inertia increases gradually with nuclear size. This case is subjected to conservation law. To conserve the total angular momentum while the nuclear size increases, the nuclear moment of inertia must increase and the rotation of the nucleus must slow down. The centrifugal stretching will come into play by decreasing the nucleons pairing correlation and the nucleus fails to preserve its spherical shape. Thus, larger nucleus lacks more in rigidity and is more deformed. The smallest values of $\Im_1$ occur when the deformed prolate minimum in the potential energy surface.

It is generally known that the effective moment of inertia of the ground-state band is smaller compared to that of β_n $(0^+_{\beta_1}, 0^+_{\beta_2})-$ and $\gamma-$ bands, $(\Im_{gr} < \Im_{\beta_n}, \Im_{\gamma})$. This arises because the Coriolis mixing of these bands with $K^\pi = 1^+_\nu$ rotational bands is more intense than the mixing of ground band state with $K^\pi = 1^+_\nu$ bands. The effect of $K^\pi = 1^+_\nu$ bands on low-lying levels is interesting to study. The intensity of mixing can be analyzed from the values of Coriolis interaction matrix elements, $(j_x)_{K,K'}$ and band head energy, ω_K.

Wave function of states ϕ^I_{MK} represents the mixture components of other bands in certain band. Tables 4.3-4.5 give the calculated wave function of states ϕ^I_{MK} for $^{152,154,156}Sm$ and Tables 4.8-4.13 give the calculated wave function of states ϕ^I_{MK} for $^{156,158,160,162,164,166}Dy$. The wave function of states ϕ^I_{MK} is obtained by solving the nuclear Hamiltonian in the form of Equation (3.2) by using the wave function of Equation (3.5). Structure of $^{152,154,156}Sm$ and $^{156,158,160,162,164,166}Dy$ can be understood by these calculated values.

The results are presented as simple two-state mixing form because of triviality. The most important thing to understand are the relationships between the pure band head energies spacings $\Delta\omega_{K,K'}$ and the value of Coriolis mixing matrix elements $(j_x)_{K,1}$, on one hand, the perturbed energy separations and the admixed wave functions on the other hand. In general, the mixing depends both on the proximity of the band head energy ω_K between two bands and on the matrix element $(j_x)_{K,1}$ [54, 75].

The actual nuclear states are complex admixtures of many components. The strong mixing of respective intrinsic excitation states will lead to the nonadiabaticity of electromagnetic transition from $0^+_{\beta_1}$, $0^+_{\beta_2}$ and γ state bands [50-52]. This is an attempt to present accurate treatment to show the realistic calculation of nuclear spectra. Rotational motion can be superimposed on the vibrational motions. The rotational and intrinsic motions are strongly coupled due to Coriolis forces. The non-adiabatic effects become more important as the rotational frequency increases. The adiabatic assumption is applied on the wave function of Equation (3.5) to separate the rotational and intrinsic motions.

4.1 Samarium isotopes $^{152,154,156}Sm$

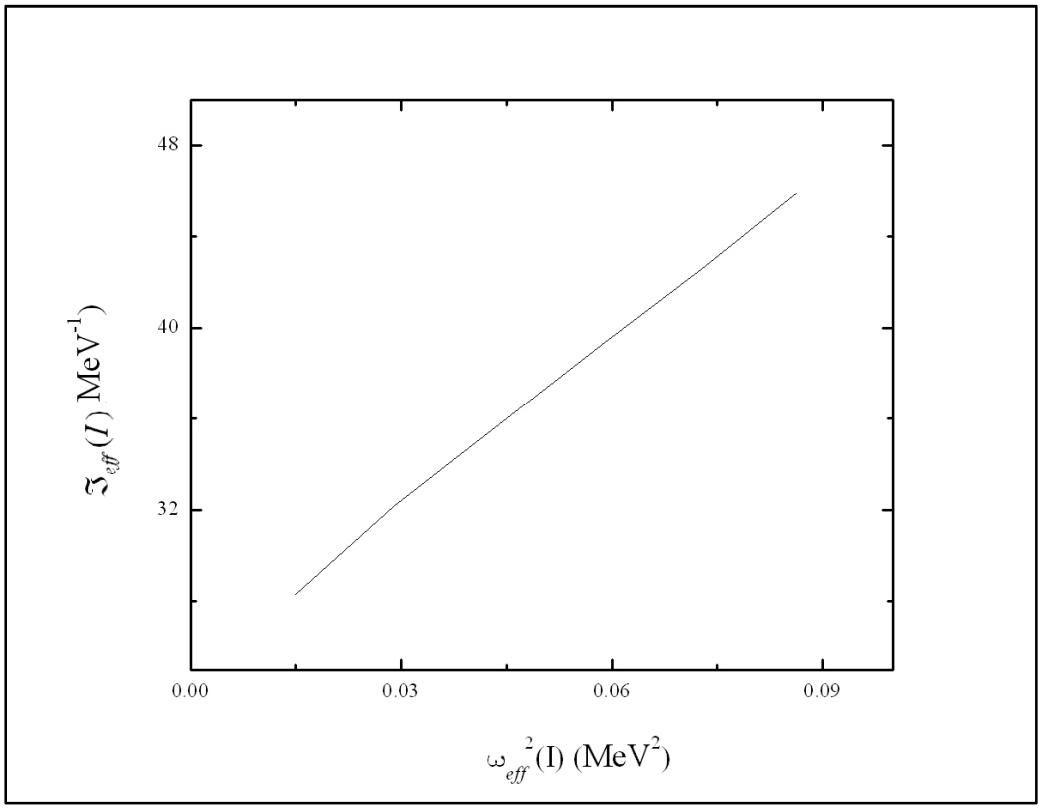

Figure 4.1 The linear dependencies of $\Im_{eff}(I)$ on $\omega_{eff}^2(I)$ for ^{152}Sm .

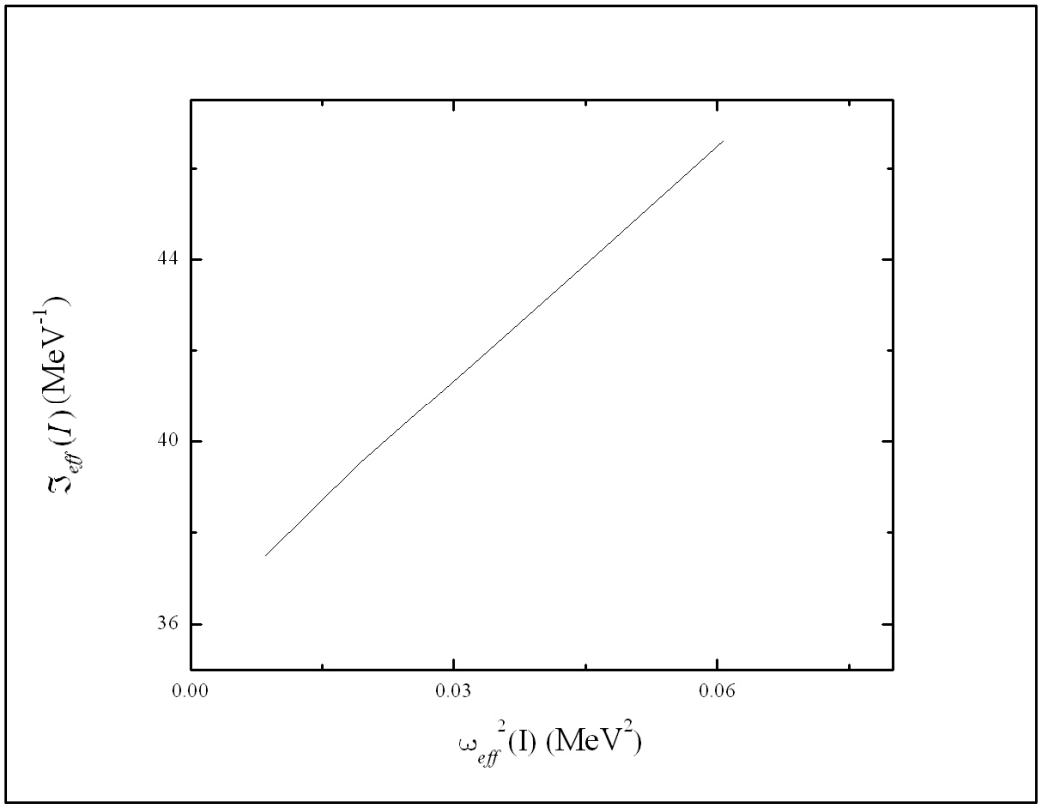

Figure 4.2 The linear dependencies of $\Im_{eff}(I)$ on $\omega_{eff}^2(I)$ for ^{154}Sm .

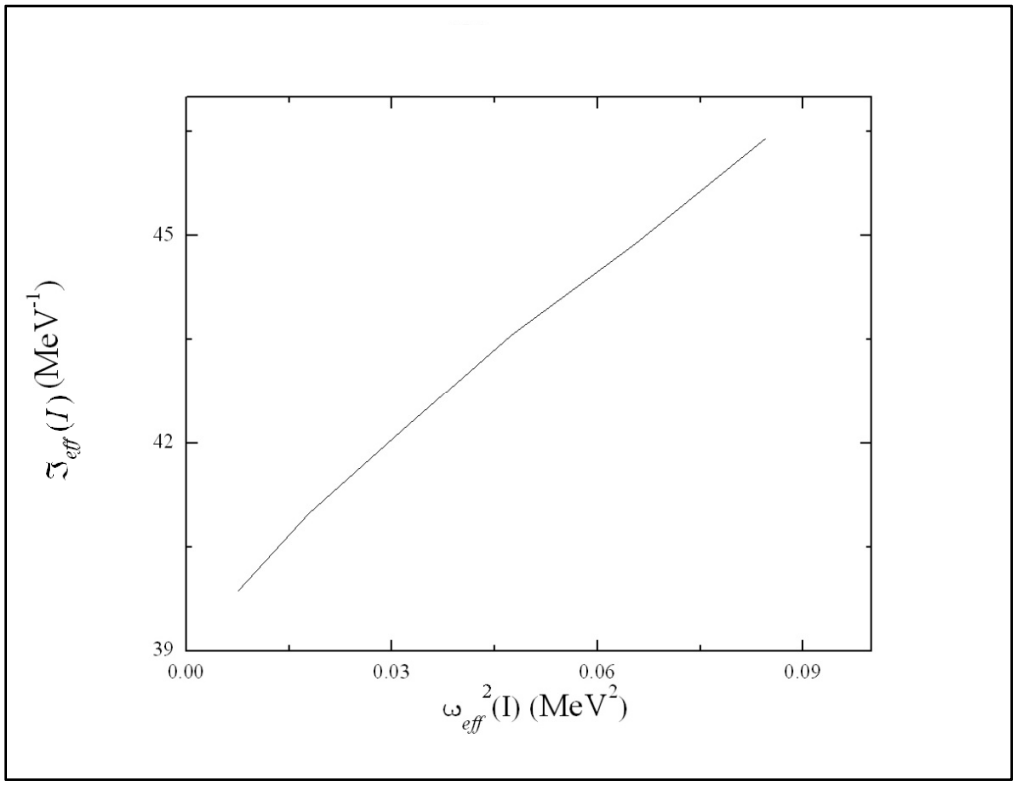

Figure 4.3 The linear dependencies of $\Im_{eff}(I)$ on $\omega_{eff}^{2}(I)$ for ^{156}Sm .

Table 4.1 Inertial parameters of rotational core used in the calculations.

Nucleus	$\Im_0$ (MeV^{-1})	$\Im_1$ (MeV^{-3})
^{152}Sm	24.74	256.57
^{154}Sm	36.07	178.88
^{156}Sm	39.22	98.36

Table 4.2 Parameters used in the calculations. Band head energies in MeV [6].

Nucleus	ω_{β_1}	ω_{β_2}	ω_1	ω_γ	$(j_x)_{gr,1}$	$(j_x)_{\beta_1,1}$	$(j_x)_{\beta_2,1}$	$(j_x)_{\gamma,1}$
^{152}Sm	0.685	1.083	3.0	1.0	0.742	0.821	0.864	0.855
^{154}Sm	1.099	1.203	3.0	1.380	0.345	0.403	0.408	0.417
^{156}Sm	1.068	-	3.0	1.365	0.749	0.872	-	0.903

Table 4.3 Structure of ^{152}Sm states.

I	gr	$0^+_{\beta_1}$	$0^+_{\beta_2}$	1^+	γ	gr	$0^+_{\beta_1}$	$0^+_{\beta_2}$	1^+	γ
	Ground-state band					$0^+_{\beta_1}$				
2	-0.9997	-0.0025	-0.0016	-0.0227	-0.0014	0.0032	-0.9994	-0.0064	-0.0326	-0.0065
4	-0.9993	-0.0065	-0.0043	-0.037	-0.0044	0.0086	-0.9982	-0.0169	-0.0536	-0.0199
6	-0.9987	-0.0109	-0.0073	-0.0483	-0.0076	0.0148	-0.9964	-0.0283	-0.0704	-0.0343
8	-0.9981	-0.0153	-0.0103	-0.0576	-0.0108	0.0211	-0.9942	-0.0397	-0.0845	-0.0485
10	-0.9975	-0.0197	-0.0132	-0.0657	-0.014	0.0275	-0.9917	-0.0508	-0.0968	-0.0621
12	-0.9968	-0.0239	-0.016	-0.0729	-0.017	0.0338	-0.9888	-0.0615	-0.1078	-0.0752
	γ					$0^+_{\beta_2}$				
2	0.0022	0.0078	-0.0302	-0.0326	-0.9990	-0.0025	-0.0075	0.9987	0.0395	-0.0316
3	-	-	-	0.0473	0.9989	-	-	-	-	-
4	-0.0069	-0.0248	0.0888	0.0630	0.9937	-0.006	-0.0182	0.9938	0.0585	-0.093
5	-	-	-	0.0698	0.9976	-	-	-	-	-
6	-0.0122	-0.0442	0.1452	0.0853	0.9846	-0.009	-0.0277	0.9855	0.0686	-0.1526
7	-	-	-	0.0866	0.9962	-	-	-	-	-
8	0.0175	0.0643	-0.1942	-0.1028	-0.9733	0.0115	0.0355	-0.9753	-0.0736	0.2049
9	-	-	-	0.1000	0.9950	-	-	-	-	-
10	-0.0226	-0.0843	0.2352	0.1168	0.9610	-0.0134	-0.0416	0.9645	0.0759	-0.2492
11	-	-	-	0.1112	0.9938	-	-	-	-	-
12	-0.0274	-0.1038	0.2691	0.1282	0.9485	-0.0149	-0.0464	0.9538	0.0766	-0.2865

Table 4.4 Structure of ^{154}Sm states.

I	gr	$0^+_{\beta_1}$	$0^+_{\beta_2}$	1^+	γ	gr	$0^+_{\beta_1}$	$0^+_{\beta_2}$	1^+	γ
	Ground-state band					$0^+_{\beta_1}$				
2	1.0	0.0002	0.0002	0.0076	0.0001	0.0003	-0.9999	-0.0037	-0.0142	-0.0011
4	-0.9999	-0.0006	-0.0005	-0.0134	-0.0004	0.0009	-0.9996	-0.0114	-0.0250	-0.0041
6	0.9998	0.0011	0.0010	0.0184	0.0009	0.0017	-0.9991	-0.0215	-0.0347	-0.0080
8	0.9997	0.0016	0.0015	0.0228	0.0013	-0.0027	0.9984	0.0329	0.0435	0.0124
10	0.9996	0.0022	0.0021	0.0266	0.0018	-0.0037	0.9975	0.0449	0.0515	0.0172
12	0.9995	0.0029	0.0026	0.0301	0.0023	-0.0048	0.9964	0.0571	0.0589	0.0221
	$0^+_{\beta_2}$					γ				
2	0.0003	0.0039	-0.9999	-0.0151	-0.0019	-0.0002	-0.0013	-0.0021	0.0139	0.9999
3	-	-	-	-	-	-	-	-	0.0216	0.9998
4	-0.0009	-0.0121	0.9996	0.0262	0.0067	-0.0008	-0.0047	-0.0075	0.0280	0.9996
5	-	-	-	-	-	-	-	-	0.0344	0.9994
6	-0.0016	-0.0228	0.9990	0.0358	0.0129	-0.0016	-0.009	-0.0145	0.0390	0.9991
7	-	-	-	-	-	-	-	-	0.0451	0.9990
8	0.0025	0.035	-0.9982	-0.0439	-0.0197	-0.0024	-0.0138	-0.0223	0.0480	0.9985
9	-	-	-	-	-	-	-	-	0.0543	0.9985
10	0.0034	0.048	-0.9972	-0.0508	-0.0265	-0.0032	-0.0187	-0.0303	0.0554	0.9978
11	-	-	-	-	-	-	-	-	0.0623	0.9981
12	0.0042	0.0612	-0.9959	-0.0568	-0.0333	-0.0040	-0.0236	-0.0383	0.0617	0.9971

Table 4.5 Structure of ^{156}Sm states.

I	gr	$0^+_{\beta_1}$	1^+	γ	gr	$0^+_{\beta_1}$	1^+	γ
	Ground-state band				$0^+_{\beta_1}$			
2	0.9999	0.0008	0.0155	0.0005	-0.0012	0.9996	0.0280	0.0043
4	0.9996	0.0025	0.0277	0.0019	-0.0039	0.9986	0.0503	0.0158
6	0.9992	0.005	0.0392	0.0039	-0.0079	0.9969	0.0715	0.032
8	0.9987	0.008	0.0499	0.0064	-0.0128	0.9944	0.0914	0.0513
10	0.9981	0.0113	0.0598	0.0091	0.0185	0.9911	0.1100	0.0723
12	0.9974	0.015	0.0689	0.0121	-0.0247	0.9871	0.1272	0.094
	γ							
2	-0.0009	-0.005	0.0277	0.9996				
3	-	-	0.0436	0.999				
4	0.0034	0.0187	-0.0564	-0.9982				
5	-	-	0.0708	0.9975				
6	0.0069	0.0377	-0.0795	-0.9961				
7	-	-	0.0947	0.9955				
8	0.0108	0.0604	-0.0983	-0.9933				
9	-	-	0.1158	0.9933				
10	-0.0149	-0.0851	0.1133	0.9898				
11	-	-	0.1346	0.9909				
12	-0.0189	-0.1104	0.1252	0.9858				

For ^{152}Sm , the Coriolis mixing matrix elements $(j_x)_{\beta_2,1} = 0.864$ MeV^{-1} and $(j_x)_{\gamma,1} = 0.855$ MeV^{-1} are considered to be larger values from others. These two comparably equal and large values Coriolis mixing matrix elements, with very small band head energies spacings $\Delta\omega_{\beta_2,\gamma} = 0.083$ MeV induced strong mixing between $0^+_{\beta_2}$ – and $\gamma-$ bands.

A large spacing of the band head energies between two bands reduces the influence of large mixing matrix element. One nice example occurs in the structure of ^{154}Sm. Coriolis mixing matrix element $(j_x)_{\gamma,1} = 0.417$ MeV^{-1} which is the highest among others and the pure band head energies spacings $\Delta\omega_{\gamma,\beta_2} = 0.177$ MeV, $\Delta\omega_{\gamma,\beta_1} = 0.281$ MeV, and $\Delta\omega_{gr,\gamma} = 1.380$ MeV. Even though the mixing matrix element is large; the large spacing reduces its effect. The strong mixing induced in this isotope is between $0^+_{\beta_1}$ – and $0^+_{\beta_2}$ – bands with Coriolis mixing matrix elements $(j_x)_{\beta_2,1} = 0.408$ MeV^{-1} and $(j_x)_{\beta_1,1} = 0.403$ MeV^{-1}. The Coriolis mixing between these bands is strengthened by the small band head energy spacings, $\Delta\omega_{\beta_2,\beta_1} = 0.104$ MeV.

The experimental energies for $0^+_{\beta_2}$ – band in ^{156}Sm isotope are not available. No calculations are done for this band. Insufficient number of states from other rotational bands and unavailability of $0^+_{\beta_2}$ – band make it difficult to explain the structure of ^{156}Sm isotope by comparison. The intensity of Coriolis mixing between $0^+_{\beta_1}$ – and $\gamma-$ bands is noticeable. This is because the Coriolis mixing matrix elements $(j_x)_{\gamma,1} = 0.903$ MeV^{-1} is the highest followed by $(j_x)_{\beta_1,1} = 0.872$ MeV^{-1} and $(j_x)_{gr,1} = 0.749$ MeV^{-1}. The Coriolis

mixing between these bands is strengthened by the closeness of band head energy, $\Delta\omega_{\gamma,\beta_1} = 0.297$ MeV.

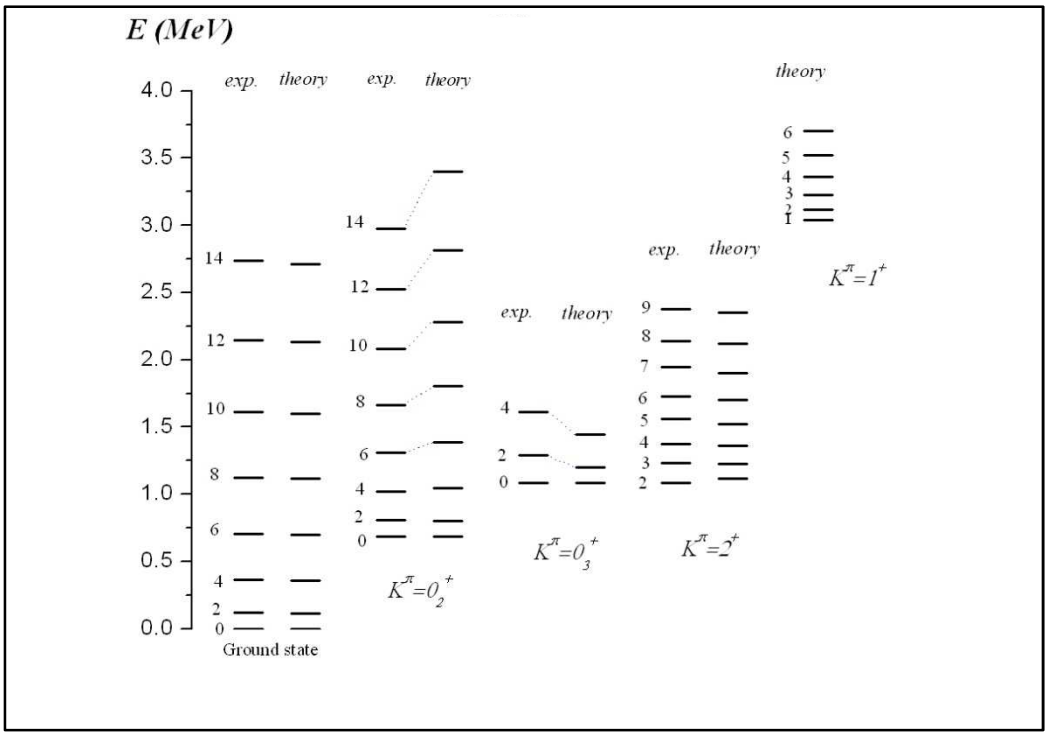

Figure 4.4 Energy spectra of positive-parity states of ^{152}Sm isotope.

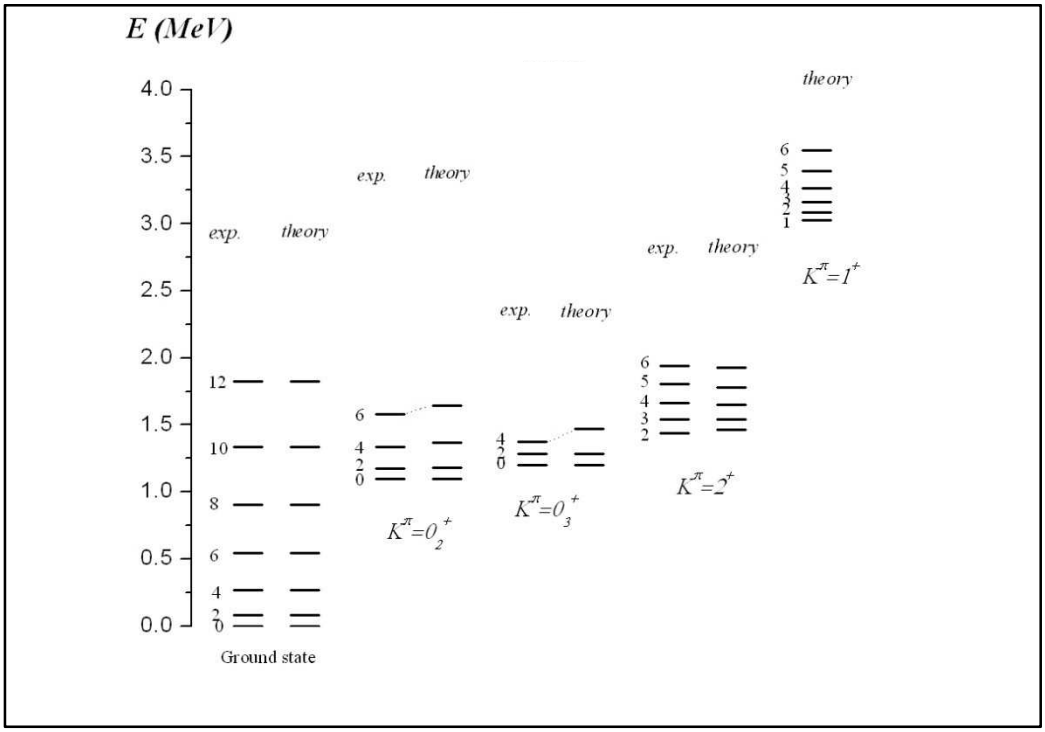

Figure 4.5 Energy spectra of positive-parity states of ^{154}Sm isotope.

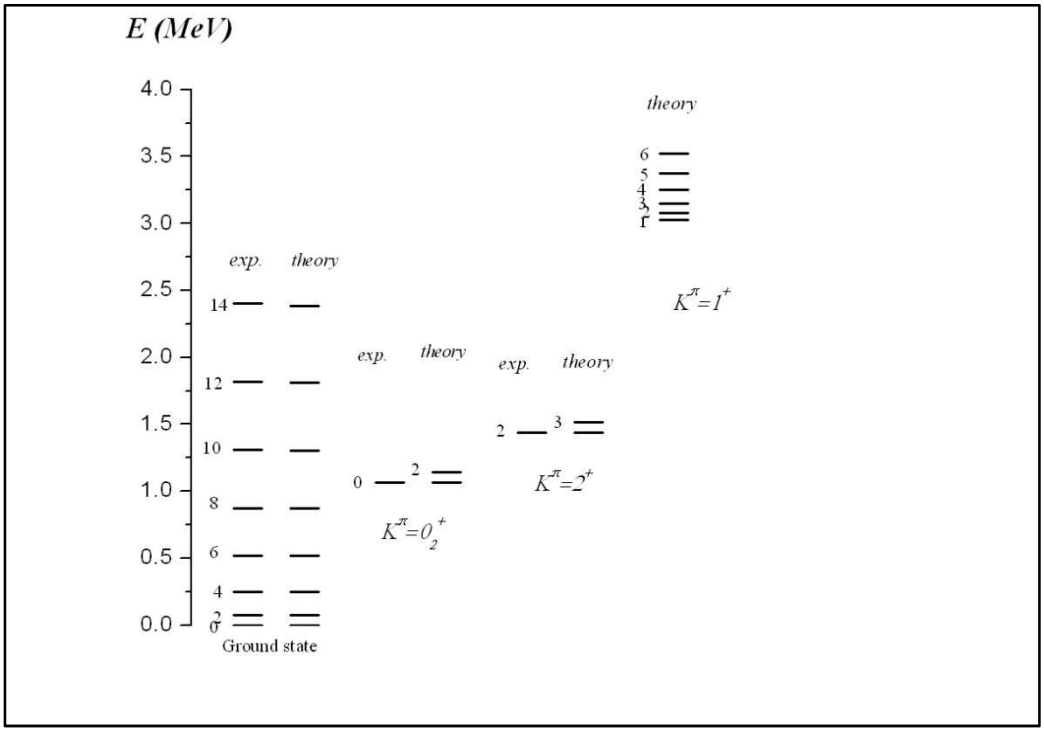

Figure 4.6 Energy spectra of positive-parity states of ^{156}Sm isotope.

The theoretical energy spectra of positive-parity states in $^{152,154,156}Sm$ are presented in Figures 4.4, 4.5 and 4.6 respectively in comparison with the experimental energies [6-9]. The theoretical energy spectra are calculated by using Equation (3.7). From the figures, we see that energy difference $\varepsilon(I) = \left| E_{theor}(I) - E_{exp}(I) \right|$ of the $0^+_{\beta_1}$ – band increases with the increase in the angular momentum *I*. At high spin, I the nonadiabaticity of energy rotational bands occurs. Two states with same spin, I and parity, π from different bands cross in that region causes Coriolis mixing. We predict the existence of s-band states to perturb the pure $0^+_{\beta_1}$ – band states.

Other than this mentioned obvious deviation, the theoretical positive-parity states energy spectra are in best agreement with the experimental data. But at higher spin, I the theoretical energies deviate from the observed energies suggests the nonadiabaticity of energy rotational bands. Few new states and collective 1^+ band are predicted.

4.2 Dysprosium isotopes $^{156,158,160,162,164,166}Dy$

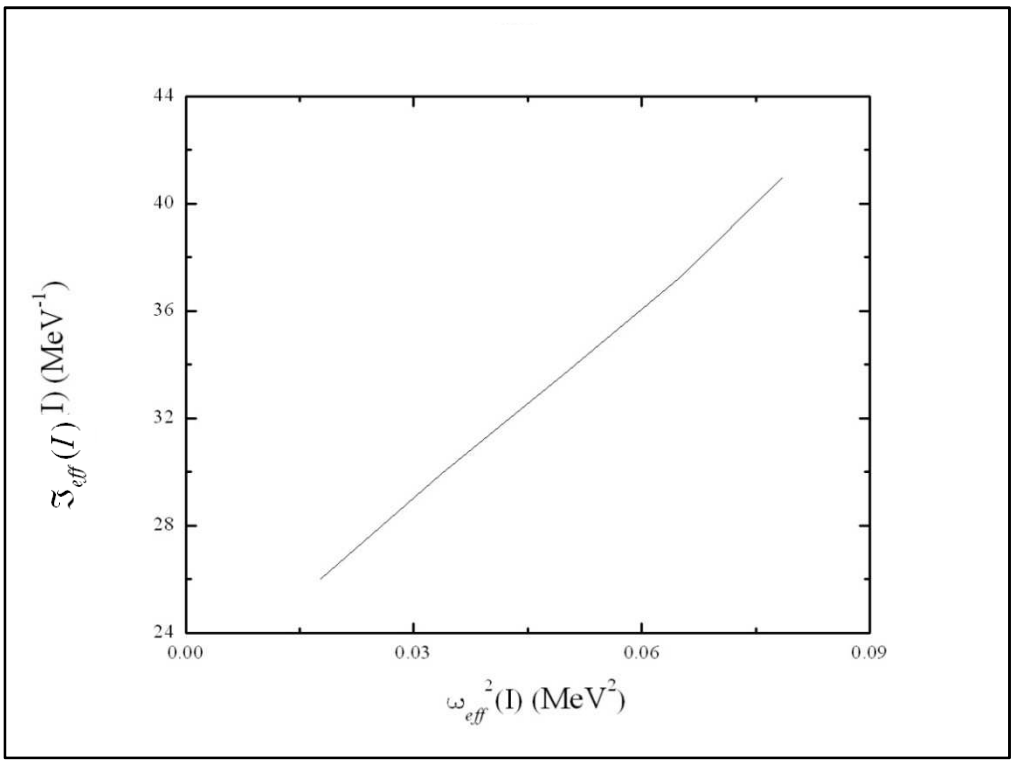

Figure 4.7 The linear dependencies of $\Im_{eff}(I)$ on $\omega_{eff}^2(I)$ for ^{156}Dy .

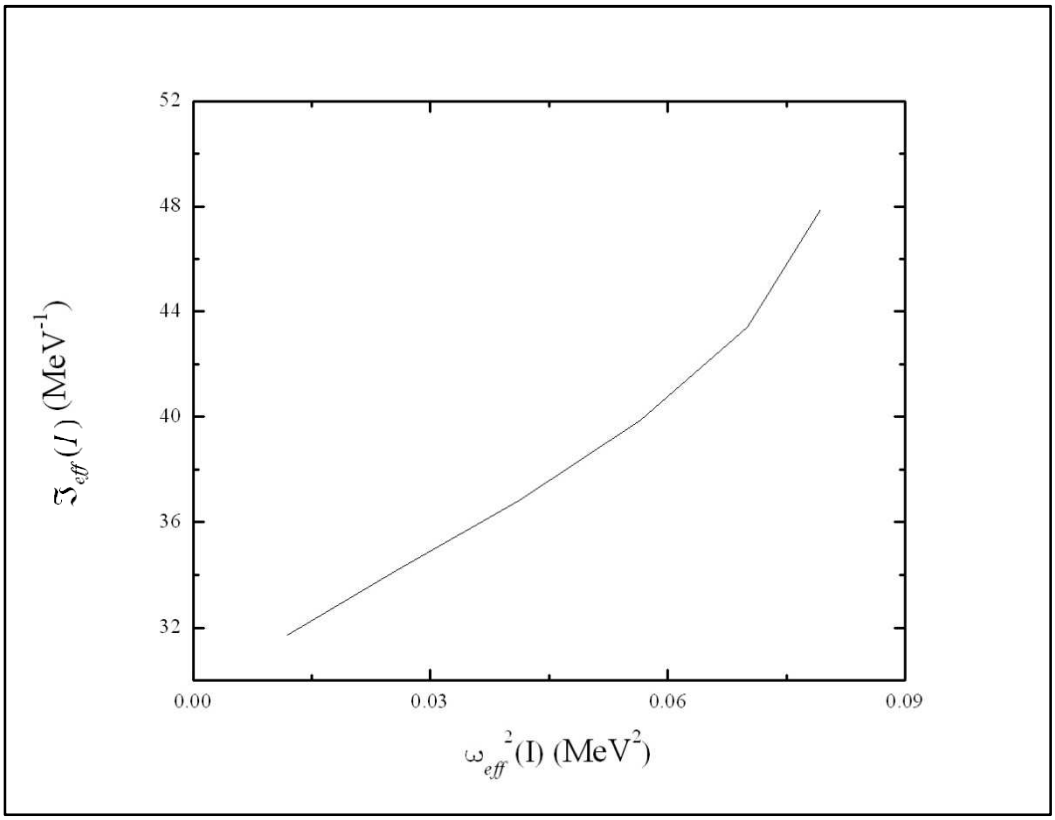

Figure 4.8 The linear dependencies of $\Im_{eff}(I)$ on $\omega_{eff}^{2}(I)$ for ^{158}Dy .

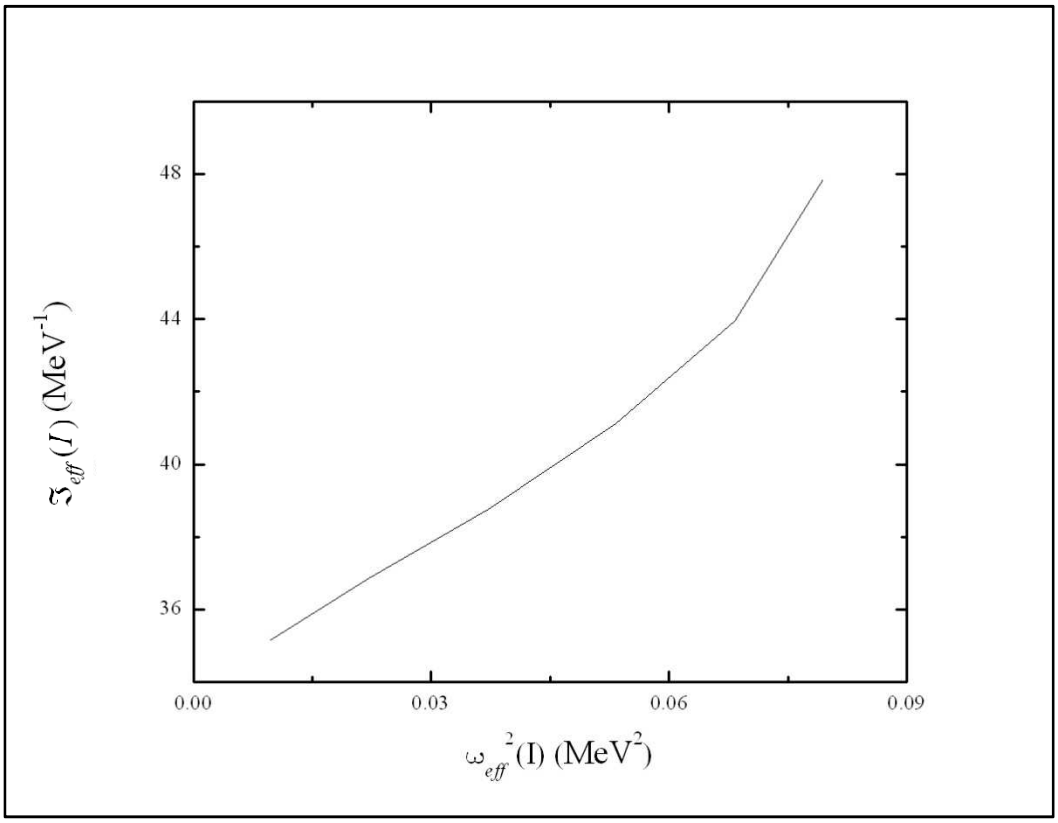

Figure 4.9 The linear dependencies of $\Im_{eff}(I)$ on $\omega_{eff}^2(I)$ for ^{160}Dy .

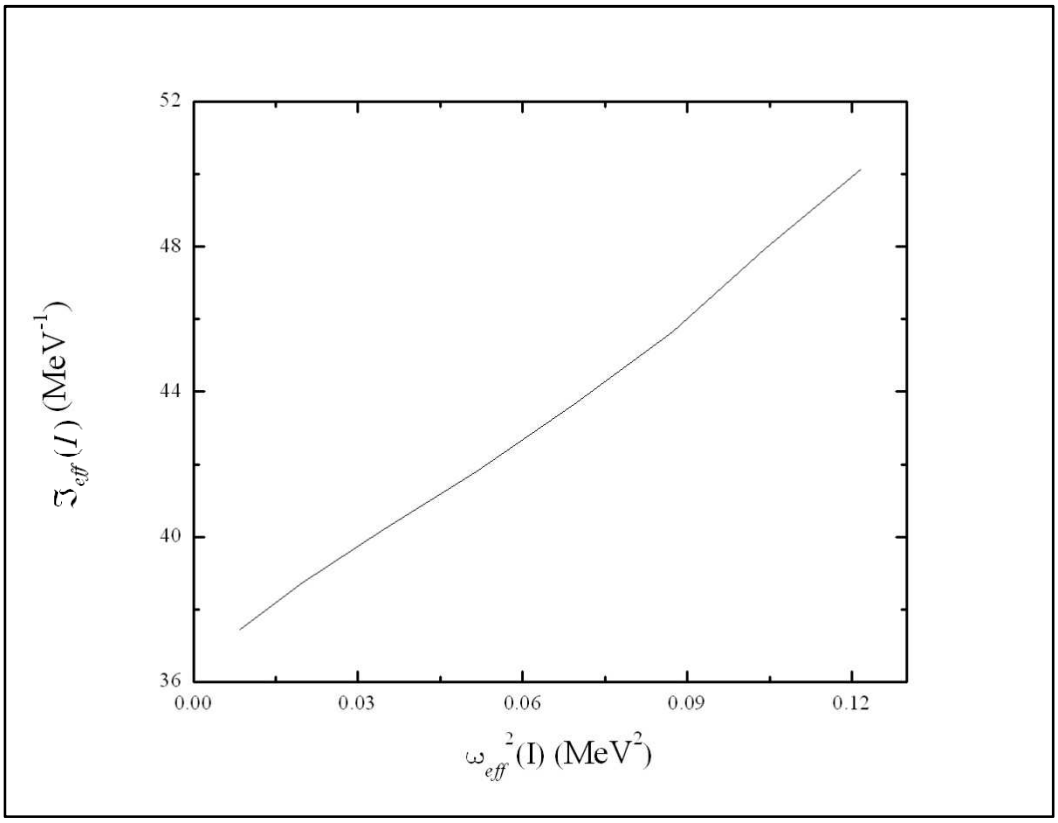

Figure 4.10 The linear dependencies of $\Im_{eff}(I)$ on $\omega_{eff}^2(I)$ for ^{162}Dy.

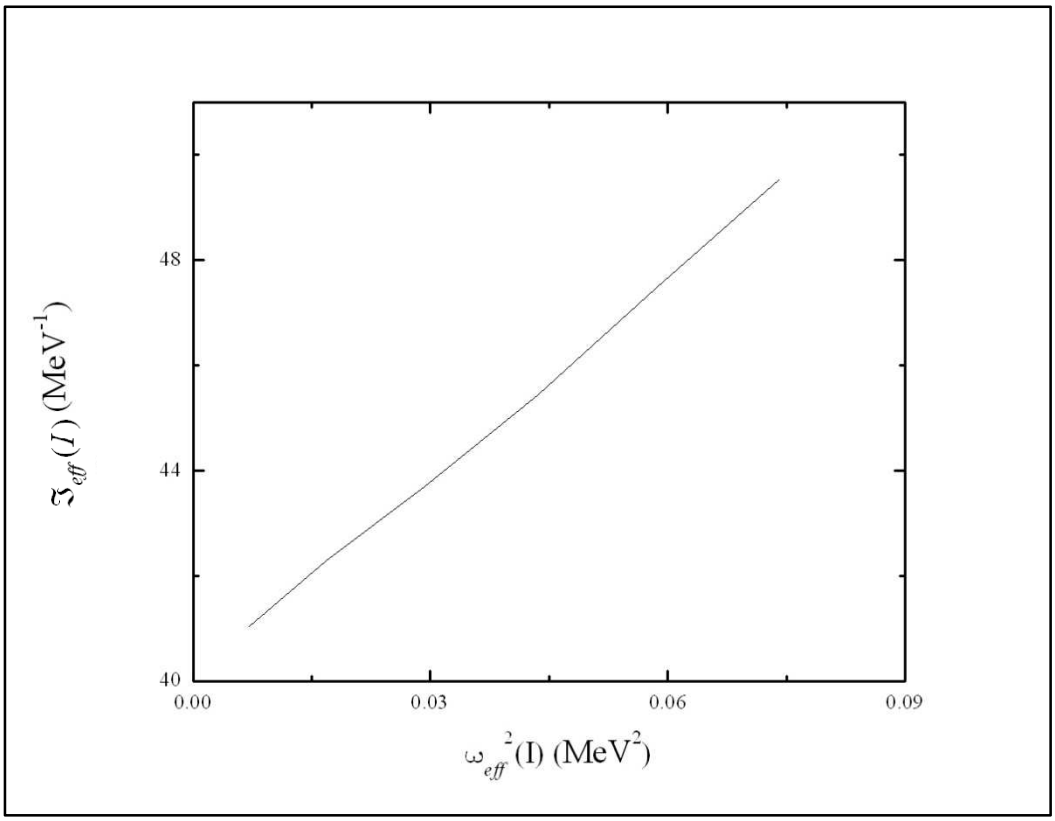

Figure 4.11 The linear dependencies of $\Im_{eff}(I)$ on $\omega_{eff}^{2}(I)$ for ^{164}Dy .

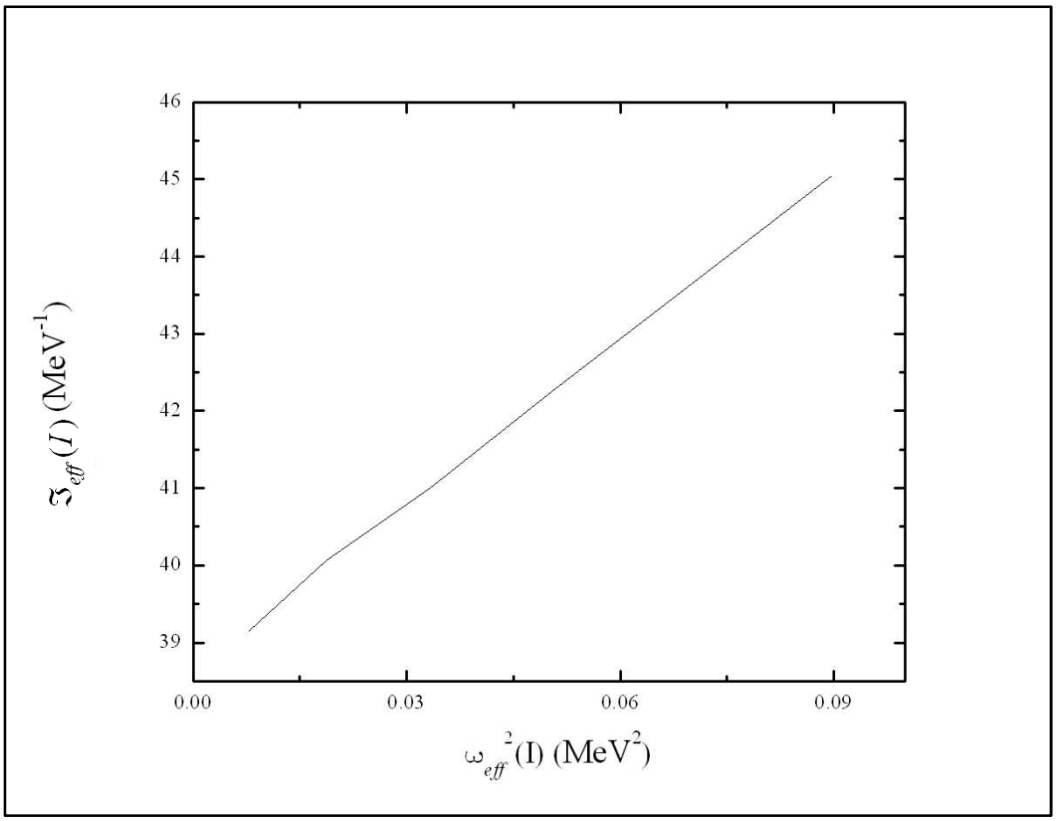

Figure 4.12 The linear dependencies of $\Im_{eff}(I)$ on $\omega_{eff}^{2}(I)$ for ^{166}Dy .

Table 4.6 Inertial parameters of rotational core used in the calculations.

Nucleus	$\Im_0$ (MeV^{-1})	$\Im_1$ (MeV^{-3})
^{156}Dy	21.93	238.13
^{158}Dy	29.69	174.26
^{160}Dy	33.96	131.07
^{162}Dy	36.61	105.77
^{164}Dy	40.25	121.09
^{166}Dy	38.68	73.81

Table 4.7 Parameters used in the calculations. Band head energies in MeV [6].

Nucleus	ω_{β_1}	ω_{β_2}	ω_1	ω_γ	$(j_x)_{gr,1}$	$(j_x)_{\beta_1,1}$	$(j_x)_{\beta_2,1}$	$(j_x)_{\gamma,1}$
^{156}Dy	0.676	1.405	3.0	0.760	1.462	1.615	1.765	1.633
^{158}Dy	0.991	1.269	3.0	0.847	2.598	2.966	2.605	2.481
^{160}Dy	1.280	1.444	1.775	0.879	1.689	2.170	2.224	2.031
^{162}Dy	1.400	1.666	1.720	0.807	0.077	0.103	0.108	0.093
^{164}Dy	1.655	1.773	3.0	0.688	0.389	0.484	0.490	0.431
^{166}Dy	1.149	-	3.0	0.780	0.174	0.205	-	0.195

Table 4.8 Structure of ^{156}Dy states.

I	gr	$0^+_{\beta_1}$	$0^+_{\beta_2}$	1^+	γ	gr	$0^+_{\beta_1}$	$0^+_{\beta_2}$	1^+	γ
	Ground-state band					$0^+_{\beta_1}$				
2	-0.9986	-0.0120	-0.0063	-0.0503	-0.0088	0.0167	-0.9913	-0.0180	-0.0753	-0.1049
4	0.9956	0.0309	0.0165	0.0833	0.0264	0.0488	-0.9496	-0.0492	-0.1336	-0.2748
6	-0.9910	-0.0515	-0.0278	-0.1111	-0.0454	0.0865	-0.8974	-0.0803	-0.1774	-0.3864
8	-0.9852	-0.0723	-0.0394	-0.1356	-0.0646	-0.1249	0.8531	0.1066	0.2081	0.4494
10	0.9782	0.0927	0.0510	0.1581	0.0834	0.1626	-0.8181	-0.1279	-0.2297	-0.4849
12	0.9701	0.1125	0.0626	0.1790	0.1017	0.1991	-0.7899	-0.1450	-0.2450	-0.5053
	γ					$0^+_{\beta_2}$				
2	0.0101	0.1093	-0.0141	-0.0518	-0.9925	-0.0111	-0.0238	0.9940	0.1041	-0.0223
3	-	-	-	0.0872	0.9962	-	-	-	-	-
4	-0.0230	-0.2891	0.0310	0.0729	0.9538	-0.0254	-0.0556	0.9852	0.1480	-0.0608
5	-	-	-	0.1259	0.9920	-	-	-	-	-
6	-0.0294	-0.4113	0.0389	0.0726	0.9073	0.0377	0.0839	-0.9766	-0.1699	0.0947
7	-	-	-	0.1534	0.9882	-	-	-	-	-
8	0.0325	0.4851	-0.0424	-0.0679	-0.8702	0.0477	0.1074	-0.9687	-0.1810	0.1230
9	-	-	-	0.1747	0.9846	-	-	-	-	-
10	0.0340	0.5312	-0.0441	-0.0631	-0.8431	-0.0558	-0.1270	0.9615	0.1866	-0.1465
11	-	-	-	0.1922	0.9814	-	-	-	-	-
12	0.0349	0.5619	-0.0451	-0.0590	-0.8231	-0.0624	-0.1434	0.9550	0.1892	-0.1663

Table 4.9 Structure of ^{158}Dy states.

I	gr	$0^+_{\beta_1}$	$0^+_{\beta_2}$	1^+	γ	gr	$0^+_{\beta_1}$	$0^+_{\beta_2}$	1^+	γ
	Ground-state band					$0^+_{\beta_1}$				
2	0.9972	0.0167	0.0115	0.0712	0.0133	-0.0230	0.9804	0.0730	0.1071	-0.1466
4	-0.9885	-0.0506	-0.0350	-0.1302	-0.0466	-0.0452	0.8839	0.1274	0.1199	-0.4314
6	-0.9713	-0.0942	-0.0658	-0.1883	-0.0886	0.0514	-0.7887	-0.1368	-0.0999	0.5888
8	-0.9453	-0.1406	-0.0992	-0.2434	-0.1327	0.0525	-0.7336	-0.1364	-0.0834	0.6584
10	-0.9125	-0.1845	-0.1316	-0.2931	-0.1736	0.0526	-0.7018	-0.1350	-0.0723	0.6937
12	-0.8765	-0.2227	-0.1605	-0.3358	-0.2086	0.0525	-0.6819	-0.1337	-0.0646	0.7143
	γ					$0^+_{\beta_2}$				
2	-0.0223	0.1339	0.0426	0.0898	0.9857	0.0164	0.0909	-0.9900	-0.0993	0.0399
3	-	-	-	0.1125	0.9936	-	-	-	-	-
4	0.0932	-0.3789	-0.1458	-0.2042	-0.8859	0.0347	0.2068	-0.9650	-0.1202	0.1018
5	-	-	-	0.1706	0.9853	-	-	-	-	-
6	-0.1862	0.4924	0.2238	0.2716	0.7739	0.0455	0.2861	-0.9395	-0.1161	0.1413
7	-	-	-	0.2136	0.9769	-	-	-	-	-
8	-0.2807	0.5236	0.2642	0.2994	0.6983	0.0515	0.3344	-0.9204	-0.1073	0.1642
9	-	-	-	0.2470	0.9690	-	-	-	-	-
10	-0.3676	0.5249	0.2823	0.3049	0.6455	0.0550	0.3648	-0.9069	-0.0991	0.1781
11	-	-	-	0.2736	0.9618	-	-	-	-	-
12	-0.4423	0.5151	0.2885	0.2989	0.6053	0.0572	0.3851	-0.8971	-0.0922	0.1872

Table 4.10 Structure of ^{160}Dy states.

I	gr	$0^+_{\beta_1}$	$0^+_{\beta_2}$	1^+	γ	gr	$0^+_{\beta_1}$	$0^+_{\beta_2}$	1^+	γ
	Ground-state band					$0^+_{\beta_1}$				
2	0.9975	0.0082	0.0075	0.0688	0.0091	-0.0288	0.9240	0.2187	0.2962	-0.0989
4	-0.9906	-0.0263	-0.0240	-0.1275	-0.0337	-0.0659	0.8016	0.3511	0.3635	-0.3127
6	0.9773	0.0523	0.0477	0.1878	0.0683	-0.0857	0.7143	0.3737	0.3281	-0.4849
8	-0.9557	-0.0836	-0.0765	-0.2487	-0.1090	0.0931	-0.6579	-0.3680	-0.2807	0.5867
10	-0.9259	-0.1171	-0.1076	-0.3073	-0.1513	0.0959	-0.6223	-0.3593	-0.2433	0.6444
12	-0.8898	-0.1497	-0.1381	-0.3608	-0.1913	0.0969	-0.5991	-0.3520	-0.2158	0.6791
	γ					$0^+_{\beta_2}$				
2	-0.0194	0.0514	0.0378	0.1397	0.9879	0.0205	0.3016	-0.9207	-0.2410	0.0540
3	-	-	-	0.1921	0.9814	-	-	-	-	-
4	-0.0771	0.1667	0.1272	0.2947	0.9291	0.0284	0.4921	-0.8450	-0.1873	0.0891
5	-	-	-	0.2846	0.9586	-	-	-	-	-
6	-0.1588	0.2619	0.2077	0.3946	0.8410	0.0304	0.5602	-0.8091	-0.1444	0.0988
7	-	-	-	0.3472	0.9378	-	-	-	-	-
8	-0.2491	0.3136	0.2564	0.4392	0.7622	0.0311	0.5894	-0.7919	-0.1187	0.1025
9	-	-	-	0.3913	0.9203	-	-	-	-	-
10	-0.3388	0.3362	0.2808	0.4490	0.7012	0.0314	0.6045	-0.7825	-0.1023	0.1042
11	-	-	-	0.4235	0.9059	-	-	-	-	-
12	-0.4216	0.3430	0.2907	0.4398	0.6532	0.0316	0.6135	-0.7768	-0.0909	0.1052

Table 4.11 Structure of ^{162}Dy states.

I	gr	$0^+_{\beta_1}$	$0^+_{\beta_2}$	1^+	γ	gr	$0^+_{\beta_1}$	$0^+_{\beta_2}$	1^+	γ
	Ground-state band					$0^+_{\beta_1}$				
2	1.0000	0.0000	0.0000	0.0030	0.0000	0.0001	-0.9998	-0.0006	-0.0213	0.0002
4	-1.0000	0.0000	0.0000	-0.0053	-0.0001	0.0002	-0.9993	-0.0018	-0.0379	0.0007
6	-1.0000	-0.0001	-0.0001	-0.0074	-0.0001	0.0005	-0.9986	-0.0035	-0.0529	0.0013
8	-1.0000	-0.0001	-0.0001	-0.0093	-0.0002	0.0008	-0.9978	-0.0055	-0.0665	0.0021
10	0.9999	0.0002	0.0002	0.0110	0.0003	0.0011	-0.9969	-0.0077	-0.0786	0.0030
12	0.9999	0.0003	0.0002	0.0125	0.0004	0.0014	-0.9959	-0.0100	-0.0895	0.0039
	γ					$0^+_{\beta_2}$				
2	0.0000	0.0001	0.0000	0.0055	1.0000	0.0004	0.0033	-0.9917	-0.1285	0.0008
3	-	-	-	0.0086	1.0000	-	-	-	-	-
4	-0.0001	0.0002	0.0002	0.0114	0.9999	0.0012	0.0099	-0.9764	-0.2156	0.0026
5	-	-	-	0.0139	0.9999	-	-	-	-	-
6	-0.0003	0.0005	0.0003	0.0163	0.9999	0.0021	0.0183	-0.9595	-0.2810	0.0049
7	-	-	-	0.0186	0.9998	-	-	-	-	-
8	-0.0004	0.0007	0.0005	0.0208	0.9998	0.0032	0.0271	-0.9440	-0.3287	0.0073
9	-	-	-	0.0228	0.9997	-	-	-	-	-
10	-0.0006	0.0011	0.0008	0.0247	0.9997	0.0041	0.0359	-0.9308	-0.3637	0.0097
11	-	-	-	0.0265	0.9996	-	-	-	-	-
12	-0.0008	0.0014	0.0010	0.0283	0.9996	-0.0051	-0.0443	0.9198	0.3898	-0.0119

Table 4.12 Structure of ^{164}Dy states.

I	gr	$0^+_{\beta_1}$	$0^+_{\beta_2}$	1^+	γ	gr	$0^+_{\beta_1}$	$0^+_{\beta_2}$	1^+	γ
	Ground-state band					$0^+_{\beta_1}$				
2	1.0000	0.0001	0.0001	0.0078	0.0002	0.0003	-0.9997	-0.0054	-0.0218	0.0005
4	0.9999	0.0004	0.0004	0.0139	0.0009	0.0010	-0.9991	-0.0172	-0.0391	0.0018
6	0.9998	0.0009	0.0008	0.0196	0.0018	-0.0020	0.9979	0.0337	0.0556	-0.0037
8	0.9997	0.0014	0.0013	0.0248	0.0029	-0.0032	0.9960	0.0533	0.0710	-0.0060
10	0.9996	0.0019	0.0018	0.0295	0.0041	-0.0046	0.9935	0.0744	0.0854	-0.0086
12	0.9994	0.0026	0.0024	0.0338	0.0054	-0.0060	0.9904	0.0962	0.0989	-0.0115
	γ					$0^+_{\beta_2}$				
2	-0.0003	0.0003	0.0002	0.0092	1.0000	-0.0003	-0.0059	0.9997	0.0239	-0.0005
3	-	-	-	0.0143	0.9999	-	-	-	-	-
4	-0.0012	0.0010	0.0009	0.0190	0.9998	-0.0010	-0.0189	0.9989	0.0419	-0.0017
5	-	-	-	0.0233	0.9997	-	-	-	-	-
6	-0.0023	0.0021	0.0019	0.0274	0.9996	0.0019	0.0369	-0.9977	-0.0574	0.0034
7	-	-	-	0.0312	0.9995	-	-	-	-	-
8	-0.0038	0.0033	0.0030	0.0350	0.9994	0.0029	0.0583	-0.9958	-0.0703	0.0053
9	-	-	-	0.0383	0.9993	-	-	-	-	-
10	-0.0054	0.0047	0.0043	0.0418	0.9991	0.0040	0.0815	-0.9934	-0.0809	0.0073
11	-	-	-	0.0447	0.9990	-	-	-	-	-
12	-0.0071	0.0062	0.0056	0.0480	0.9988	0.0051	0.1053	-0.9904	-0.0894	0.0092

Table 4.13 Structure of ^{166}Dy states.

I	gr	$0^+_{\beta_1}$	1^+	γ	gr	$0^+_{\beta_1}$	1^+	γ
	Ground-state band				$0^+_{\beta_1}$			
2	1.0000	0.0000	0.0037	0.0000	-0.0001	1.0000	0.0069	-0.0002
4	1.0000	0.0001	0.0066	0.0002	-0.0002	0.9999	0.0125	-0.0007
6	1.0000	0.0003	0.0093	0.0004	-0.0004	0.9998	0.0176	-0.0015
8	0.9999	0.0004	0.0118	0.0006	-0.0007	0.9997	0.0224	-0.0024
10	0.9999	0.0006	0.0142	0.0009	-0.0010	0.9996	0.0268	-0.0034
12	0.9999	0.0008	0.0163	0.0011	-0.0013	0.9995	0.0308	-0.0046
	γ							
2	-0.0001	0.0002	0.0045	1.0000				
3	-	-	0.0071	1.0000				
4	-0.0002	0.0006	0.0094	1.0000				
5	-	-	0.0258	0.7800				
6	0.0005	-0.0012	-0.0137	-0.9999				
7	-	-	0.0157	0.9999				
8	0.0008	-0.0020	-0.0177	-0.9998				
9	-	-	0.0195	0.9998				
10	0.0012	-0.0029	-0.0213	-0.9998				
11	-	-	0.0229	0.9997				
12	0.0015	-0.0038	-0.0246	-0.9997				

In the structure of ^{156}Dy, a large spacing of the band head energies between two bands reduces the influence of large mixing matrix element. Coriolis mixing matrix element $(j_x)_{\beta_2,1} = 1.765$ MeV^{-1} which is the highest among others and the pure band head energies spacings $\Delta\omega_{\beta_2,gr} = 1.405$ MeV, $\Delta\omega_{\beta_2,\beta_1} = 0.729$ MeV, and $\Delta\omega_{\beta_2,\gamma} = 0.645$ MeV. Even though the mixing matrix element is large; the large spacing reduces its effect. Strong mixing is induced between $0^+_{\beta_1}-$ and $\gamma-$ bands due to the small pure band head energies spacing $\Delta\omega_{\beta_1,\gamma} = 0.084$ MeV.

The band head energies spacings play a very important role in two-state mixing. Even a small mixing matrix element can induce strong mixing if the band head energies spacing is small. One nice example occurs in the structure of ^{158}Dy. Coriolis mixing matrix element $(j_x)_{\gamma,1} = 2.481$ MeV^{-1} which is the smallest among others and the pure headband energies spacings $\Delta\omega_{\gamma,\beta_1} = 0.144$ MeV, $\Delta\omega_{\gamma,gr} = 0.847$ MeV,and $\Delta\omega_{\gamma,\beta_2} = 0.422$ MeV.

Now, let us have a look at the structure of ^{160}Dy. We can see that the strong mixing is induced between $0^+_{\beta_1}-$ and $0^+_{\beta_2}-$ bands. The Coriolis mixing matrix elements $(j_x)_{\beta_2,1} = 2.224$ MeV^{-1} and $(j_x)_{\beta_1,1} = 2.170$ MeV^{-1} which are considerably large matrix elements. The pure band head energies spacings $\Delta\omega_{\beta_2,\beta_1} = 0.164$ MeV is very small. Conversely, the Coriolis mixing matrix element $(j_x)_{gr,1} = 1.689$ MeV^{-1} which is the lowest among others. Small mixing is induced between the ground state and $0^+_{\beta_2}-$ bands. Even though the Coriolis

mixing matrix element of $0^+_{\beta_2}-$ band is very large, the Coriolis mixing effect is reduced by small Coriolis mixing matrix element of ground state band and large headband energies spacings $\Delta\omega_{\beta_2,gr}=1.444$ MeV.

For ^{162}Dy, the Coriolis mixing matrix elements $(j_x)_{\beta_2,1}=1.080$ MeV^{-1} and $(j_x)_{\beta_1,1}=1.030$ MeV^{-1} are considered to be larger values from others. Even though these two Coriolis mixing matrix elements are comparable, the band head energies spacings $\Delta\omega_{\beta_2,1^+}=0.054$ MeV is very small compared to $\Delta\omega_{\beta_2,\beta_1}=0.266$ MeV. Therefore, large mixing is strikingly induced between $0^+_{\beta_2}-$ and 1^+ bands.

For ^{164}Dy isotope, the Coriolis mixing matrix elements $(j_x)_{\beta_2,1}=0.490$ MeV^{-1} and $(j_x)_{\beta_1,1}=0.484$ MeV^{-1} are nearly equal and considered to be larger values from others. Due to closeness of $0^+_{\beta_1}-$ and $0^+_{\beta_2}-$ bands with band head energies spacings $\Delta\omega_{\beta_2,\beta_1}=0.118$ MeV, the mixing between these two bands is noticeably induced. The intensity of Coriolis mixing of these two bands with other low-lying state bands is approximately equal.

The experimental energies for $0^+_{\beta_2}-$ band in ^{166}Dy isotope are not available. No calculations are done for this band. There is not so much comparison can be done to explain the structure of ^{166}Dy isotope. The intensity of Coriolis mixing between $0^+_{\beta_1}-$ and 1^+ bands is the highest compared to mixing of the ground state and $\gamma-$ bands with 1^+ band. This is because the Coriolis mixing matrix

element $(j_x)_{\beta_1,1} = 0.205$ MeV^{-1} is the highest followed by $(j_x)_{\gamma,1} = 0.195$ MeV^{-1} and $(j_x)_{gr,1} = 0.174$ MeV^{-1}. The pure band head energies spacings $\Delta\omega_{\beta_1,1^+} = 1.851$ MeV is smaller than $\Delta\omega_{\gamma,1^+} = 2.220$ MeV supports the strong mixing between $0^+_{\beta_1}$ – and 1^+ bands.

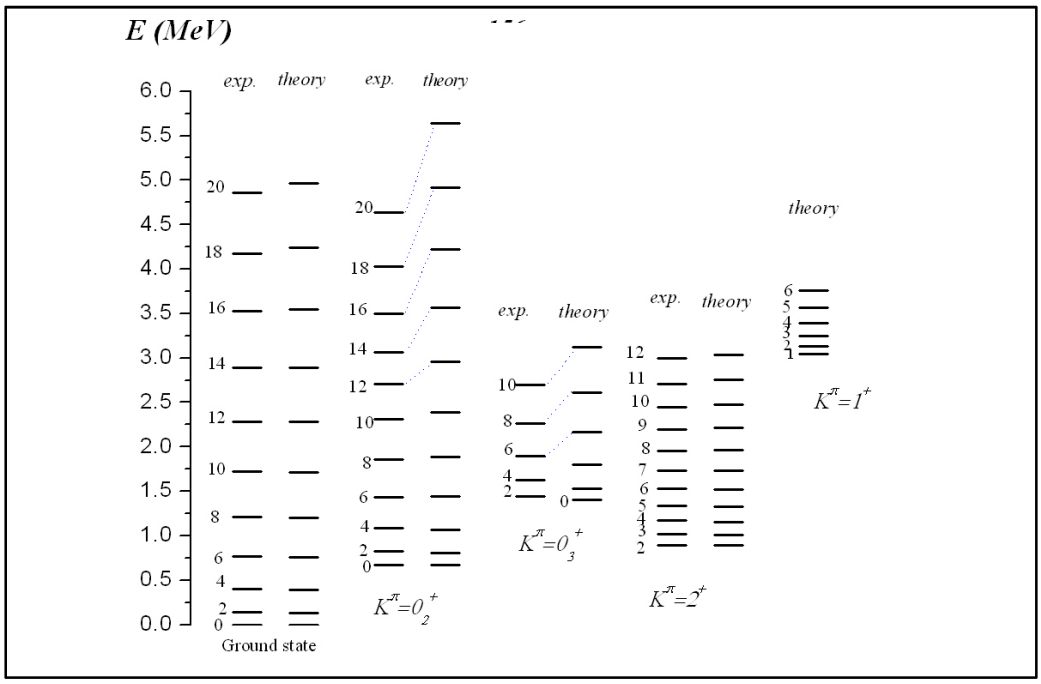

Figure 4.13 Energy spectra of positive-parity states of ^{156}Dy isotope.

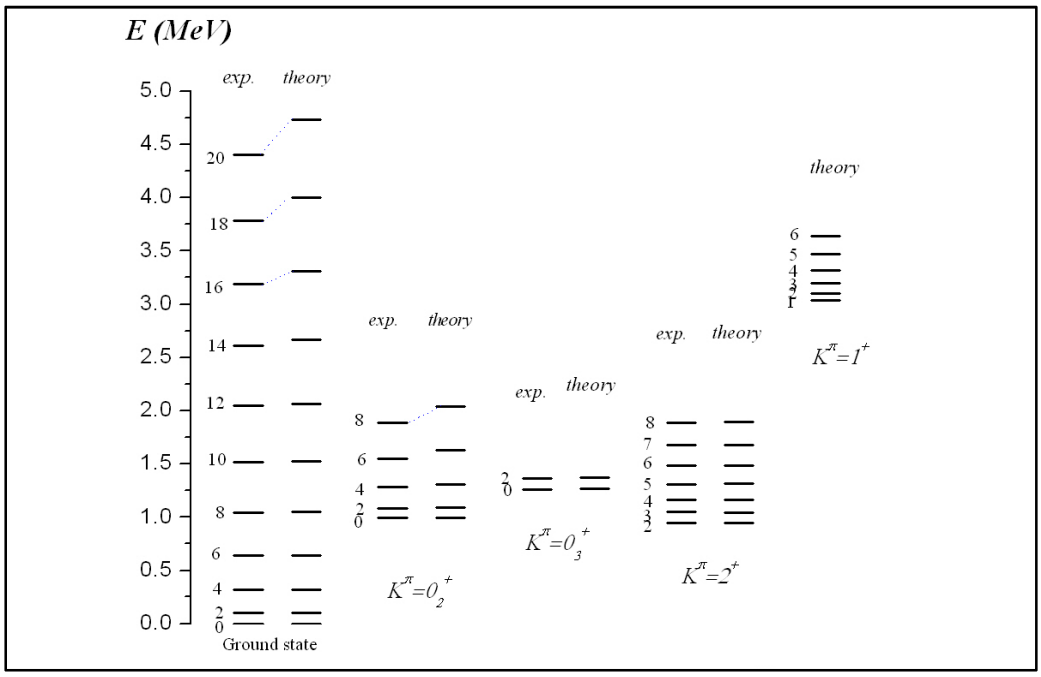

Figure 4.14 Energy spectra of positive-parity states of ^{158}Dy isotope.

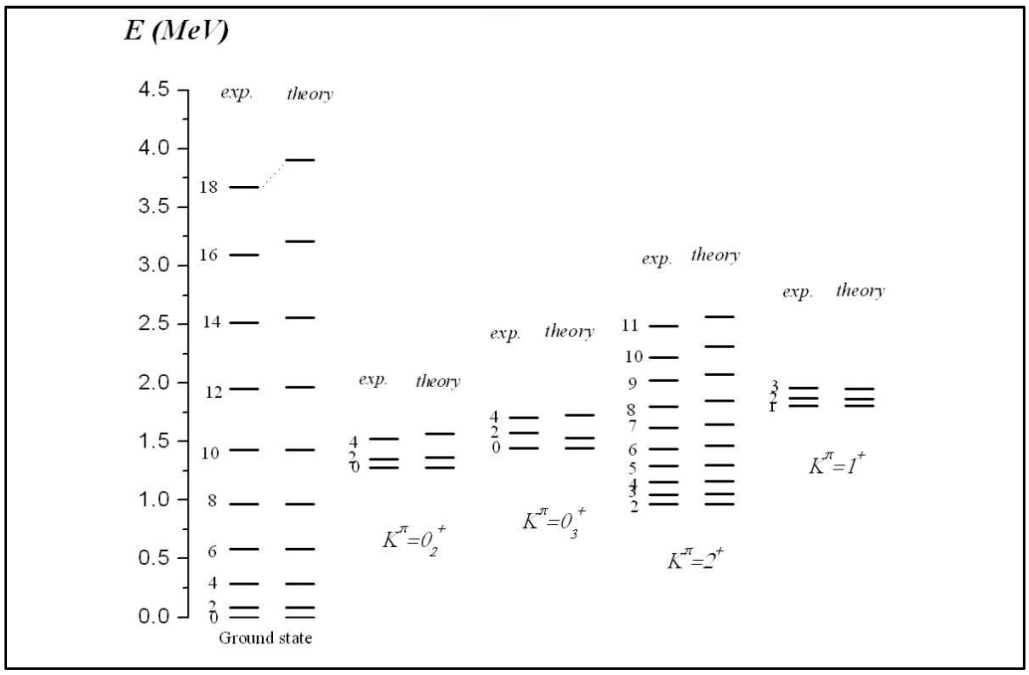

Figure 4.15 Energy spectra of positive-parity states of ^{160}Dy isotope.

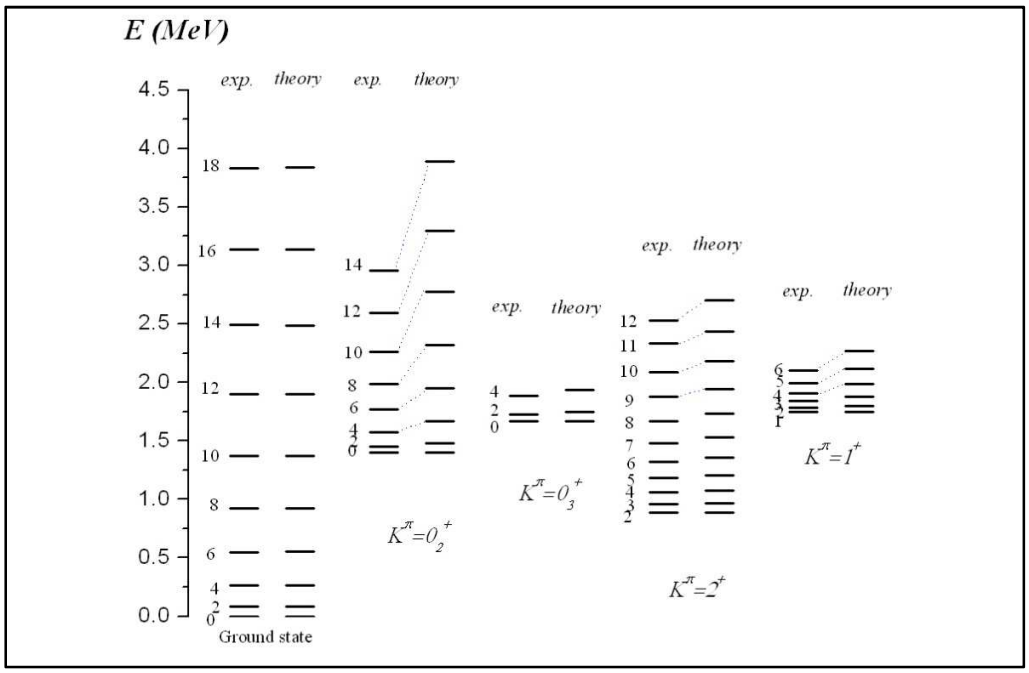

Figure 4.16 Energy spectra of positive-parity states of ^{162}Dy isotope.

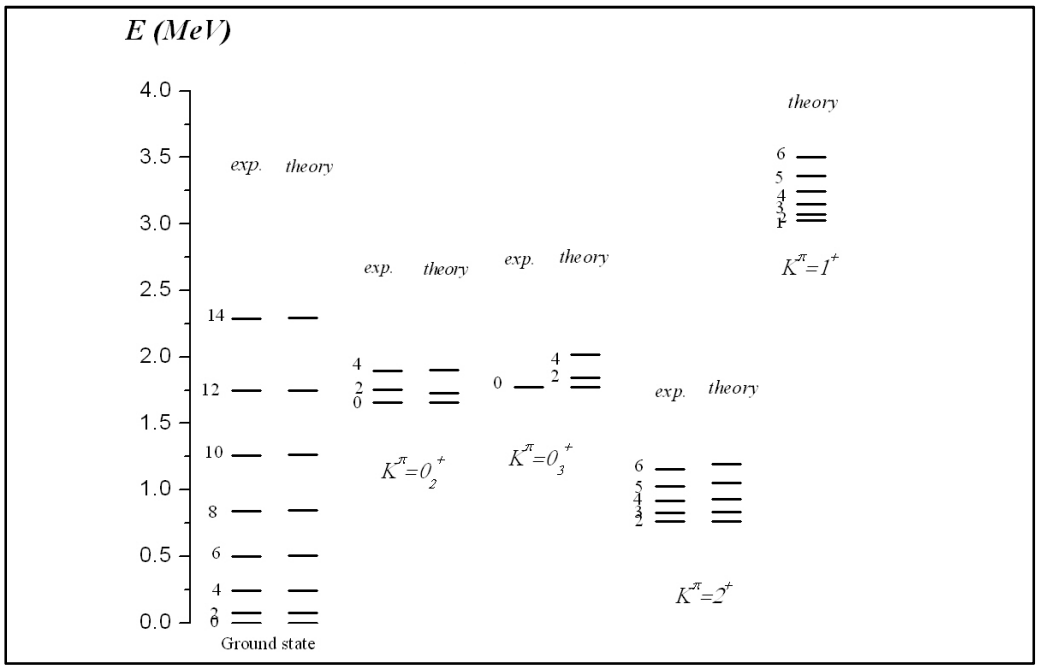

Figure 4.17 Energy spectra of positive-parity states of ^{164}Dy isotope.

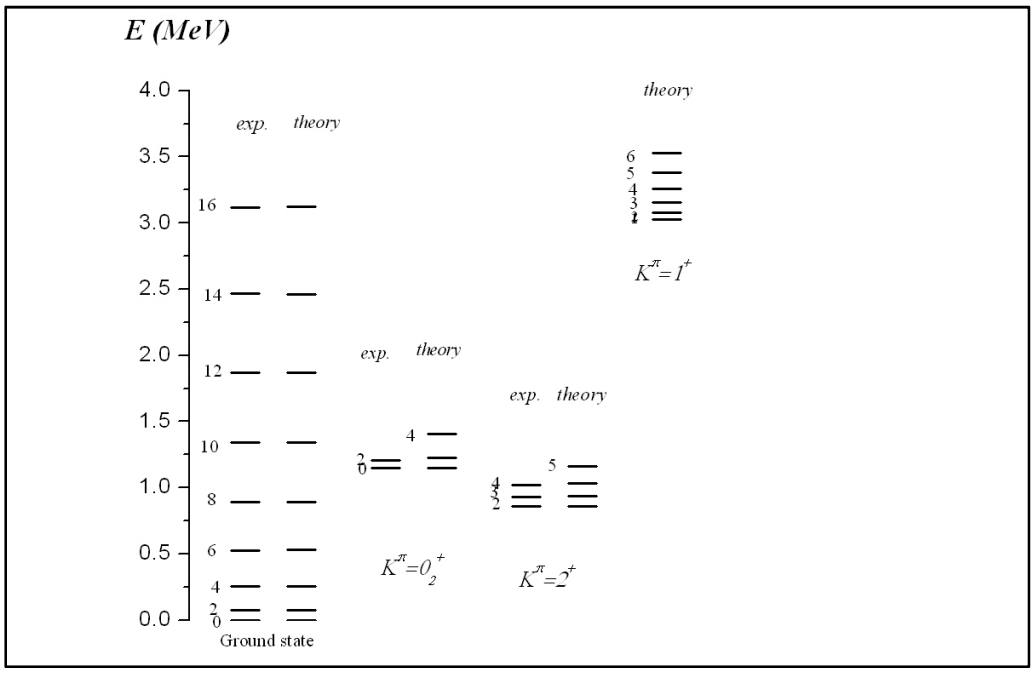

Figure 4.18 Energy spectra of positive-parity states of ^{166}Dy isotope.

The theoretical energy spectra of positive-parity states in $^{156,158,160,162,164,166}Dy$ are presented in Figures 4.13-4.18 respectively in comparison with the experimental energies [6, 10-15]. The total energy of states are calculated by using Equation (3.7). The rotational behaviour is included in the energies for each intrinsic excitation.

The experimental energies are reproduced very well by using Equation (3.7), but they are clearly deviated as I increases. The energy difference between the theoretical and experimental energies $\varepsilon_q^{\sigma}(I) = \left| E_{theor}(I) - E_{\exp}(I) \right|$ increases with the increase in the angular momentum I especially the β_n- bands of ^{156}Dy and ^{162}Dy isotopes. At high spin I, the nonadiabaticity of energy rotational bands occurs. The understanding of these deviations in physics is due to the Coriolis mixing between states. This Coriolis mixing is taken into account in the calculation of the total energy of states. Two states must be with same spin I and parity π from different bands must stay close in order to be involved in the Coriolis mixing. The closeness of any two bands is represented by the value of the band head energies spacings $\Delta\omega_{K,K'}$.

In ^{156}Dy and ^{162}Dy isotopes, we predict the existence of s-band states to perturb the pure $0^+_{\beta_1}$ – band states due to large deviations from the experimental energies. Other than this mentioned obvious deviation, the experimental positive-parity states energy spectra are reproduced. But at higher spin I, the theoretical energies deviate from the observed energies suggests the nonadiabaticity of energy rotational bands. Few new states and collective 1^+ band are predicted.

For other isotopes, insufficient number of states of rotational bands especially $0^+_{\beta_2}$ − band makes it difficult to see the occurrence of nonadiabaticity of energy rotational β_n $(0^+_{\beta_1},\ 0^+_{\beta_2})$ − bands at high spin. However, few states still can be predicted by the model.

CHAPTER 5

CONCLUSIONS

5.1 Concluding Remarks

In adiabatic limit, the Coriolis coupling between rotational and intrinsic motion is small. The rotational frequency is very small compared to the frequency of intrinsic motion for a given angular momentum. A pure rotation apart from the intrinsic motion is defined yielding the observable pure rotational spectrum. To make a good approximation, the Coriolis coupling is then treated as perturbation in the Harris cranking model.

Phenomenological model is exploited to show the deviation of energy spectrum of positive parity states in even-even deformed nuclei from the adiabatic theory. The calculations are done by taking into account the Coriolis mixing of the $K^{\pi}=1^{+}$ collective bands with low-lying ground (gr), β_n $(0^{+}_{\beta_1},0^{+}_{\beta_2})-$, $\gamma-$ vibrational and rotational bands. Few parameters fitted to this model are calculated.

Energy of rotational core is calculated by using the Harris parameterization of the angular momentum and energy. The real root of cubic equation of Harris parameterization of the angular momentum gives the value of rotational angular frequency of rotational core. The adjustable inertial parameters of rotational core, $\Im_0$ and $\Im_1$ for $^{152,154,156}Sm$ and $^{156,158,160,162,164,166}Dy$ nuclei are calculated from the Harris two-parameter formula.

Coriolis rotational states mixing matrix elements $(j_x)_{K,K'}$ and $\gamma-$ band head energies ω_γ are determined by using the least square fitting method of a

diagonalizing matrix. The mixing components of the states are represented by the calculated values of the wave function of the nuclear states $\phi^{I}_{M,K}$. The value of the mixing component explained why deviation occurred. In general, the strength of states mixing is influenced by the values of Coriolis interaction matrix elements, $(j_x)_{K,K'}$ and the pure headband energies spacings $\Delta\omega_{K,K'}$. Larger values of Coriolis interaction matrix elements, $(j_x)_{K,K'}$ and the closeness between band head energies, ω_K lead to strong states mixing.

Energy spectra for the isotopes $^{152,154,156}Sm$ and $^{156,158,160,162,164,166}Dy$ are calculated. The levels appears in bands, each characterized by quantum number K^{π}. The experimental data is well reproduced at low spin I. However, it is observed the energy levels within a band do not follow the law of $E_{rot}(I) \sim I(I+1)$ expected for rotor at high spin I. This is from the fact that the rotational and intrinsic motions are strongly coupled. With the agreement between the theoretical and experimental data, few states that have never been observed experimentally are predicted.

5.2 Future Work

Very clear-cut problems to be solved in coming years are listed. A number of topics that deserved future intensive theoretical efforts to bring us closer to the physical insights of nucleus are:

1. Calculation of the probability of electromagnetic transitions in even-even deformed nuclei.
2. Study of the back bending phenomenon by the description of state-mixing.

3. Study of the nuclear isomerism and the K-forbidden transition.

Last, but not least, a point of current interest is to study the $K^{\pi}=1^{+}$ collective bands that have magnetic characteristic. Taking into account the Coriolis mixing of the isovector collective M1 states with low-lying states will lead to the non-adiabaticity of electromagnetic properties to occur. The orbital Ml low-lying excitation strength is correlated with the E2 excitation strength to the first excited 2^{+} states in heavy deformed even-even nuclei.

REFERENCES

[1] Beauford, R. (2010). An Introduction to the Geology of the Rare Earth Elements and Associated Mineral Ores. Retrieved from: rareearthelements.us/ree_geology

[2] Chandler, D.L. (8 Apr 2012). Clean Energy Could Lead to Scarce Materials. Retrieved from: web.mit.edu/newsoffice/2012/rare-earth-alternative-energy-0409.html

[3] Natural Resources Canada. (5 Jul 2012). Rare Earth Minerals and Metals Processing R&D. Retrieved from: www.nrcan.gc.ca/minerals-metals/technology/4475

[4] Kidela Capital Group. (10 May 2011). Rare Earth Processing 101. Retrieved from:www.kitco.com/ind/kidela/may102011.html

[5] Koerth-Baker, M. (2012). 4 Rare Earth Elements That Will Only Get More Important. Retrieved from:www.popularmechanics.com/technology/engineering/news/important-rare-earth-elements#slide-1

[6] Begzhanov, R. B., Belinkiy, V. M., Zalyubovskiy, I. I. and Kuznichenko, A. B. (1989). Handbook on Nuclear Physics Vol. **1** and **2**. Tashkent: FAN.

[7] Cohen, A. A. (1996). *Nucl. Data Sheets* **79**(1): 24-76.

[8] Reich, C. W. (2009). *Nucl. Data Sheets* **110**: 2278-2313.

[9] Reich, C. W. (2003). *Nucl. Data Sheets* **99**: 263-772.

[10] Reich, C. W. (2003). *Nucl. Data Sheets* **99**: 910-956.

[11] Helmer, R. G. (2004). *Nucl. Data Sheets* **101**: 415-444.

[12] Reich, C. W. (1996).*Nucl. Data Sheets* **78**: 603-661.

[13] Reich, C. W. (2007). *Nucl. Data Sheets* **108**: 1819-1907.

[14] Singh, B. (2001). *Nucl. Data Sheets* **93**: 249-299.

[15] Baglin, C. M. (2008). *Nucl. Data Sheets* **109**: 6-20.

[16] Trajdos, M. and Zajac, K. (1989). Nucleon Pairs as the Building Blocks of a Nucleus. *Acta Phys. Pol. B* **20**(9): 815-822.

[17] Zamfir, N. V., Casten, R. F., Caprio, M. A., Beausang, C. W., Krucken, R., Novak, J. R., Cooper, J. R., Cata-Danil, G. and Barton, C. J. (1999). $B(E2)$ Values and Phase Coexistence in ^{152}Sm. *Phys. Rev. C* **60**(5), 054312: 1-11.

[18] Casten, R. F. and Zamfir, N. V. (2001). Empirical Realization of a Critical Point Description in Atomic Nuclei. *Phys. Rev. Lett.* **87**(5), 052503: 1-4.

[19] Kulp, W. D., Wood, J. L., Garret, P. E. et al. (2005). Identification of a Pairing Isomeric Band in ^{152}Sm. *Phys. Rev. C* **71**(4), 041303: 1-4.

[20] Youngblood, D. H., Lui, Y. W., Clark, H. L., John, B., Tokimoto Y. and Chen, X. (2004). Isoscalar $E0-E3$ Strength in ^{116}Sn, ^{144}Sm, ^{154}Sm and ^{208}Pb. *Phys. Rev. C* **69**(3), 034315: 1-14.

[21] Burke, D. G. (2002). Search for Experimental Evidence Supporting the Multiphonon Description of Excited States in ^{152}Sm. *Phys. Rev. C* **66**(2), 024312: 1-8.

[22] Klug, T., Dewald, A., Werner, V., von Brentano, P. and Casten, R. F. (2000). The $B(E2:4_2^+ \rightarrow 2_2^+)$ Value in ^{152}Sm and $\beta-$Softness in Phase Coexisting Structures., *Phys. Lett. B* **495**: 55-62.

[23] Hellstrom, M., Fogelberg, B., Spanier, L. and Mach, H. (1990). Energy Levels and Transition Probabilities in the Neutron-Rich Lanthanide Nucleus ^{156}Sm. *Phys. Rev. C* **41**(5): 2325-2332.

[24] Garret, P. E. (2001). Characterization of the β Vibration and 0_2^+ States in Deformed Nuclei. *J. Phys. G Nucl. Partic.* **27**: R1-R22.

[25] Raman, S. and Nestor Jr., C. W. (1989). Predictions of $B(E2:0_1^+ \rightarrow 2_1^+)$ Values for Even-even Nuclei. *Atom. Data and Nucl. Data* **42**(1): 1-54.

[26] Jing-ye Zhang, Caprio, M. A., Zamfir, N. V. and Casten, R. F. (1999). Phase/Shape Coexistence in ^{152}Sm in the Geometric Collective Model. *Phys. Rev. C* **60**(6), 061304: 1-5.

[27] Bjerregaard, J. H., Hansen, O. and Nathan, O. (1966). The (t,p) Reaction with Even Isotopes of Sm. *Nucl. Phys.* **86**(1): 145-166.

[28] Helmer, R. G. and Burson, S. B. (1960). Decay of ^{166}Dy. *Phys. Rev.* **119**(2): 788-795.

[29] Burke, D. G. (1988). Studies of $^{158,160,162,164,166}Dy$ Levels with the (t,p) Reaction. *Nucl. Phys. A* **483**(2): 221-243.

[30] Grotdal, T., Nybo, K. and Thorsteinsen, T. (1968). Collective Vibrational States in Even Dysprosium Nuclei. *Nucl. Phys. A* **110**(2): 385-399.

[31] Sheng, Z., Ren, Z. and Jiang, W. (2010). Investigations on Ground-State Properties of Deformed Nuclei in Relativistic Mean Field Theory with Parameter Set FSUGold. *Nucl. Phys. A* **832**: 49-61.

[32] Struble, G. L., Mann, L. G., Lanier, R. G. and Buckley, W. M. (1981). Influence of Complex States and Deformation on Neutron Pairing Vibrations in the Even *Sm* Isotopes. *Phys. Rev. C* **23**(6): 2447-2458.

[33] Maggie, K. and Kirsten, S. (2005). The Periodic Table. Retrieved from: www.hobart.k12.in.us/ksms/PeriodicTable/index.htm

[34] Chemical Periodic Table. Chemicool.com (5 May 2012). Samarium. Retrieved from:http://www.chemicool.com/elements/samarium.html

[35] Buzzle. (2012). Samarium Uses. Retrieved from:www.buzzle.com/articles/samarium-uses.html

[36] Chemical Periodic Table. Chemicool.com (5 May 2012). Dysprosium. Retrieved from:http://www.chemicool.com/elements/dysprosium.html

[37] Ring, P. and Schuck, P. (2005). The Nuclear Many-Body Problem. New York: Springer.

[38] Soloviev, V. (1976). Theory of complex nuclei. Oxford: Pergamon Press.

[39] Krane, K. and Halliday, D. (1987). Introductory nuclear physics. New York: Wiley.

[40] Bohr, A. and Mottelson, B. R. (1953). Interpretation of Isomeric Transitions of Electric Quadrupole Type. *Phys. Rev.* **89**(1): 316.

[41] Bohr, A. and Mottelson, B. R. (1998). Nuclear Structure. Singapore: World Scientific.

[42] Iudice, N. L. and Palumbo, F. (1978). New Isovector Collective Modes in Deformed Nuclei. *Phys. Rev. Lett.* **41**(22): 1532-1534.

[43] Faessler, A. (1997). Magnetic Dipole Properties in Deformed Nuclei. *Prog. Part. Nucl. Phys.* **38**: 195-212.

[44] Pietralla, N., von Brentano, P., Herzberg, R. D., Kneissl, U., Iudice, N. L., Maser, H., Pitz, H. H. and Zilges, A. (1998). Systematics of the Excitation Energy of the 1^+ Scissor Mode and Its Empirical Dependence on the Nuclear Deformation Parameter. *Phys. Rev. C* **58**(1): 184-190.

[45] De Franceschi, G. and Palumbo, F. (1984). Reformulation of the Two-Rotor Model. *Phys. Rev. C* **29**(4): 1496-1509.

[46] Iudice, N. L. (1995). Semiclassical Versus Microscopic Descriptions of Scissors Modes. *Prog. Part. Nucl. Phys.* **34**: 309-318.

[47] Iudice, N. L., Palumbo, F., Richter, A. and Wortche, H. J. (1990). Semiclassical Description of the Scissor Mode: Possible Improvements and Intrinsic Limitations. *Phys. Rev. C* **42**(1): 241-246.

[48] Iudice, N. L. and Richter, A. (1993). Scissors Mode and Nuclear Deformation. A Phenomenological Model Independent Analysis. *Phys. Lett. B* **304**(3-4): 193-197.

[49] Iudice, N. L. and Palumbo, F. (1979). Positive Parity Isovector Collective States in Deformed Nuclei. *Nucl. Phys. A* **326**(1): 193-208.

[50] Itoh, M., Sakaguchi, H., Ishikawa T. et al. (2001). Giant Monopole Resonance in Deformed Nuclei. *Nucl. Phys. A* **687:** 52c-57c.

[51] Richter, A. (1985). Nuclear Structure. *Proceedings of the Niels Bohr Centennial Conference.* North-Holland: Amsterdam. p. 469.

[52] Nesterenko, V. O., Usmanov, Ph. N., Okhunov, A. A. and Fahlander, C. (1993). Non-adiabatic Behaviour of E2 Transition in ^{166}Er. *J. Phys. G Nucl. Partic.* **19**: 1339-1348.

[53] Usmanov, Ph. N. and Mikhailov, I. N. (1997). Effects of Non-adiabatics of collective motion in even-even deformed nuclei. *Fiz. Elem. Chastits At. Yadra* **28**: 887-950.

[54] Okhunov, A. A. (2006).Electric Properties of Levels of ^{156}Dy Rotational Bands. *Phys. Atom. Nucl.* **69**(4): 593-597.

[55] Bohr, N. (1936). Neutron Capture and Nuclear Constitution. *Nature* **137**: 344.

[56] Nilsson, S. G. and Ragnarsson, I. (1995). Shapes and Shells in Nuclear Structure. New York: Cambridge University Press.

[57] Krane, K. S. *(*1988). Introductory Nuclear Physics, New York and Singapore: John Wiley and Sons.

[58] von Weizsacker, C. F. (1935). Zur Theorie der Kermassen. *Z. Phys.* **96**: 431-458.

[59] Jelley, N. A. (1990). Fundamentals of Nuclear Physics. New York: Cambridge University Press.

[60] Mayer, M. G. and Jensen, J. H. D. (1955). Elementary Theory of Nuclear Shell Structure. New York and London: John Wiley & Sons.

[61] Rowe, D. J. (2010). Nuclear Collective Motion: Models and Theory. Singapore: World Scientific.

[62] Telfer, R. (26 Oct 1998). The Spin-Orbit Effect. Retrieved from: www.pha.jhu.edu/~rt19/hydro/node.html

[63] Rainwater, J. (1950). Nuclear Energy Level Argument for a Spheroidal Nuclear Model. *Phys. Rev.* **79**(3) : 432.

[64] Scharff-Goldhaber, *G.* and Weneser, J. *(*1955*).* System of Even-even Nuclei. *Phys. Rev*. **98***:* 212-214(L).

[65] Greiner, W. and Maruhn, J. (*1996*). Nuclear Models. Berlin: Springer.

[66] Wheldon, C. (1999). Deformation. Retrieved from: www.wheldon.talktalk.net/thesis/thesis/node10.html

[67] Nave, C. R. (1997). Electric Quadrupole Moments of Nuclei. Retrieved from: hyperphysics.phy-astr.gsu.edu/hbase/nuclear/elequad.html

[68] Burcham, W. E. and Jobes, M. (1995). Nuclear and Particle Physics. Harlow, UK: Pearson Education Limited.

[69] Belyaev, S. T. (1968). Collective Excitations in Nuclei. New York: Gordon and Breach Science Publishers.

[70] Roy, R. R. and Nigam, B. P. (2005). Nuclear Physics: Theory and Experiment. New Delhi: New Age International (P) Limited, Publishers.

[71] Hornyark, W.E. (1975). Nuclear Structure. New York San Francisco and London: Academic Press, Inc.

[72] Xiaofeng Wang. (2007). Exotic Collective Excitation at High Spin: Triaxial Rotation and Octupole Condensation**.** Unpublished doctoral dissertation, University of Notre Dame, Notre Dame, Indiana.

[73] Siemens, P. J. and Jensen, A. S. (1987). Many-Body Physics with the Strong Interaction. New York: Addison-Wesley Publishing Company, Inc.

[74] Heyde, K. (2004). Basic Ideas and Concepts in Nuclear Physics: An Introductory Approach. Bristol: Institute of Physics Pub.

[75] Casten, R. F. (2000). Nuclear Structure from a Simple Perspective. Oxford University Press.

[76] Vertes, A., Nagy, S., Klencsar, Z. and Lovas, R.G. (2003). Handbook of Nuclear Chemistry: Basics of Nuclear Science. Kluwer Academic Publishers,

[77] Wilets, L. and Jean, M. (1956).Surface Oscillations in Even-Even Nuclei. *Phys. Rev.* **102** (3): 788-796.

[78] Stephens, F. S. (1975). Coriolis Effects and Rotation Alignment in Nuclei. Review of Modern Physics, 47(1), 43-65.

[79] Wheldon, C. (1999). *K*-isomerism at High-spin Beyond the Fusion Limit**.** Unpublished doctoral dissertation, University of Surrey, Guildford, United Kingdom.

[80] Inglis, D. R. (1954). Particle Derivation of Nuclear Rotation Properties Associated with a Surface Wave. *Phys. Rev.* **96**(4): 1059.

[81] Inglis, D. R. (1956). Nuclear Moments of Inertia due to Nucleon Motion in a Rotating Well. *Phys. Rev.* **103**(6): 1786.

[82] Harris, S. M. (1965). Higher Order Corrections to the Cranking Model. *Phys. Rev.* **138**: B509.

[83] Okhunov, A. A., Kassim, H.A., and Usmanov, Ph.N. (2011). Determination of Moment of Inertia for $^{162\text{-}168}$Hf and $^{164\text{-}176}$Yb Deformed Nuclei. *Sains Malaysiana* **40**(1): 1-3.

[84] Rowley, N. (2009). Natural Reference for Nuclear High-spin States. *Phys. Rev. C* **80**: 024323.